Ph.D. DISSERTATION

A STUDY ON EFFICIENCY MAXIMIZATION AND SYSTEM IMPLEMENTATION OF MICROWAVE POWER TRANSMISSION

마이크로웨이브 무선전력전송의 효율 최대화와 시스템 제작에 관한 연구

BY

HOYEOL KIM

FEBURARAY 2023

DEPARTMENT OF ELECTRICAL AND
COMPUTER ENGINEERING
COLLEDGE OF ENGINEERING
SEOUL NATIONAL UNIVERSITY

A STUDY ON EFFICIENCY MAXIMIZATION AND SYSTEM IMPLEMENTATION OF MICROWAVE POWER TRANSMISSION

지도 교수 남 상 욱

이 논문을 공학박사 학위논문으로 제출함
2023 년 2 월

서울대학교 대학원
전기 • 컴퓨터공학부
김 호 열

김호열의 공학박사 학위논문을 인준함
2023 년 2 월

위 원 장 _____ 이 정 우 _____ (인)

부위원장 _____ 남 상 욱 _____ (인)

위 원 _____ 이 범 선 _____ (인)

위 원 _____ 이 정 해 _____ (인)

위 원 _____ 오 정 석 _____ (인)

Abstract

In this thesis, research on the maximum power transfer efficiency (PTE) of microwave wireless power transmission (MPT) and the optimization algorithm for efficient system was presented. First, an optimization algorithm was studied to obtain an optimal transmit signal to maximize PTE during MPT using an array antenna. There are two important factors to consider in MPT. The first is to minimize the effect of electromagnetic waves on the human body, and the second is to charge multiple receivers simultaneously. Therefore, we propose an optimization algorithm that satisfies each of the two cases and derives the maximum PTE. Furthermore, we study an optimization algorithm that provides the necessary guidelines for designing a practical MPT system. An algorithm that can calculate the efficiency boundary of an MPT system through a fast channel prediction method was proposed. Additionally, an MPT method of a hybrid beamfocusing architecture has been proposed. The main contents of the study are as follows.

First, we propose a novel convex optimization algorithm for exciting transmit antennas of MPT systems that transmit maximum power under certain specific absorption rate (SAR) constraints for human safety. The method of converting the initial NP-hard problem into a convex optimization problem has been described in detail. A single receiver is placed next to the box-shaped phantom model, and the algorithm is applied to the MPT scenario where

multiple transmit antennas surround them. The channel response between the transmitter and receiver and the electric field response of the phantom required for the optimization process were obtained using electromagnetic simulation. The received power and PTE of the proposed optimization technique were compared with the time-reversal (TR) technique at 0.9 GHz. We show that optimization (OPT) techniques can transfer more power than TR techniques with lower PTEs within the SAR limit and that the proposed techniques can be applied to various MPT scenarios.

Second, we develop an optimization method for MPT capable of charging multiple receivers. The optimization algorithm finds the optimal transmit signal for transferring the desired power to multiple receivers with maximum PTE. As a transmitter and receiver, we designed a 5×5 rectangular patch array antenna and a single patch antenna operating at 10 GHz. The operation process of the MPT system using the optimization method is analyzed. In addition, considering the various scenarios, we compare the power transfer efficiency of the PTE of each receiver's received power and optimization technique with the multi-receiver TR technique. The OPT algorithm generates multiple beams to charge multiple receivers simultaneously. We also validate that in MPT systems OPT technology can accurately transfer power to receivers at the desired rate with larger PTEs than TR technology.

Third, we study an efficient method for finding PTE for practical microwave and mmWave wireless power transmission systems

consisting of transmitter and receiver array antennas. The PTE boundary of the MPT system is obtained by formulating it as a convex optimization problem that maximizes the power received from the receiver array under transmit power constraints. The channel state information (CSI) between each element of transmitter and receiver is an input parameter of the proposed CVP. CSI is estimated using the Friis transmission equation of the array antenna and the Active Element Pattern (AEP) because transmitter and receiver are assumed to be large arrays. For MPT systems designed at 10 GHz and 24 GHz, the estimated PTE boundaries were compared with previous studies, varying the distance and tilt angle between transmitter and receiver. In addition, the calculation time required for each method was compared. We show that the proposed method provides faster and more accurate PTE boundaries without electromagnetic simulation of MPT systems consisting of transmitter and receiver array antennas.

Finally, we investigate a hybrid beamfocusing method for MPT. We propose an optimization algorithm to obtain an optimal coefficient of phase shifters and amplitude controllers with maximum RF power transfer efficiency (RF−PTE) for the hybrid beamfocusing architecture. The optimization algorithm is proposed by iteratively solving the alternative optimization problem. The algorithm is simulated by applying it to an MPT system with a transmitter and receiver composed of patch array antennas operating at 10 GHz. Additionally, we implement a test bed

operating at 5.8 GHz. Through the simulations and experiments, the amplitude controllers of partially-connected hybrid beamfocusing architecture can be reduced by half compared with the fully digital beamfocusing to achieve the optimal RF-PTE. Therefore, an economical and less complex MPT system can be implemented by using the hybrid beamfocusing method.

Keywords: Microwave wireless power transmission, array antenna, power transfer efficiency, convex optimization

Student Number: 2016-20889

Table of Contents

List of Figures

Chapter 1. Introduction

1.1. Classification of Wireless Power Transmission

The wireless charging is basically installed in most mobile devices related to portable terminals, and furthermore, it is predicted that charging terminals can be removed in new device models in the future. If so, in the future, charging of the mobile device including the portable terminal will only be performed using the wireless power transmission (WPT) device. Currently, the wireless charging service adopts a method in which a wireless power transmission unit and a wireless charging reception unit charge with probability and contactless in a frequency band of several hundred kHz through a magnetic induction method. Technology through magnetic induction is currently being applied not only to wireless charging of 15W mobile devices, but also to several kW wireless power supplies for electric vehicles or electric mobility devices (electric bicycles, kickboards, home/industrial robots, etc.). Therefore, it is expected to be applied to more diverse electronic devices in the future. In addition, it has the advantage of maintaining high efficiency even in high voltage power and being able to develop through relatively inexpensive parts, so it is quickly coping with existing wired charging services. However,

the WPT method using the magnetic field has a limitation on the degree of freedom of the charging position as the charging device rapidly deteriorates even at a slight distance from the WPT device. In addition, to charge multiple devices at the same time, the complexity of the transmission device configuration increases, making it less effective. It is not easy to apply to small IoT and wearable devices because it utilizes tens/hundreds of kHz bands. Therefore, to solve this problem, research on the application of multiple transmission coils, magnetic beamforming, and magnetic resistance method through impedance matching change to charge multiple devices and increase the degree of freedom of charging position in near-field magnetic field coupling situations is being actively conducted.

Wireless Power Consortium (WPC) and Airfuel, which are standard groups for wireless charging, are also paying attention to establishing standards for more convenient wireless charging services through the development of related technologies. In the WPT technology using a magnetic field, the WPT unit and the receiving unit are electromagnetically tight-coupled or loose-coupled. As the resonance frequency and impedance parameters change if the location or load of the receiver changes slightly, the power transfer efficiency reacts sensitively and requires detailed control of the inductive/capacitive/resistance coupling. In addition, the implementation of magnetic field coupling theory and system for charging multiple devices is complicated, and the wavelength is

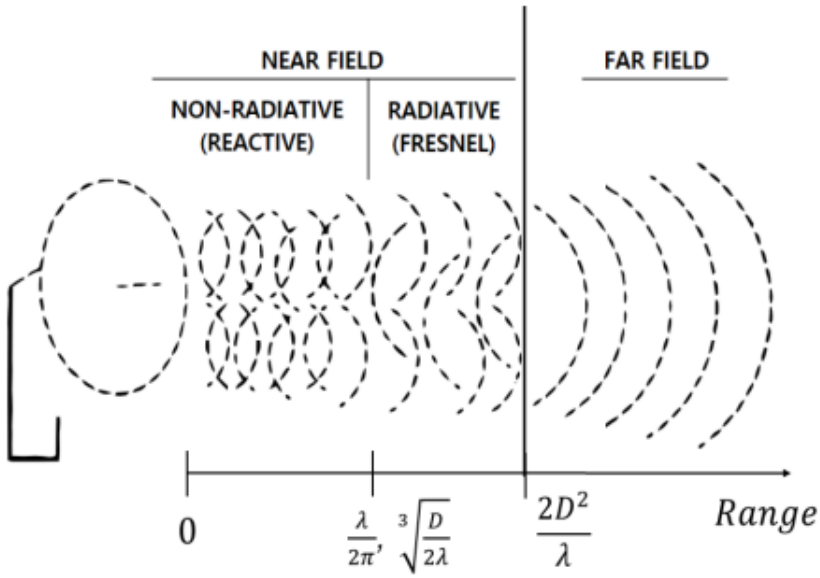

Fig. 1. 1. Distance region of wireless power transfer

long in the frequency band of several kHz to several tens MHz, making it difficult to focus the signal to a long distance. Therefore, since microwave WPT (MPT) uses sub-GHz and several GHz bands rather than conventional magnetic field coupling, the higher the frequency,

the same the magnitude of the electric field and the magnetic field, making it easier to transmit wireless power to multiple devices and control the beamforming of the transmitter.

The criteria for field region in WPT can basically be explained through the concept of near-field and far-field in radio wave and antenna theory. The distance field of radio waves can be defined as

a propagation region that varies depending on the distance from the transmission antenna by the operation of the electromagnetic (EM) wave. In addition, it can be seen that it has different EM radiation characteristics depending on the near-field and far-fields. The near-field and far-field can be divided into mathematical expressions by farunhofer distance [2]. The Fraunhofer distance can be expressed as the wavelength of the radio wave divided by twice the square of the antenna length, as shown in Fig. 1. 1.

The intensity of the EM field in the near-field is much greater than that of the magnetic field in the area near the WPT source. Therefore, the WPT source and the wireless power reception unit are influenced by the strong reaction component and affect each other according to the change in the load current of the transmission unit and the reception unit. In a far-field, EM waves emitted from a wireless power source proceed in the form of spherically waves, and spherical waves that have traveled a very long distance look like plane waves in a narrow range. In conclusion, in the classification of WPT technology, the boundaries of distance cannot be accurately divided, but it can be defined as a position that does not affect the propagation characteristics and impedance of the wireless power receiver even if the load current and electric charge change.

The radiative near field does not contain reactive field components from the source antenna, since it is far enough from the antenna that back-coupling of the fields becomes out of phase

with the antenna signal, and thus cannot efficiently return inductive or capacitive energy from antenna currents or charges. The energy in the radiative near field is thus all radiative energy, although its mixture of magnetic and electric components are still different from the far field. Further out into the radiative near field (one half wavelength to 1 wavelength from the source), the E and H field relationship is more predictable. In most cases, the receiver is located in the radiative near-field or far-field of microwave WPT (MPT). However, if the frequency is increased, there is a high probability that the receiver is located in the radiative near-field.

In general, MPT system consists of transmit array antenna and receive array antenna as shown in Fig. 1. 2. he far-field was calculated while increasing the frequency when the physical size of the transmitter was fixed. For example, if the physical size is 0.25 m x 0.25 m and the frequency is 0.9 GHz, 2.45 GHz, 5.8 GHz and 24.5 GHz, the far-field reference distance is 0.38 m, 1 m, 2.4 m and 10 m, respectively. In general, the MPT specification is determined to receive a power of several W with reference distance of 1m [3]. However, as you can see from the data above, the distance of 1m is radiative near-field at frequencies above 5.8GHz. Therefore, it is necessary to charge power to the receiver by controlling both the amplitude and phase of the transmission antenna to transmit maximum power. This paper defines the method of focusing on power by controlling the amplitude and phase in MPT as the beam focusing method. The optimal magnitude phase

can be obtained using the optimization problem if the channel information between the transmitter and the receiver is known. A detailed explanation is given in the main part.

1.2. Power efficiency of wireless power transmission system

Fig. 1. 2 shows the block diagram from the transmitter's dc source to the receiver's dc output, which constitutes the overall MPT system. The MPT system consists of a power source connected to the transmit antenna system, a wireless channel, and a receiving antenna system connected to a rectifying circuit whose DC output is managed by a dc-to-dc converter that supplies energy to the battery-free device [4, 5]. The MPT system consists of transmit array antenna and receive array antenna as shown in Fig. 1. 3. Fig. 1. 2 also summarizes the amount of power that is monitored on each subsystem connection port. The exact value for these quantities can be used to calculate the overall system efficiency as a product of the following ratios: The P_{BIAS} the dc power required on the transmitter side, the P_{RX} is the RF power available on the transmit antenna input port, the P_{RX} is the RF power received by the antenna, the P_{DC} is the rectifier output power, and the P_{ST} is the dc-dc converter output power. All of these quantities depend on the operating frequency, architecture of MPT system and dimension of MPT system.

The first factor is the DC-RF conversion efficiency of the power supply. The second factor is determined by transmit and receive antenna characteristics, radio channel characteristics, and transmission signals. This depends on frequency and can be

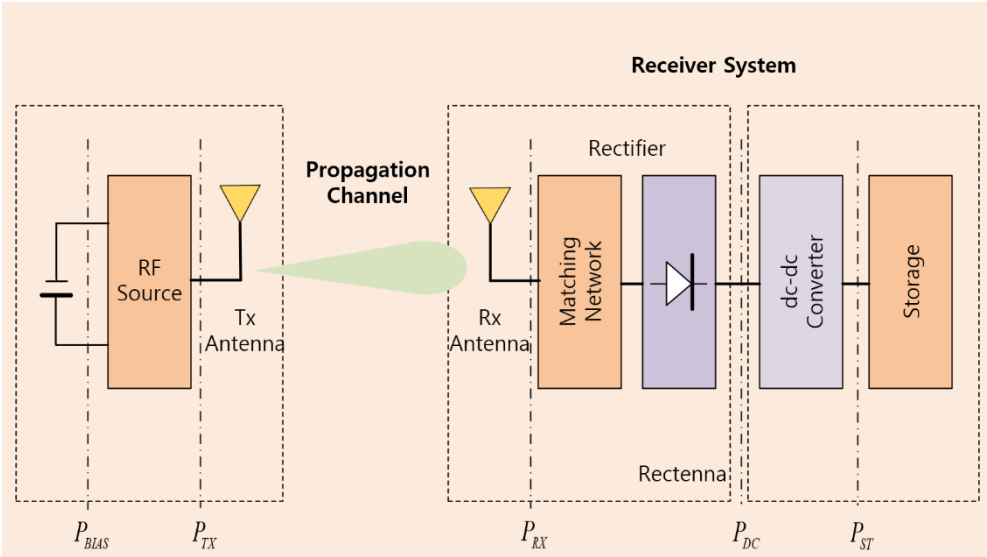

Fig. 1. 2. The building blocks of a microwave wireless power transmission system, along with the power quantities involved. Tx: transmitter; Rx: receiver.

calculated based on EM theory. Research is being actively conducted to accurately evaluate these contributions [6-8] The third factor is the RF-DC conversion efficiency of the rectifier. Because the entire MPT system consists of connections of nonlinear circuits, the behavior of the MPT system depends heavily on the relevant power level and waveform of RF signal and can be accurately quantified only if the behavior of these blocks is known accurately. The last factor is the dc-to-dc conversion efficiency of the optimized power management device. In this paper, we focused on RF efficiency. RF efficiency varies greatly depending on the distribution of signals applied to the transmitting antenna when there is a given transmitting antenna and receiving antenna.

Therefore, when the optimal signal is found, the maximum power can be transmitted to the receiver. That is, RF efficiency can be maximized. Therefore, it is necessary to find a transmission signal that maximizes the power transfer efficiency (PTE) between the transmitter and the receiver on a given MPT system, or to find a method to design an efficient MPT system before that.

1.3. Microwave Wireless Power Transmission Technologies

Initial research and development of MPT technology focused on transmitting large amounts of power from several m to several km due to the difficulty of applying to small devices due to the large size, low performance, and integration of high-frequency parts [9]. In addition, the use of MPT was limited due to the low maturity of mobile devices and large amounts of IoT device technologies and little spread of commercialization. However, since the 2010s, the spread of mobile devices and IoT devices has increased the inconvenience of always supplying power and replacing battery, and research and development for commercialization is underway as MPT has received attention as a technology that can solve these problems. However, MPT using ultra-high frequency reduces the WPT efficiency in inverse proportion to the distance square compared to the energy transmission distance, so the received power is bound to decrease as the distance from the transmitter increases. The receiver may receive desired wireless power by transmitting the transmit power by greatly increasing the transmit power or increasing the directivity of the antenna. However, due to problems such as radio wave interference with surrounding wireless signals/electronic devices, influence on the human body, heat generation in the surrounding environment, and the price of

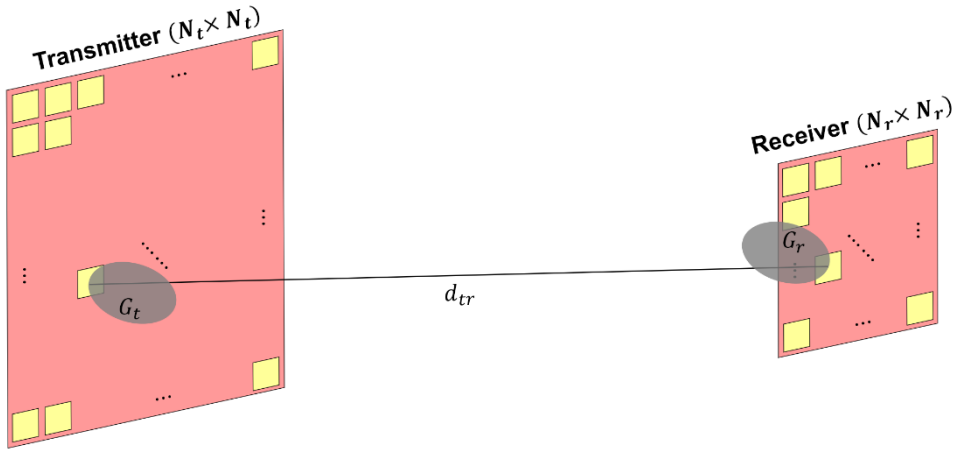

Fig. 1. 3. The example of MPT system with transmitter and receiver array antennas

parts, transmit power cannot be greatly increased to infinity. In addition, the directivity of the antenna is also limited in implementation according to the size and shape of the service device. Therefore, in order to overcome the free space path loss when transmitting wireless power, research on methods for focusing wireless power on devices that receive power and reducing the surrounding radio waves and human environment is being actively conducted. Research on beamforming as a method of utilizing ultra-high frequency of MPT technology and focusing wireless power is being actively conducted.

In particular, technology for retro-directive beamforming is being developed as a method for finding the location of the receiving device and focusing power. Retro-direct beamforming transmits a pilot signal from the receiving side to locate the location of the

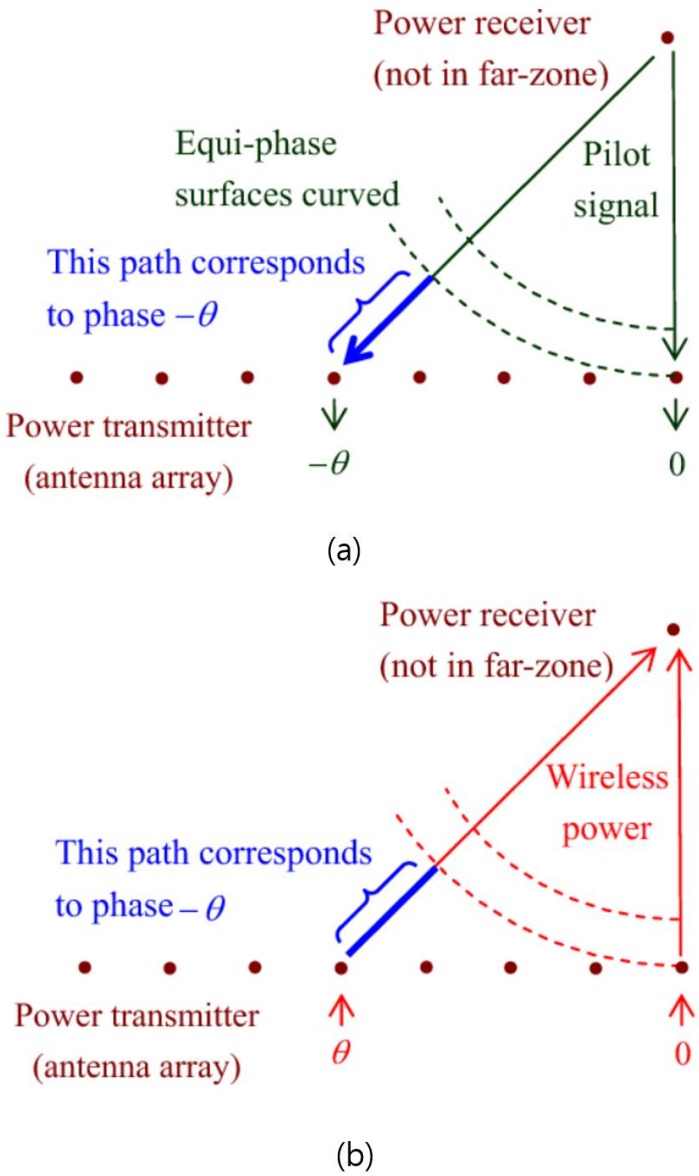

Fig. 1. 4. Retro-directive beamforming technology (a) Wireless power receiver broadcasts pilot signal to wireless power transmitter. (b) Wireless power transmitter sends power to wireless power receiver.

wireless power receiving unit. Next, it detects the phase difference of the pilot signal input from the wireless power transmitter side, which consists of a phased array antenna structure, and applies a negative phase value for the difference to transmit wireless power

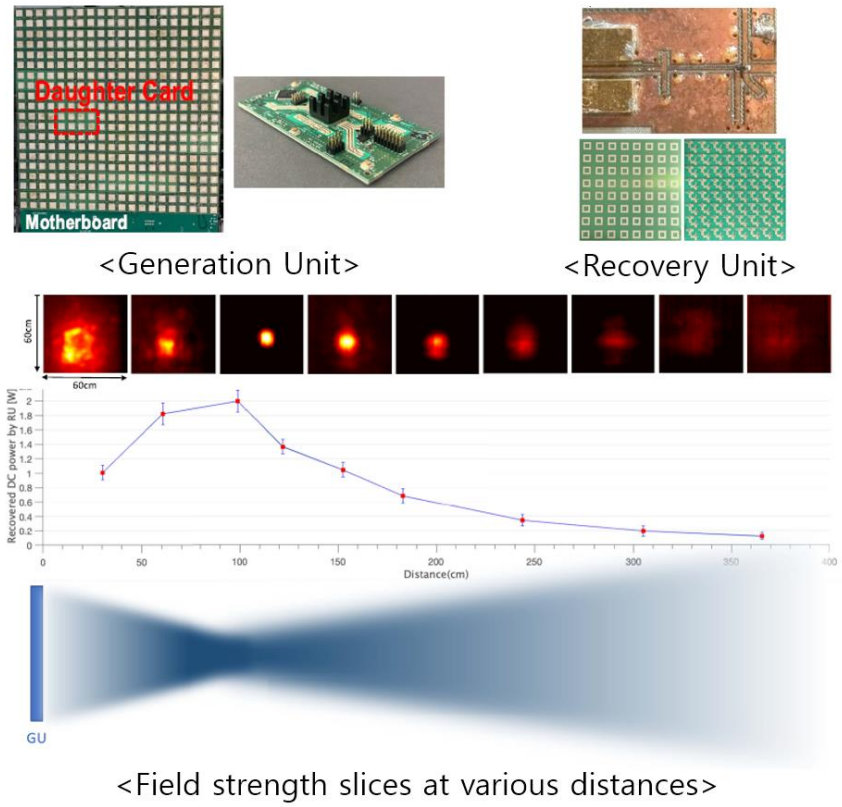

Fig. 1. 5. Microwave and mmWave wireless power transmission researches in the Hajimiri Lab [14].

[10], [11]. As shown in Fig. 1. 4, when phase-conjugate is applied to the incident angle input to each phase array antenna to transmit wireless power, the wireless power is beamformed and transmitted in the direction of the receiving unit that transmits the pilot signal. The Time-Reversal method, which is a method of transmitting signals in proportion to the reception size of pilot signals used in phase-conjugation, was also studied [12].

Since a few years ago, research on wireless power beamforming has been published in IEEE Wireless Power Transfer Conference

(IEEE WPTC) and related journals. Research at Kyoto University shows that the retro-directive beamforming method can maximize PTE in multi-path environments of wireless power beams [13]. The PTE of the retro-directive beamforming is higher than that of the single beam, and the efficiency is higher in the multi-path environment generated by the wall. This technology is typically being commercialized for MPT products by implementing a direction-of-arrival (DOA) location estimation technology by Osia, and many other related companies are applying beamforming through similar methods. In addition, a method of finding the optimal transmission signal after feedback the received signal using orthogonal matrix as the basis of the transmission signal was also studied [14].

Another technology that focuses power for MPT is being studied using a millimeter wave (mmWave). In 5G mobile communication, the mmWave frequency band (over 24 GHz) allows a much higher radiation power density than the low frequency regulation with an acceptable transfer EIRP (Effective Isotropic Radiated Power) limit of 75 dBm in the Federal Communications Commission (FCC) [15]. In addition, mmWave can minimize the array antenna size of the wireless power receiving device, and compensate for high path loss in high frequency bands using very large gains. On the other hand, due to the high gain characteristics, the directional angular coverage of the antenna is limited. However, millimeter waves have a very short wavelength and strong straightness, so they are good

for focusing and controlling beams, and research and development to apply them as long-distance WPT technology is currently underway. Hajimiri's research group at the California Institute of Technology recently developed a technology that enables WPT of 2W or more at a distance of 1m or more of transmission and reception in the 10GHz band [3]. As shown in Fig. 1. 5, it is possible to focus wireless power at a desired location through RF Lensing by controlling the transmission unit of the 20×20 (400 elements) array. In addition, the Tentzeris study group at Georgia Tech developed a wireless power reception rectenna with an incident power density of −6 dBm/cm2 with a transmission power of 25 dBm in the range of 2.83 m in the 5G frequency band, 28 GHz [15].

1.4. Human Safety Regulation in terms of Electromagnetic field

One of the factors to consider in the commercialization of MPT is the human safety problem of EM field. Since the MPT transmitter transmits relatively large power compared to other electronic devices, the magnitude of EM waves in the air is large. Therefore, the system should be developed in consideration of the effect of EM field on the human body. Standard is made to protect against adverse human health effects associated with exposure to electromagnetic fields [16]. Protection against effects associated with electrical stimulation, tissue and systemic heating has been considered and applies to all human body exposures except patient exposures, either under the direction of the physician and medical professional or under the direction of the physician. It is not limited to the purpose of preventing interference with medical devices and other devices that may exhibit sensitivity to radio frequency (RF) fields. The regulations are expressed in terms of basic restrictions (BRs) and maximum permissible exposure (MPE) values. The BRs are limits on internal fields, specific absorption rate (SAR), and current density. The MPEs are limits on external fields and induced and contact current.

The SAR is one of the representation of BRs and is defined as

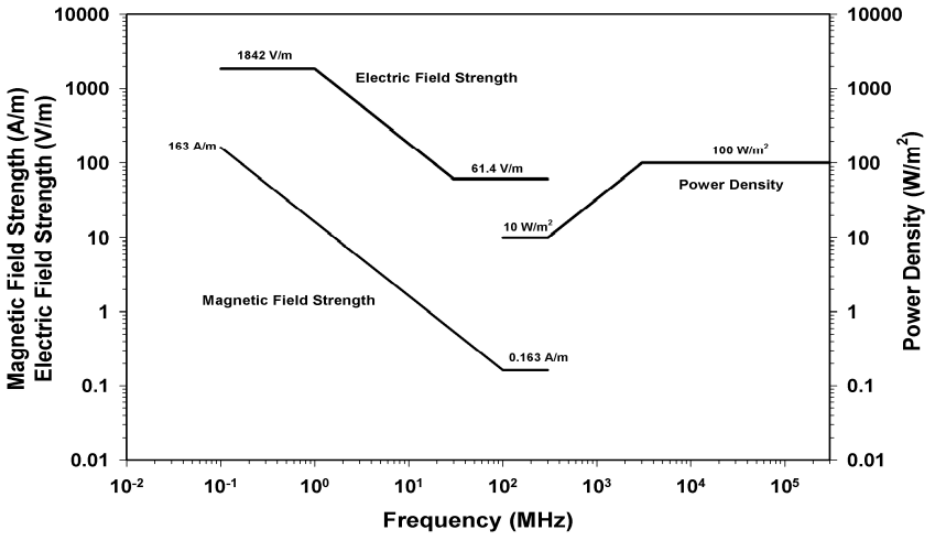

Fig. 1. 6. Graphic representation of maximum permissible exposure.

the time derivative of incremental energy absorbed by an incremental mass contained in a volume element of given density. It can be expressed as $\mathrm{SAR} = {\sigma|E|^2}/{\rho}$ by electric field at a point, where σ, E and ρ are conductivity of the tissue (S/m), mass density of the tissue (kg/m^3) and rms electric field strength in tissue (V/m), respectively. In addition, the maximum local SAR averaged over a specified volume or mass.

The whole-body-average BRs were calculated based on the abuse health effects associated with the whole-body heating. SAR is averaged over the appropriate averaging times as shown in Fig.1. 6. Whole-body SAR and localized SAR are defined respectively. Localized SAR is averaged over any 10g of tissue (defined as a tissue volume in the shape of a cube). Localized exposure SAR

were set to prevent excessive temperature rise in body parts that may result from local exposure or non-uniform exposure. The orientation of the cube used for SAR averaging must also correspond to the coordinate axis used for experimental measurement or numerical calculation procedures.

Since it is difficult to determine whether exposure complies with BR, MPE is provided below to protect against heating-related side effects for the convenience of exposure assessment. If humans are exposed to electromagnetic energy at radio frequencies from 100 kHz to 300 GHz, MPE is shown in Fig. 1. 6 as a function of frequency in terms of plane wave free-space power density (S) equivalent to RMS electricity (E) and magnetic field strength.

1.5. Reference

[1] G. Lipworth et al., “Magnetic metamaterial superlens for increased range wireless power transfer,” Sci. Rep. 4, 2014.

[2] K. T. Selvan et al., “Fraunhofer and fresnel distances,” IEEE Antennas Propag. Mag., Vol.59, No.4, 2017, pp.12−15.

[3] A. Hajimiri, B. Abiri, F. Bohn, M. Gal−Katziri and M. H. Manohara, "Dynamic Focusing of Large Arrays for Wireless Power Transfer and Beyond," in IEEE Journal of Solid−State Circuits, vol. 56, no. 7, pp. 2077−2101, July 2021.

[4] A. Costanzo, M. Dionigi, D. Masotti, M. Mongiardo, G. Monti, L.Tarricone, and R. Sorrentino, “Electromagnetic energy harvesting and wireless power transmission: A unified approach,“ Proc. IEEE, vol. 102, no. 11, pp. 1692–1711, Nov. 2014.

[5] A. Costanzo and D. Masotti, "Smart Solutions in Smart Spaces: Getting the Most from Far−Field Wireless Power Transfer," in IEEE Microwave Magazine, vol. 17, no. 5, pp. 30−45, May 2016.

[6] J. −H. Kim, Y. Lim and S. Nam, "Efficiency Bound of Radiative Wireless Power Transmission Using Practical Antennas," in IEEE Transactions on Antennas and Propagation, vol. 67, no. 8, pp. 5750−5755, Aug. 2019.

[7] H. Sun and W. Geyi, "Optimum Design of Wireless Power Transmission Systems in Unknown Electromagnetic Environments," in IEEE Access, vol. 5, pp. 20198−20206, 2017.

[8] B. Clerckx and E. Bayguzina, "Waveform Design for Wireless

Power Transfer," in IEEE Transactions on Signal Processing, vol. 64, no. 23, pp. 6313-6328, 1 Dec.1, 2016.

[9] W. C. Brown, “The history of power transfer by radio waves,” IEEE Trans. Microw. Theory Tech., 1984.

[10] X. Wang et al., “Retro-directive beamforming versus retro-reflective beamforming with applications in wireless power transmission,” Progress In Electromagnetics Research, 2016.

[11] T. Sasaki et al., "Study on multipath retrodirective for microwave power transmission," IEEE WPTC’18, 2018.

[12] W. Geyi, Foundations of Applied Electrodynamics, USA, NY, New York:Wiley, 2010.

[13] T. Sasaki et al., "Study on multipath retrodirective for efficient and safe indoor microwave power transmission," IEEE WPTC’19, 2019

[14] J. H. Park, N. M. Tran, S. I. Hwang, D. I. Kim and K. W. Choi, "Design and Implementation of 5.8 GHz RF Wireless Power Transfer System," in IEEE Access, vol. 9, pp. 168520-168534, 2021, doi: 10.1109/ACCESS.2021.3138221.

[15] A. Eid et al., “5G as a wireless power grid,” Nature scientific reports, 2021.

[16] IEEE Recommended Practice for Determining the Peak Spatial-Average Specific Absorption Rate (SAR) in the Human Head from Wireless Communications Devices: Measurement Techniques," in IEEE Std 1528-2013 (Revision of IEEE Std 1528-2003) , vol., no., pp.1-246, 6 Sept. 2013

Chapter 2. Power Transfer Efficiency Maximization considering human safety

2.1 Motivation

Microwave wireless power transmission (MPT) has been an area of research since the 1960s and is nowadays attracting increasing attention owing to the widespread use of wireless devices, such as mobile phones, Internet-of-Things devices, sensors, and implant devices [1], [2]. Various types of MPT have been studied theoretically and experimentally [1]–[13]. Large phased-array for long distance MPT were studied in the 1960s [3], [4], and MPT techniques using retro-directive arrays [5], [6] and time-reversal (TR) techniques for indoor environments [7]–[10] have also been reported. In addition, waveform design for improving the RF–DC efficiency of a rectifier has been investigated [11], [12].

The goal in the MPT research is to transfer the maximum power from a transmitter to a receiver. Time-reversal (TR) technique is known as the optimum technique for maximizing PTE in free space [7]; it flips the received signal in time to refocus the original field as an incoming wave [8] and can be interpreted as a phase-conjugation technique in the frequency domain. In practical cases, the electromagnetic field (EMF) cannot be fully restored using a finite transmitting antenna array, and hence, there is a PTE

boundary in terms of the transmitting area and transfer distance [9]. Although TR is the best solution for MPT even in practical cases with maximum PTE, EMF issues should be considered when designing MPT systems.

In general, EM waves cause thermal heating in the body and may be hazardous to humans. Therefore, the specific absorption rate (SAR), which measures the EM energy absorbed per unit mass of tissue, is used to limit EM wave exposure. A SAR limit of 1.6 W/kg averaged over 1 g of local tissue proposed in the ANSI/IEEE C95.1 standard was recommended by the Federal Communications Commission (FCC) [13]. In particular, the use of an MPT system close to the body makes it more dangerous than other wireless devices because MPT systems employ high power in their transmitter. Therefore, considering human safety is one of the most important issues in MPT research. A few researchers have checked whether their wireless power transfer (WPT) systems satisfy the SAR limit after system implementation [14]–[16]. However, human safety must be considered during the design process of WPT systems.

In this chapter, we propose a convex optimization algorithm that can control the electric field (E−field) in the body not to exceed the SAR limit and transfer maximum power to the receiver when the receiver is positioned near body. A similar optimization technique was used in hyperthermia research to focus the E−field without input power constraints [17]. In this study, we formulate

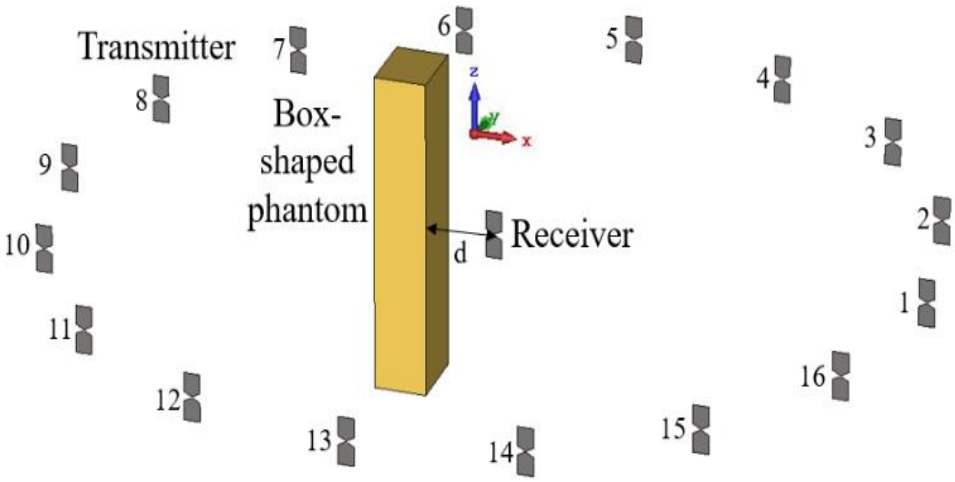

Fig. 2. 1. 3D MPT scenario with 16 transmitters and a receiver comprising bowtie half-lambda dipole antennas and a small box-shaped phantom near the receiver

the optimization algorithm that maximizes the power received by the receiver and includes a total input power constraint. The proposed algorithm is applied to several MPT scenarios with multiple transmitting antennas and one receiver near a box-shaped phantom model. Full-wave numerical simulation is used to compare the performance, received power, and PTE of the proposed optimization (OPT) technique with those of the TR technique. The differences in the performance for different distances and the worst-case scenario are analyzed in detail. With the proposed optimization algorithm, the MPT system transfers more power to the receiver in every scenario compared with the TR technique.

2.2 Optimization problem formulation

The optimization problem is formulated for an MPT scenario with N transmitting antennas around a receiving antenna located near a human phantom model as shown in Fig. 2. 1. When a unit voltage is applied to each transmitting antenna, the E−field produced by each antenna at position r in the human phantom model is expressed as

$$\overline{\overline{E}}(r) = \begin{bmatrix} e_{x0}(r) & e_{x1}(r) & \cdots & e_{xN-1}(r) \\ e_{y0}(r) & e_{y1}(r) & \cdots & e_{yN-1}(r) \\ e_{z0}(r) & e_{z1}(r) & \cdots & e_{zN-1}(r) \end{bmatrix}^T \quad (2-1)$$

where $e_{xn}(r)$, $e_{yn}(r)$, and $e_{zn}(r)$ refer to the x, y, and z components of the E−field at r in the phantom excited by the n−th transmitting antenna, respectively. Consider a transmitting signal vector $\mathbf{S} = [s_0, s_1 \cdots s_{N-1}]^T$. The n−th element of $\mathbf{S}$, $s_n = v_n e^{j\psi_n}$, represents the excitation of a complex voltage to the n−th transmitting antenna, where v_n and ψ_n are the amplitude and phase of the signal, respectively. The total E−field vector at position r in the human phantom model when the signal $\mathbf{S}$ is excited by N transmitting antennas is expressed as

$$\mathbf{E}(\mathrm{r},\mathbf{S}) = \overline{\overline{E}}(r)^T \mathbf{S} = \begin{bmatrix} E_x(r,\mathbf{S}) \\ E_y(r,\mathbf{S}) \\ E_z(r,\mathbf{S}) \end{bmatrix} \tag{2-2}$$

where $E_x(r,\mathbf{S})$, $E_y(r,\mathbf{S})$, and $E_z(r,\mathbf{S})$ are the x, y, and z components of the E-field, respectively. The components of the E-field vector are expressed as $\sum_{n=0}^{N-1} e_{xn}(r)s_{xn}$, $\sum_{n=0}^{N-1} e_{yn}(r)s_{yn}$, and $\sum_{n=0}^{N-1} e_{zn}(r)s_{zn}$, respectively. In the proposed optimization problem, (2-2) is used to formulate the SAR constraint. The received voltage on the receiving antenna can be obtained as $V_R(\mathbf{S}) = \sum_{n=0}^{N-1} h_n s_n = \mathbf{H}^T\mathbf{S}$ with $\mathbf{H} = [h_0, h_1 \cdots h_{N-1}]^T$, where $h_n = A_n e^{j\phi_n}$ is the channel response between the n-th transmitting antenna and the receiver. A_n and ϕ_n are the amplitude and phase of the channel response, respectively.

With the channel response and the E-field, the optimal transmitted signal $\mathbf{S}$ should be found to maximize the received power considering the limit of the total transmitted power and the SAR constraint, i.e.,

$$\max \quad P_R(\mathbf{S}) \tag{2-3}$$

$$\text{Subject to} \quad \frac{\|\mathbf{S}\|_F^2}{R} \le P \tag{2-4}$$

$$\frac{\sigma|\mathbf{E}(r,\mathbf{S})|_F^2}{\rho} \le SAR, r \in \Psi. \tag{2-5}$$

$P_R(\mathbf{S})$ is the target function, and is proportional to the received power at the receiver. $P_R(\mathbf{S})$ can be expressed as $|V_R(\mathbf{S})|^2$. The limited transmitted power constraint is expressed in (2−4), where R and P refer to the radiation resistance of the transmitting antenna under matching conditions and the total transmitted power, respectively. The SAR regulation in the human phantom model is expressed as constraint (2−5) using the SAR definition, where σ and ρ refer to the electric conductivity and the density of the human phantom model, respectively. In this optimization problem, the optimal phase of the transmitted signal can be easily obtained; the condition that $P_R(\mathbf{S})$ is maximum is met when all the polynomial terms of $V_R(\mathbf{S})$ are positive and real. Therefore, the optimal phases of the transmitted signal must be of opposite sign to the phase of the transfer function, i.e.,

$$\psi_n^* = -\phi_n \tag{2-6}$$

In terms of the optimal amplitude of the transmitted signal, the optimization problem in (2−3)–(2−5) is not a convex problem and belongs to the class of the NP−hard problems. Fortunately, the problem can be transformed to a convex problem.

2.3 Transformation to Convex Optimization Problem

Equations (2−3)–(2−5) can be transformed to an equivalent problem by introducing an auxiliary variable t.

$$\min \quad 1/t \tag{2−7}$$

$$\text{subject to} \quad \frac{\|\mathbf{S}\|_F^2}{R} \leq P \tag{2−8}$$

$$t/P_R(\mathbf{S}) \leq 1 \tag{2−9}$$

$$\frac{\sigma|\mathbf{E}(r,\mathbf{S})|_F^2}{\rho} \leq SAR, r \in \Psi. \tag{2−10}$$

This optimization problem is not a geometric program (GP) because the left sides of (2−9) and (2−10) are not posynomials. The reason is that the denominator of the left side of (2−9) is a posynomial and the left side of (2−10) consists of negative and positive terms. To make this optimization problem a convex problem, the left sides of (2−9) and (2−10) need to be transformed to a posynomial. The idea is to use the upper bound of $\mathrm{t}/P_R(\mathbf{S})$ as a monomial function [18]. $P_R(\mathbf{S})$ can be expressed as a posynomial function using the optimal phases of the transmitted signal, ψ_n^*. Let $\{f_k(\mathbf{S})\}$ be the monomial terms in posynomial $P_R(\mathbf{S}) = |V_R(\mathbf{S})|^2 = \sum_{k=0}^{K-1} f_k(\mathbf{S})$. K is $\mathrm{N}(\mathrm{N}+1)/2$. The upper bound can be obtained using

the fact that the arithmetic mean is larger than or equal to the geometric mean. Therefore, $\sum_{k=0}^{K-1} f_k(\mathbf{S}) \geq \prod_{k=0}^{K-1} \left(\frac{f_k(\mathbf{S})}{x_k}\right)^{x_k}$ with $x_k \geq 0$ and $\sum_{k=0}^{K-1} x_k = 1$, such that the upper bound to the left side of (9) can be approximated by a monomial, i.e.,

$$t / P_R(\mathbf{S}) \leq t \prod_{k=0}^{K-1} \left(\frac{f_k(\mathbf{S})}{x_k} \right)^{-x_k} \tag{2-11}$$

If the original constraint (2-9) is tightened by (2-11), (2-9) can be replaced by

$$t \prod_{k} \left(\frac{f_k(\mathbf{S})}{x_k} \right)^{-x_k} \leq 1 \tag{2-12}$$

Fortunately, a set of $\{x_k\}$ that tightens the original constraint can be found via an iterative computation method [19], [20]. This method will be explained in detail in the last part of this section. As a result, the left side of (2-9) is transformed to a monomial, i.e., a posynomial.

In this next step, the left side of (2-10) is transformed to a posynomial. As $\mathbf{E}(r, \mathbf{S})$ consists of the x, y, and z components of the E-field, we obtain

$$|\mathbf{E}(r,\mathbf{S})|_F^2 = \sum_{n=0}^{N-1}|e_{xn}(r)|^2 v_n^{\ 2} + \sum_{n=0}^{N-1}|e_{yn}(r)|^2 v_n^{\ 2} + \sum_{n=0}^{N-1}|e_{zn}(r)|^2 v_n^{\ 2}$$
$$+2\sum_{i=0}^{N-1}\sum_{j=0,i\neq j}^{N-1}\left[e_{xi}(r)\mathrm{s}_i\, e_{xj}(r)^*\mathrm{s}_j^{\ *} + e_{yi}(r)\mathrm{s}_i\, e_{yj}(r)^*\mathrm{s}_j^{\ *} + e_{zi}(r)\mathrm{s}_i\, e_{zj}(r)^*\mathrm{s}_j^{\ *}\right] \quad (2-13)$$

The first three terms of the right side of (2−13) are posynomials, whereas all the components of the last term are not. $|\mathbf{E}(r,\mathbf{S})|_F^2$ is a real value, hence the right side must be a real value. Therefore, (2−13) can be replaced by

$$|\mathbf{E}(r,\mathbf{S})|_F^2 = \sum_{n=0}^{N-1}|e_{xn}(r)|^2 v_n^{\ 2} + \sum_{n=0}^{N-1}|e_{yn}(r)|^2 v_n^{\ 2} + \sum_{n=0}^{N-1}|e_{zn}(r)|^2 v_n^{\ 2}$$
$$+2\sum_{i=0}^{N-1}\sum_{j=0,i\neq j}^{N-1}|e_{xi}(r)||e_{xj}(r)|v_i v_j\cos\theta_l + 2\sum_{i=0}^{N-1}\sum_{j=0,i\neq j}^{N-1}|e_{yi}(r)||e_{yj}(r)|v_i v_j\cos\theta_l$$
$$+2\sum_{i=0}^{N-1}\sum_{j=0,i\neq j}^{N-1}|e_{zi}(r)||e_{zj}(r)|v_i v_j\cos\theta_l \quad (2-14)$$

where $\theta_l = \psi_i - \psi_j + \phi_i - \phi_j$ for i and j ranging from 0 to N−1, $i > j$, and $\mathrm{i} \neq \mathrm{j}$. Equation (2−14) can be expressed as $|E(r,\mathbf{S})|^2 = P(r,\mathbf{S}) - N(r,\mathbf{S})$, where $P(r,\mathbf{S})$ and $N(r,\mathbf{S})$ are the sums of the positive terms and negative terms, respectively. Therefore, the inequality in (2−10) is transformed to $\frac{\sigma P(r,\mathbf{S})}{\rho SAR+\sigma N(r,\mathbf{S})} \leq 1$ and the same technique used to transform (2−9) into (2−11) can be applied. Let $\{f_e(\mathbf{S})\}$ be the monomial terms in a posynomial $\rho SAR + \sigma N(r,\mathbf{S}) = \sum_{e=0}^{E-1} f_e(r,\mathbf{S})$. Therefore, the following inequality holds:

$$\rho SAR + \sigma N(\mathrm{r}, \mathbf{S}) \geq \prod_{e=0}^{E-1} \left(\frac{f_e(\mathrm{r}, \mathbf{S})}{x_e} \right)^{x_e} \tag{2-15}$$

where $x_e \geq 0$ and $\sum_{e=0}^{E-1} x_e = 1$. E is the number of positive terms of $\rho SAR + \sigma N(r, \mathbf{S})$ that is not constant with position r.

Finally, the transformed optimization problem can be expressed as

$$\min \quad 1/t \tag{2-16}$$

$$\text{subject to} \quad \frac{\|\mathbf{S}\|_F^2}{R} \leq P \tag{2-17}$$

$$t \prod_{k=0}^{K-1} \left(\frac{f_k(\mathbf{S})}{x_k} \right)^{-x_k} \leq 1 \tag{2-18}$$

$$\sigma P(r, \mathbf{S}) \prod_{e=0}^{E-1} \left(\frac{f_e(r, \mathbf{S})}{x_e} \right)^{-x_e} \leq 1, \ r \in \Psi. \tag{2-19}$$

The transformed optimization problem expressed by (2−16)–(2−19) is the standard GP and a convex problem [18]. The precondition for this optimization problem is that the set of $\{x_k\}$ and $\{x_e\}$ satisfy the tight bounds of (2−11) and (2−15). An iterative computation method can be used to find the set of $\{x_k\}$ and $\{x_e\}$

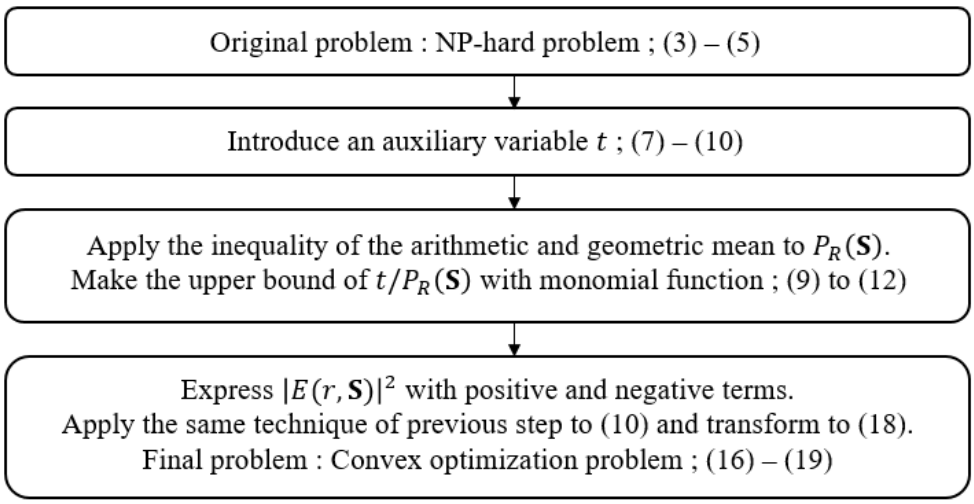

Fig. 2. 2. Flowchart of transformation of the original problem into a convex optimization problem

using the approach in [15] and [16] in which the standard GP (2−16)–(2−19) is solved for an updated set of $\{x_k\}$ and $\{x_e\}$ at each iteration. To compute $\{x_k\}$ and $\{x_e\}$, the following equations are used:

$$x_k^{(i+1)} = f_k(\mathbf{S}^{(i)}) / \left|V_R(\mathbf{S}^{(i)})\right|^2, \qquad (2-20)$$

$$x_e^{(i+1)} = f_e(r,\mathbf{S}^{(i)}) / \left[\rho \mathrm{SAR} + \sigma \mathrm{N}(r,\mathbf{S}^{(i)})\right] \qquad (2-21)$$

These satisfy the conditions that $x_k \geq 0$, $\sum_{k=0}^{K-1} x_k = 1$, $x_e \geq 0$, and $\sum_{e=0}^{E-1} x_e = 1$ at iteration *i*. Start with any feasible set S and compute $\{x_k\}$ and $\{x_e\}$ using (2−20) and (2−21). Assuming the solved set of $\mathbf{S}^{(i)}$ at iteration *i*, compute $x_k^{(i+1)}$ and $x_e^{(i+1)}$ at iteration $i+1$ and

solve problem (2−16)–(2−19) to obtain $\mathbf{S}^{(i+1)}$. Repeat the iterative computation until convergence. The tight bound conditions of (2−11) and (2−15) and the global optimal solution for our MPT system can be found through this iterative method. A summary of the transformation of the original problem (2−3)–(2−5) into the convex optimization problem (2−16)–(2−19) is shown in Fig. 2. 2.

2.4 MPT Simulation Scenario

The 3D WPT scenario considered for simulation is depicted in Fig. 2. 1; the transmitting antenna is a circular array with a radius of 1.5 m comprising 16 bowtie half-lambda dipoles with an operating frequency of 0.9 GHz each. The width, length, thickness, and edge-cutting angle of the bowtie antenna are 55 mm, 143 mm, 0.018 mm, and 55°, respectively. The receiver consists of a single antenna identical to the transmitter and is located at the center of the transmitting array. The phantom is located at a distance d away from the center of the receiver. The dimensions of the phantom are 0.18 m × 0.233 m × 0.96 m, and its dielectric constant, conductivity, and density are 42, 1 S/m, and 1 g/cm^3, respectively, as specified in IEC 62232 [21]. The transmitter and receiver are located on the same plane, namely $z = 0$ (center of the phantom). This study considered only the periodic circular array. However, the proposed optimization algorithm can also be used for aperiodic 2-D arrays, such as the one shown in [22].

A full-wave numerical simulation is performed at 0.9 GHz using CST Microwave Studio to obtain E-field data inside the box-shaped phantom for each transmitting antenna. The optimal phases of the transmitted signals can be found using the channel response between the receiver and each transmitting antenna. With the E-field data and the channel responses, the optimal amplitudes of the

transmitted signals can be obtained via a MATLAB program using a convex optimization solver, such as CVX [23]. The points for the SAR constraints in the optimization are located 8 mm apart as specified in the IEEE SAR measurement report [24]. They are selected to be 1 mm inside the skin of the phantom because the E-field amplitude is rapidly attenuated with the depth of penetration in the phantom.

The simulation steps are as follows. The optimization region in the phantom consists of several planes. First, the plane, z=0, is chosen because the closest point on the phantom from the receiver is at z = 0; then, the optimization algorithm is applied to the phantom plane using the E-field obtained on the selected plane. Then, full-wave numerical simulation is performed using the optimized solution to check if there are any other planes that contain maximum SAR points exceeding 1.6 W/kg averaged over 1 g of the local tissue. If any other plane is detected to have such a point exceeding the SAR constraint, optimization is performed by including that plane. Then, full-wave numerical simulations are used to assess the validity of the solution. These steps are repeated until the maximum SAR is less than or equal to 1.6 W/kg in the entire phantom. The final results, which are the SAR of the box-shaped phantom and the received power satisfying the SAR regulation on the entire phantom, are obtained. In addition, full-wave numerical simulations are performed using the TR technique. A pilot signal transmitted from the receiver is measured at each

transmitting antenna. Then, the transmitter excites the phase-conjugated signal of the measured signal to obtain the results of the TR technique.

The MPT scenarios are simulated with various distances between the phantom and the receiver. We simulate MPT scenarios in which the distance varied from 40 mm to 200 mm. The phantom is located closest to the receiver when d=40 mm, which is the worst-case scenario according to the SAR test report published by the FCC [25]. In addition, scenarios with either 8 or 16 transmitting antennas are simulated.

2.5 Numerical Results

The results of the proposed optimization technique are compared with those of the TR technique as a reference for MPT. In the time-harmonic case, the TR technique transmits the phase-conjugated signal of the pilot signal generated from the receiver at each transmitting antenna [7]. The received power relative to the transmitted power for each distance d between the phantom and receiver is shown in Fig. 2. 3.

2.5.1 Worst-Case Analysis

In this subsection, the worst case of the MPT scenario is explained in detail. The received power of the OPT technique is the same as that of the TR technique up to a transmitted power of 195 W, as shown in the black solid line in Fig. 2. 3. TR is the optimal solution of the OPT technique until the maximum SAR of the phantom exceeds the limit with the maximum PTE [7]. The received power and the maximum SAR of the TR technique increase proportionally with the transmitted power. It is due to the fact that the PTE of the TR technique and the proportion of the transmitted power at each transmitting antenna are constant even if the transmitted power changes. Therefore, for a transmitted power higher than 195 W with TR technique, the maximum SAR

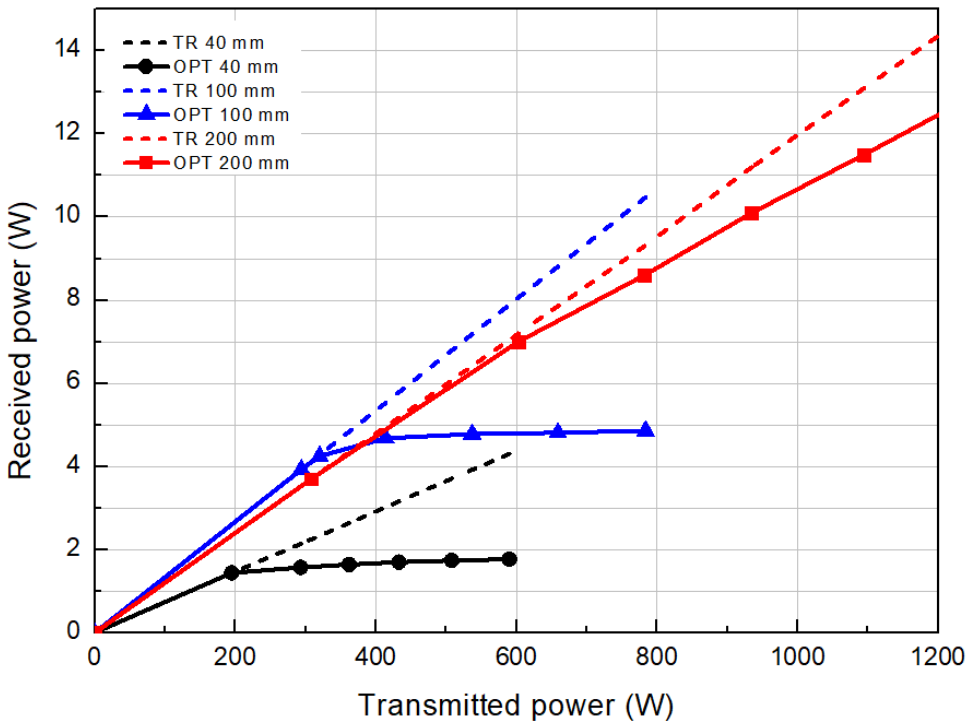

Fig. 2. 3. Comparison of the received power on the receiver using the optimization and time-reversal techniques at 0.9 GHz with 16 transmitting antennas. The solid lines represent the optimization technique. The dashed lines represent the calculated results of the time-reversal technique, which cannot be obtained considering SAR constraints. The black, blue, and red lines indicate distances of 40 mm, 100 mm, and 200 mm, respectively. The symbols indicate the simulated points

exceeds the limit of 1.6 W/kg. If the SAR constraint is not considered, the TR technique can transfer more power, as shown by the black dashed line in Fig. 2. 3. On the other hand, the OPT technique, which uses the optimal input signal obtained via the optimization algorithm, makes the peak E-field in the phantom lower even for a transmitted power higher than 195 W. As a result, the maximum SAR is maintained at 1.6 W/kg, and the received

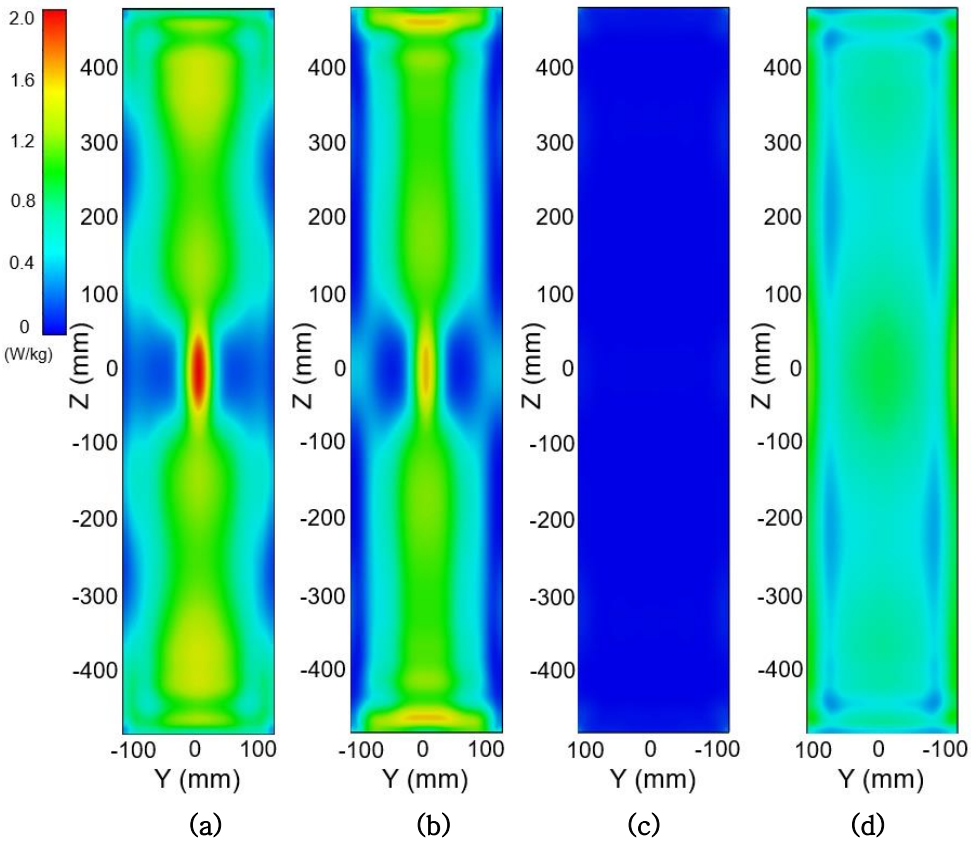

Fig. 2. 4. Magnitude of the SAR distribution in the front and rear of the box-shaped phantom relative to the receiver when the received power is 1.76 W, which is the maximum received power for the OPT technique in the worst-case MPT scenario: (a) front and (c) rear distributions using the time-reversal technique; (b) front and (d) rear distributions using the proposed optimization technique.

power saturates to 1.76 W as the transmitted power increases. Therefore, the OPT technique transfers more power than the TR technique, and the results show that the proposed optimization algorithm can be used in the worst-case MPT scenario.

The SAR distribution of the box-shaped phantom is displayed in Fig. 2. 4 for the worst-case WPT scenario with a transmitted power of 600 W to elucidate the operation of the OPT technique.

The magnetic field distribution is not shown here because the phantom is located in the far-field region of the transmitting antenna even though it should be considered to be in the near-field region [26]. The input reflection coefficient of the receiver is increased in the worst-case scenario due to the near-phantom effect compared with other scenarios. However, it does not affect the comparison result between TR and OPT because its effect is included equally in both these cases. When the TR technique is used, the maximum SAR is 2 W/kg at the phantom in front of the receiver, which exceeds the SAR limit (1.6 W/kg), as shown in Fig. 2. 4(a). However, with the OPT technique, the maximum SAR is 1.6 W/kg, and the SAR is relatively uniformly distributed on the phantom and is below 1.6 W/kg, as shown in Fig. 2. 4(b) and (d).

It is worth noting that the SAR distributions on the rear of the phantom using the TR and OPT techniques are clearly different, as shown in Fig. 2. 4(c) and (d). The SAR obtained through the TR technique is approximately zero because the channel responses of the transmitting antennas at the rear of the phantom and receiver are significantly lower than those of the other antennas. However, the SAR obtained through the OPT technique has a higher but limited value. According to the ANSI/IEEE C95.1 standard, only the peak SAR is relevant when assessing human safety [13]. Therefore, in the OPT technique, the value of the SAR need not be zero anywhere in the phantom, and the transmitters behind the phantom transmit more power than those in the TR technique even

though the channel responses between the receiver and transmitters are lower. This is because the target of the optimization problem is to maximize received power and not the PTE. Therefore, the PTE of the OPT technique is equal to or lower than that obtained via the TR technique. Because of this difference between the TR and OPT techniques, the maximum SAR of the TR technique exceeds 1.6 W/kg whereas the OPT technique satisfies the SAR regulation when both receive same power.

2.5.2 Effect of Separation Between Receiver and Phantom

The performance of the OPT and TR techniques with respect to the distance between the receiver and the phantom is shown in Fig. 2. 3. In addition, the maximum received power and the PTE while satisfying the SAR constraint are reported in Table 2. 1. The maximum received power of both techniques is increased by increasing the distance between the receiver and the phantom. When the TR technique is used, the maximum received power for a distance of 200 mm is 157% higher than in the 40 mm case. If the separation is larger, the EMF loss on the phantom decreases because the transmitter focuses EMF on the receiver. In addition, the PTE of the TR technique increases by 67% because the number of non-line of sight (NLOS) paths between the transmitting

antennas and the receiver decreases from seven to three. The magnitude of the channel response of the line of sight (LOS) paths is larger than that of the NLOS paths by a factor of 3 or more, as listed in Table 2. 2. Therefore, the PTE of the TR technique is higher when the separation is larger because the number of NLOS paths decreases. NLOS paths by a factor of 3 or more, as listed in Table 2. 2. Therefore, the PTE of the TR technique is higher when the separation is larger because the number of NLOS paths decreases.

TABLE 2. 1. Performance Comparison of TR and OPT Techniques with 16 Transmitting Antennas satisfying the SAR Constraint

Distance between receiver and phantom	Time-Reversal		Optimization	
	Maximum Received Power (W)	PTE (%)	Maximum Received Power (W)	PTE (%)
40 mm	1.43	0.73	1.76	0.29
100 mm	3.93	1.43	4.86	0.62
200 mm	3.70	1.22	15.6	0.87

TABLE 2. 2. Excitation of 16 Transmitting Antennas at the point of Maximum Received Power satisfying the SAR constraint

Distance / Transmitter number	40 mm		100 mm		200 mm	
	TR (V)	OPT (V)	TR (V)	OPT (V)	TR (V)	OPT (V)
1	8.77	8.08	8.40	2.65	5.42	4.69
2 (16)	8.22	7.43	8.40	6.43	4.90	1.31
3 (15)	7.12	7.11	8.64	10.40	5.16	12.11
4 (14)	4.93	4.20	7.44	9.69	8.00	31.91
5 (13)	3.29	7.22	5.76	5.20	9.30	12.00
6 (12)	1.92	7.32	3.60	8.16	7.74	10.61
7 (11)	0.82	3.34	3.34	12.55	4.64	16.71
8 (10)	0.27	17.02	1.90	0	1.29	2.73
9	0.82	6.14	0.22	23.77	1.14	12.31

In the OPT technique, the maximum received power increases by 781% for a distance of 200 mm compared with the 40 mm case, which is higher than that of the TR technique by a factor of 5. The OPT algorithm prioritizes LOS paths to transfer more power to the receiver because of the larger magnitude of the channel response than on the NLOS paths. Therefore, the transmitting antennas assign as much power as possible to the LOS paths in such a way that the maximum SAR of the phantom does not exceed the SAR limit. Next, the OPT algorithm excites the transmitting antennas having NLOS paths without increasing the peak SAR because almost all the EMF is absorbed in the rear of the phantom. Therefore, having many LOS paths is advantageous in order to increase the maximum received power and PTE. In other words, the number of LOS paths is the degree of freedom of the optimization algorithm.

The excitation of each transmitting antenna when the maximum power is transferred for each distance is presented in Table 2. 2. To analyze how the transmitted power is wasted when using the OPT technique compared with the TR technique, the figure of merit (FOM) is defined as the OPT to TR ratio in terms of the transmitted power on each path. If more power than the proportion of the channel response in the TR technique is assigned to an NLOS path, the PTE of the entire MPT system decreases. For a distance of 40 mm, the paths between transmitters 6 through 9 and the receiver are NLOS paths, and hence the amplitudes of the channel responses

are lower than on the other paths, as shown in the TR results. The FOMs of the NLOS paths are larger than 14, whereas those of the other paths are lower than 5. Therefore, the PTE of the OPT technique is much lower than that of the TR technique. The paths between transmitters 8 and 9 and the receiver are NLOS paths for distances of 100 mm and 200 mm. FOM of path 9 is only dominantly larger than those of other paths in both cases. Therefore, the rate at which the PTE decreases when using the OPT technique compared with the TR technique at distances of 100 mm and 200 mm are less than that at a distance of 40 mm.

The maximum received power with the OPT technique is 23% higher than with the TR technique, although the PTE is 60% lower for a distance of 40 mm, as presented in Table I. The PTE of the OPT technique decreases because of several NLOS paths. However, the rate at which the maximum received power increases compared with the TR technique becomes higher as the distance increases. For a distance of 200 mm, the maximum received power is 322% higher and the PTE is 29% lower with OPT technique than the TR technique. Note that the OPT technique outperforms the TR technique in every scenario, particularly when the distance is 200 mm. It is found that the results with a SAR limit of 2 W/kg averaged over 10 g of local tissue show that more power can be received with the OPT than the TR technique. The PTE in this study is quite low because the antennas used have omnidirectional patterns and the number of transmitting antennas is inadequate to focus the EMF.

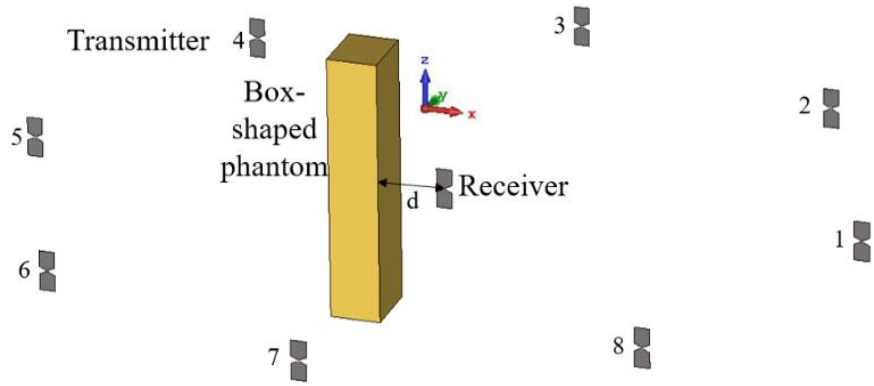

Fig. 2. 5. 3D MPT scenario with 8 transmitters and a receiver comprising bowtie half-lambda dipole antennas and small a box-shaped phantom near the receiver.

TABLE 2. 3. Performance Comparison of TR and OPT Techniques with 8 Transmitting Antennas satisfying the SAR Constraint

Distance between receiver and phantom	Time-Reversal		Optimization	
	Maximum Received Power (W)	PTE (%)	Maximum Received Power (W)	PTE (%)
40 mm	1.43	0.28	1.56	0.18
100 mm	3.85	0.54	4.6	0.41
200 mm	3.35	0.49	5.76	0.38

2.5.3 Effect of the Number of Transmitting Antennas

The scenario with a lower number of transmitting antennas, i.e. eight, is considered as shown in Fig. 2. 5. The performances of the TR and OPT techniques are presented in Table 2. 3. The PTE of the TR technique decreases by more than 50% compared with the scenario with 16 transmitting antennas because the electric area of the transmitter is reduced by 50% [9]. When the number of transmitting antennas decreases at a distance of 200mm, it is noted that the increasing rate of the LOS path number to the total path number is lower compared with other scenario, which explains larger decreasing rate of PTE of the OPT technique. The maximum received power of the OPT and TR techniques are slightly lower compared with the corresponding cases with 16 transmitting antennas. These results demonstrate that the OPT technique can be used even with a small number of transmitting antennas. In all cases, the maximum received power obtained using the OPT technique is higher than that obtained using the TR technique, even though the PTE of the OPT technique is lower.

2.6 Summary

In this chapter, the new convex optimization algorithm for the design of an MPT system that transfers the maximum allowable power while satisfying a SAR constraint for human safety was proposed. The optimization problem for our MPT scenario is formulated and transformed into an equivalent convex optimization problem using various techniques, and the optimal amplitudes and phases of the transmitting antenna array are obtained. The results are then compared with those obtained using the TR technique, which is known as the optimal solution in MPT. The optimization technique can receive higher power with a lower PTE compared with the TR technique in the worst-case scenario, which is clearly explained with the SAR distributions in the phantom and excitation signals. The received power and PTE are calculated for various distances between the receiver and phantom and for different number of transmitting antennas. The results indicate that the OPT technique transfers more power to the receiver than the TR technique in the MPT scenarios considered, particularly in the case where the distance between the receiver and phantom is larger. In addition, the maximum received power obtained using the OPT technique is higher than that obtained using the TR technique even for a lower number of transmitting antennas. Therefore, the OPT technique outperforms the TR technique in terms of faster charging

via MPT for every scenario considered. The results of this study, which considered practical MPT scenarios, is expected to be useful for implementing the proposed optimization algorithm during the design of MPT systems with SAR constraints to ensure human safety.

2.7 Reference

[1] B. Strasner and K. Chang, "Microwave Power Transmission: Historical Milestonesnd System Components," in Proceedings of the IEEE, vol. 101, no. 6, pp. 1379–1396, June 2013.

[2] A. Costanzo and D. Masotti, "Smart Solutions in Smart Spaces: Getting the Most from Far-Field Wireless Power Transfer," in IEEE Microwave Magazine, vol. 17, no. 5, pp. 30–45, May 2016. doi: 10.1109/MMM.2016.2525119[3] W. C. Brown, “Experiments involving a microwave beam to power and position a helicopter,” IEEE Trans. Aerosp. Electron. Syst., vol. AES-5, no. 5, pp. 692–702, Sep. 1969.

[4] P. E. Glaser, “Power from the sun: Its future,” Science, vol. 162, no. 3856, pp. 857–861, 1968.

[5] Y. Li and V. Jandhyala, "Design of Retrodirective Antenna Arrays for Short-Range Wireless Power Transmission," in IEEE Transactions on Antennas and Propagation, vol. 60, no. 1, pp. 206–211, Jan. 2012.

[6] M. Ettorre, W. A. Alomar, and A. Grbic, “2-D Van Atta array of wideband, wideangle slots for radiative wireless power transfer systems,” IEEE Trans. Antennas Propag., vol. 66, no. 9, pp. 4577–4585, Sep. 2018.

[7] W. Geyi, Foundations of Applied Electrodynamics, USA, NY, New York:Wiley, 2010.

[8] J. de Rosny, G. Lerosey and M. Fink, "Theory of

Electromagnetic Time-Reversal Mirrors," in IEEE Transactions on Antennas and Propagation, vol. 58, no. 10, pp. 3139-3149, Oct. 2010.

[9] J. Kim, Y. Lim and S. Nam, "Efficiency Bound of Radiative Wireless Power Transmission Using Practical Antennas," in IEEE Transactions on Antennas and Propagation, vol. 67, no. 8, pp. 5750-5755, Aug. 2019.

[10] R. Ibrahim et al., "Experiments of Time-Reversed Pulse Waves for Wireless Power Transmission in an Indoor Environment," in IEEE Transactions on Microwave Theory and Techniques, vol. 64, no. 7, pp. 2159-2170, July 2016

[11] A. Boaventura, D. Belo, R. Fernandes, A. Collado, A. Georgiadis and N. B. Carvalho, "Boosting the Efficiency: Unconventional Waveform Design for Efficient Wireless Power Transfer," in IEEE Microwave Magazine, vol. 16, no. 3, pp. 87-96, April 2015.

[12] B. Clerckx and E. Bayguzina, "Waveform Design for Wireless Power Transfer," in IEEE Transactions on Signal Processing, vol. 64, no. 23, pp. 6313-6328, 1 Dec.1, 2016.

[13] IEEE Standard for Safety Levels With Respect to Human Exposure to Radio Frequency Electromagnetic Fields, 3 kHz to 300 GHz, IEEE Standard C95.1-2005, Apr. 2006.

[14] C. Liu, Y. Guo, H. Sun and S. Xiao, "Design and Safety Considerations of an Implantable Rectenna for Far-Field Wireless Power Transfer," in IEEE Transactions on Antennas and

Propagation, vol. 62, no. 11, pp. 5798−5806, Nov. 2014.

[15] G Kim, S Boo, S Kim and B Lee*, “Control of Power Distribution for Multiple Receivers in SIMO Wireless Power Transfer System,” J. Electromagn. Eng. Sci., vol. 18, no. 4, pp. 221−230, 2018

[16] M. Koohestani, M. Zhadobov and M. Ettorre, "Design Methodology of a Printed WPT System for HF−Band Mid−Range Applications Considering Human Safety Regulations," in IEEE Transactions on Microwave Theory and Techniques, vol. 65, no. 1, pp. 270−279, Jan. 2017.

[17] D. A. M. Iero, T. Isernia and L. Crocco, "Focusing Time−Harmonic Scalar Fields in Complex Scenarios: A Comparison," in IEEE Antennas and Wireless Propagation Letters, vol. 12, pp. 1029−1032, 2013.

[18] R. J. Duffin and E. L. Peterson, “Geometric programming with signomials,” J. Optim. Theory Appl., vol. 11, no. 1, pp. 3–35, 1973.

[19] M. Chiang, “Geometric programming for communication systems,” in Foundations and Trends in Communications and Information Theory. Delft, The Netherlands: Now Publishers, 2005.

[20] C. S. Beightler and D. T. Philips, Applied Geometric Programming. Hoboken, NJ, USA: Wiley, 1976.

[21] IEC, “Determination of RF field strength and SAR in the vicinity of radiocommunication base stations for the purpose of evaluating human exposure”, IEC 62232, May 2011.

[22] A. F. Morabito, “Power synthesis of mask-constrained shaped beams through maximally-sparse planar arrays,” Telkomnika (Telecommun. Comput. Electron. Control), vol. 14, no. 4, pp. 1217–1219, 2016.

[23] M. Grant, S. Boyd, and Y. Ye, “CVX: MATLAB software for disciplined convex programming,” 2015. [Online]. Available: http://cvxr.com/cvx/

[24] IEEE Recommended Practice for Determining the Peak Spatial-Average Specific Absorption Rate (SAR) in the Human Head from Wireless Communications Devices: Measurement Techniques," in IEEE Std 1528-2013 (Revision of IEEE Std 1528-2003) , vol., no., pp.1-246, 6 Sept. 2013

doi: 10.1109/IEEESTD.2013.6589093

[25] UL Verification Services INC, "SAR EVALUATION REPORT", Energous Corporation, 3590, North First Street, San Jose, CA 95134, USA, 2017. Accessed on Sept. 19, 2017. [Online]. Available: https://fccid.io/2ADNG-MS300/RF-Exposure-Info/SAR-report-V3-368490

[26] N. Kuster and Q. Balzano, “Energy absorption mechanism by biological bodies in the near field of dipole antennas above 300 MHz,” IEEE Trans. Veh. Technol., vol. 41, pp. 17–23, 1992.

Chapter 3. Power Transfer Efficiency Maximization for multiple receivers

3.1 Motivation

Recently, the demand for powering widespread electronic devices and sensors in homes and offices, such as the Internet of things and 5G, has increased the academic and industrial interests in microwave wireless power transmission (MPT) [1][2]. Particularly, the operating frequency has increased to the millimeter-wave (mmWave) range owing to the use of 5G and the possibility of improving the efficiency. When multiple electronic devices need to be charged through MPT, each device requires different amounts of power as it relies on the charging state of the device. Therefore, an MPT system that can obtain the maximum power transfer efficiency (PTE) and supply power to each receiver with a specified power ratio is essential. PTE is defined as ratio of received power at port of receivers and transmitted power at port of transmitter.

Researches have been presented to wirelessly charge multiple receivers in various fields [3]-[8]. In particular, various methods aimed at charging multiple receivers through MPT have been explored [9]-[15]. Studies on MPT have focused on waveform optimization for multiple rectennas that uses a multi-sine signal

[9][10]. Additionally, multi-beamforming antennas and systems have been proposed for MPT [11]–[13]. However, these studies have not reported a method for achieving the maximum PTE, which is the core aspect of MPT. Moreover, the accurate charging of each receiver with the desired power has not been addressed thus far. Furthermore, although the optimization problem of MPT for multiple receivers has been solved using a scattering matrix [14] and non-convex quadratically constrained quadratic program (QCQP) [15], these methods do not ensure a general optimum solution when the desired ratio of the received power is unequal. The time-reversal (TR) technique is considered to be an effective method for maximizing PTE. However, in practical cases that focus on human safety [16] and charging multiple receivers, TR is not the ideal solution for MPT.

In this chapter, an efficient MPT system that can charge multiple receivers using a convex optimization algorithm was proposed. An optimization method is proposed to design the optimal signal that can charge receivers at the maximum total PTE while simultaneously satisfying the desired charging power ratio. Initially, we formulated an optimization problem that can maximize the PTE under the constraint of charging multiple receivers with the desired received power ratio (RPR). The initial optimization problem was transformed into a convex optimization problem (CVP) using several ideas. A 5 × 5 rectangular patch array antenna and patch element antenna operating at 10 GHz were designed as the

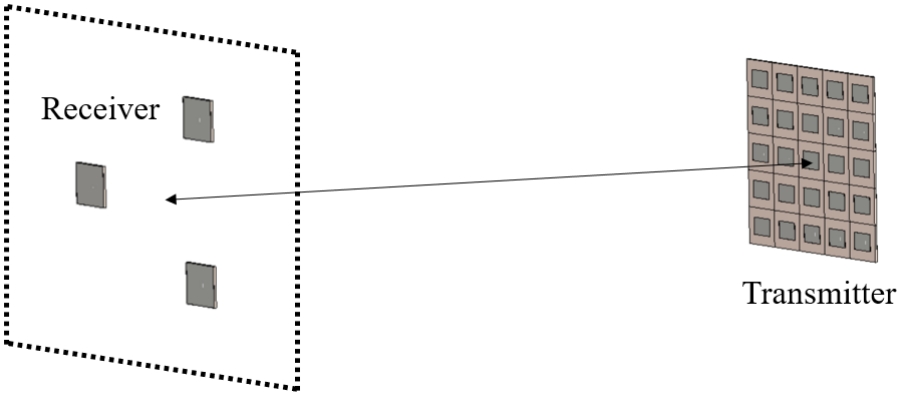

Fig. 3. 1. Microwave wireless power transmission (MPT) system comprising a transmitter and three receivers positioned on the same plane.

transmitter and receiver, respectively. The operation of the WPT system was analyzed using the proposed optimization method, and the MPT system was simulated using a three-dimensional full electromagnetic simulator, namely CST Microwave Studio. We considered several scenarios with multiple receivers at various positions in the radiative near-field region of the transmitter. The electric field (E-field) distribution, which is known to indicate multi-beamforming of the MPT system, was analyzed. Furthermore, performance parameters, such as PTE, received power, and the actual RPR at the receivers of the proposed optimization (OPT) technique were compared with the results of the TR technique. Based on the experimental results, we determined that the MPT system precisely transfers power to multiple receivers using the proposed optimization method.

3.2 Optimization Problem Formulation

This optimization problem is aimed to transfer power to the multiple receivers with the desired ratio and maximum power transmission to achieve maximum PTE. The problem is applied for an MPT system with N transmitting antennas at arbitrary positions and M receivers. Let a transmitted signal vector be $\mathbf{S} = [s_1, s_1 \cdots s_N]^T$. The n−th element of S, $s_n = v_n e^{j\psi_n}$, expresses the input voltage for the n−th transmitting antenna. v_n and ψ_n are the amplitude and phase of the transmitted signal, respectively. The voltage received at the m−th receiving antenna can be obtained with $V_{Rm}(\mathbf{S}) = \sum_{n=1}^{N} h_{m,n} s_n = \mathbf{H}_m^T \mathbf{S}$. Assuming the channel response is known to the transmitter, the optimization problem aims at finding the optimal set of S. The problem maximizes the total received power of multiple receivers subject to constraints, the limited total transmitted power and the ratio of the received power of each receiver, i.e.,

$$\max \quad P_R(\mathbf{S}) \tag{3-1}$$

$$\text{subject to} \quad \frac{\|\mathbf{S}\|_F^2}{R} \leq P \tag{3-2}$$

$$\frac{|V_{R_1}(\mathbf{S})|^2}{|V_{R_m}(\mathbf{S})|^2} \leq \beta_m, 2 \leq \mathrm{m} \leq \mathrm{M}. \tag{3-3}$$

The objective function, $P_R(\mathbf{S})$, is set to proportional to the total power received at multiple receivers and expressed as

$\sum_{m=1}^{M}|V_{Rm}(\mathbf{S})|^2$. Under a given total transmit power condition, maximizing the total received power is equivalent to maximizing the PTE. The total transmit power of optimal signal is constrained by the inequality (3−2), where R and P are the port impedance and the limited transmitted power of MPT system, respectively. The received power of each receiver is expressed as its ratio to the power of the first receiver as in (3−4): β_m is the ratio of the received power of the m−th to the 1st receiver. The problem (3−1)–(3−3) is not convex [17]. The problem, however, can be converted into a GP, i.e. convex problem, as shown in [16].

Divide $\mathbf{S}$ into $\mathbf{S}_1, \cdots, \mathbf{S}_M$ where M is the number of the receivers, i.e., $\mathbf{S} = \sum_{m=1}^{M}\mathbf{S}_m$ and $\mathbf{S}_m = [s_{m,1}, s_{m,2} \cdots s_{m,N}]^T$. The n−th element of $\mathbf{S}_m$, $s_{m,n} = v_{m,n}e^{j\psi_{m,n}}$, expresses the input voltage for the n−th transmitting antenna, where $v_{m,n}$ and $\psi_{m,n}$ refer to the amplitude and phase of the transmitted signal, respectively. Now, we can determine the phase of the transmitting signal with the same approach used in the TR technique, i.e., $\psi_{m,n} = -\phi_{m,n}$.

The problem (3−1)–(3−3) can be transformed to the equivalent epigraph problem form. By transforming the left sides of constraints into posynomials, this optimization problem can be converted to a convex problem. $|V_{Rm}(\mathbf{S})|^2$ can be expressed as $P_m(\mathbf{S}) - N_m(\mathbf{S})$. $P_m(\mathbf{S})$ and $N_m(\mathbf{S})$ are the sums of absolute value of the positive and negative terms of polynomial, respectively, i.e., posynomials. Subsequently, $P_R(\mathbf{S})$ can be expressed as $\sum_{m=1}^{M}[P_m(\mathbf{S}) - N_m(\mathbf{S})]$, and problem (3−1)–(3−3) transform into

problem (3−4)–(3−7).

$$\min \quad 1/t \tag{3-4}$$

$$\text{subject to} \quad \frac{\|\mathbf{S}\|_F^2}{R} \le P \tag{3-5}$$

$$\frac{t+\sum_{m=1}^{M} N_m(\mathbf{S})}{\sum_{m=1}^{M} P_m(\mathbf{S})} \le 1 \tag{3-6}$$

$$\frac{P_1(\mathbf{S})+\beta_m N_m(\mathbf{S})}{N_1(\mathbf{S})+\beta_m P_m(\mathbf{S})} \le 1, 2 \le m \le M \tag{3-7}$$

The idea is to upper bound $[t+\sum_{m=1}^{M} N_m(\mathbf{S})]/\sum_{m=1}^{M} P_m(\mathbf{S})$ by a posynomial function [18]. The upper bound is obtained with the inequality of arithmetic and geometric means. Consider $\{p_k(\mathbf{S})\}$ as a set of monomial terms in the posynomial $\sum_{m=1}^{M} P_m(\mathbf{S}) = \sum_{k=1}^{K} p_k(\mathbf{S})$. K is the number of positive terms of $\sum_{m=1}^{M} P_m(\mathbf{S})$. Because $\sum_{k=1}^{K} p_k(\mathbf{S}) \ge \prod_{k=1}^{K} \left(\frac{p_k(\mathbf{S})}{x_k}\right)^{x_k}$ with $x_k \ge 0$ and $\sum_{k=1}^{K} x_k = 1$, $\sum_{k=1}^{K} x_k = 1$ is upper bounded by a posynomial.

In this step, the above concept is applied to convert the left side of (3−7) into a posynomial. Consider $\{f_z(\mathbf{S})\}$ as a set of monomial terms in a posynomial $N_1(\mathbf{S}) + \beta_m P_m(\mathbf{S}) = \sum_{z=1}^{Z_m} f_z(\mathbf{S})$. Hence, for a given choice of $\{x_k\}$ and $\{x_z\}$, the initial problem is replaced by an equivalent convex problem, i.e.,

$$\min \quad 1/t \tag{3-8}$$

$$\text{subject to} \quad \frac{\|\mathbf{S}\|_F^2}{R} \leq P \tag{3-9}$$

$$(t + \sum_{m=1}^{M} N_m(\mathbf{S})) \prod_{k=1}^{K} \left(\frac{P_m(\mathbf{S})}{x_k}\right)^{-x_k} \leq 1 \tag{3-10}$$

$$(P_1(\mathbf{S}) + \beta_m N_m(\mathbf{S})) \prod_{z=1}^{Z_m} \left(\frac{f_z(\mathbf{S})}{x_z}\right)^{-x_z} \leq 1, 2 \leq \mathrm{m} \leq \mathrm{M} \tag{3-11}$$

where $x_z \geq 0$ and $\sum_{z=1}^{Z_m} x_z = 1$. Z_m is the number of positive terms of $N_1 + \beta_m P_m(\mathbf{S})$.The transformed optimization problem (3-16)-(3-19) is the standard GP, i.e., a convex problem [17]. An iterative computation method using the approach in [19] can be used to find the sets of $\{x_k\}$ and $\{x_z\}$.

3.3 MPT Simulation Scenario with Array Antennas

Fig. 3. 1 depicts the MPT system used in this study, which comprises a 5 × 5 patch array antenna as the transmitter and several patch antennas as receivers. The antennas of the transmitter and receiver were designed using a 1-mm-thick and 15-mm-long Rogers RT/Duroid 5880 square substrate with a dielectric constant of 2.2. The single element in the patch array antenna was designed as a rectangle with dimensions of 6.5 × 9.5 mm and coaxial feed, as illustrated in Fig. 3. 2. The dimensions of the patch array antenna were set based on the targeted operating frequency of 10 GHz, and the interval of each element is half the wavelength. The receiver was designed as a rectangular patch antenna with dimensions of 6 × 9.8 mm. These antennas were simulated using the CST Microwave Studio. The receivers were positioned on the same plane, as depicted in Fig. 3. 1. The distance between the transmitter and receiver planes was set to 350 mm, which is the radiative near-field region of the transmitter. We considered multiple positions of the three receivers and various ratios of the received power in this study as shown in Fig. 3. 3.

The proposed optimization algorithm serves as the core of the MPT system; therefore, its implementation is essential. Initially, the pilot signal is transmitted from the receiver to the transmitter,

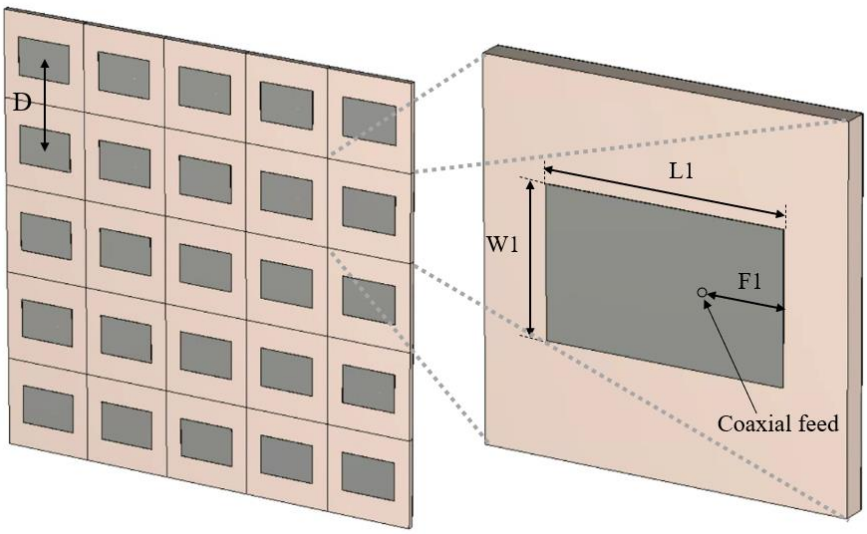

Fig. 3. 2. Designed (a) 5 × 5 patch array antenna as transmitter and (b) the element patch antenna. D = 15 mm, W1 = 6.5 mm, L1 = 9.5 mm, F1 = 2.98 mm.

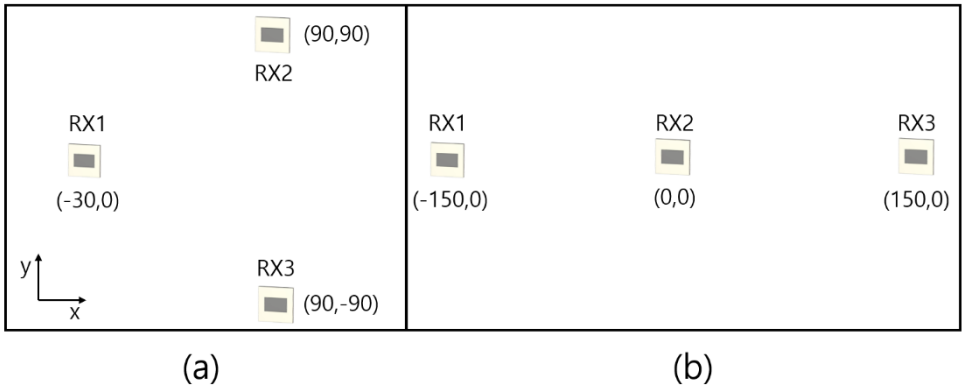

Fig. 3. 3. Positions of the three receivers as viewed from the transmitter. Each position of the receiver is marked adjacent to the antenna relative to the origin, which is the center of the transmitter plane. (a) Scenario 1: Triangular arrangement; (b) Scenario 2: Linear arrangement. Three receivers are placed on the same plane 350 mm away from the transmitter

and the transmitter calculates the channel response between the receiver and transmitter based on the received pilot signal. In this study, this process was simulated using CST Microwave Studio.

The optimal transmitted signals are then obtained using the proposed optimization method via a convex optimization solver, namely CVX [20]. Finally, the transmitter transmits the optimal power signal obtained using the optimization method. To perform a comparative analysis, the transmitted signal of the TR technique was calculated using the multi-receiver TR technique that calculates the transmitted signal based on the received pilot signals of each receiver.

3.4 Numerical Results

Table 3. 1 summarizes the comparison of the received power and PTE considering all scenarios of the OPT and multi−receiver TR techniques. In the OPT technique, the ratio of the received power was equal to the desired value in all cases. By contrast, large errors were observed in the desired and actual RPRs in the case of the multi−receiver TR technique. In scenarios 1 and 2, the actual ratios of the received power were 1:0.43:3.43 and 1:1:3.95, respectively, when the desired RPR was 1:1:2 considering the TR technique. Therefore, the PTE of the OPT technique was greater than that of the multi−receiver TR technique.

Fig. 3. 4 and 3. 5 illustrate the E−field distributions of scenarios 1 and 2, respectively, when OPT technique is used. As depicted in Fig. 3. 4 (a), (b), and (c), three multibeam were generated in scenario 1 when the RPR was 1:1:1. As the receiver was placed on different xz planes, we selected the planes y = 0 mm, y = −45 mm, and y = 45 mm to indicate the beams for receivers 1, 2, and 3, respectively. Additionally, we compared the E−field distributions of different RPRs. When the RPR was 1:1 for receivers 2 and 3, the E−field magnitude of the beam was equal. Conversely, when the RPR was 1:2 for receivers 2 and 3, the E−field magnitude of the beam for receiver 3 was larger than that of receiver 2. Fig. 3. 5 illustrates the multibeam generated in scenario 2. Herein, when the RPR was 1:1:1, two beams targeted receivers 1 and 3, whereas

TABLE 3. 1. Performance Comparison of OPT and TR Techniques Considering the Scenario with three Receivers (Fig. 3. 3)

Desired ratio of the received power			RX1 (mW)	RX2 (mW)	RX3 (mW)	PTE (%)
Scenario 1	1:1:1	TR	4.9	3.4	3.4	1.17
		OPT	4.9	4.9	4.9	1.48
	1:1:2	TR	2.3	1.0	7.9	1.11
		OPT	3.6	3.6	7.3	1.48
Scenario 2	1:1:1	TR	4.1	4.1	4.1	1.22
		OPT	4.2	4.2	4.2	1.25
	1:1:2	TR	1.9	1.9	7.5	1.13
		OPT	3.0	3.0	6.0	1.20

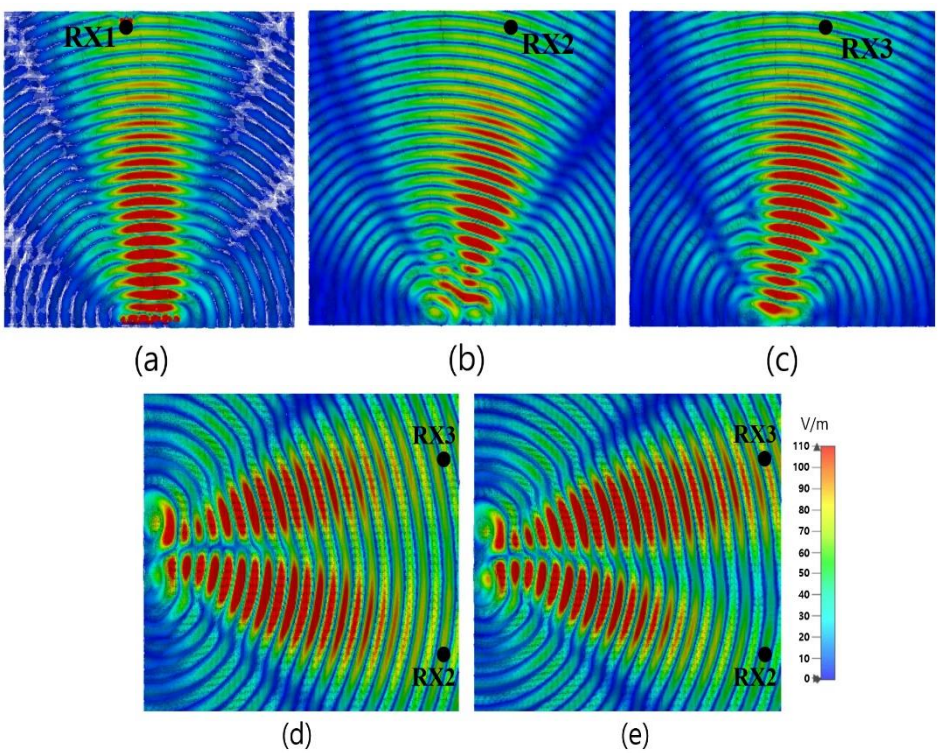

Fig. 3. 4. Electric field distribution of scenario 1 when the optimization (OPT) technique is used. (a) y = 0 mm, (b) y = −45 mm, and (c) y = 45 mm plane when the received power ratio (RPR) is 1:1:1. x = 45 mm plane when the RPR is (d) 1:1:1 and (e) 1:1:2. The three receivers are charged simultaneously.

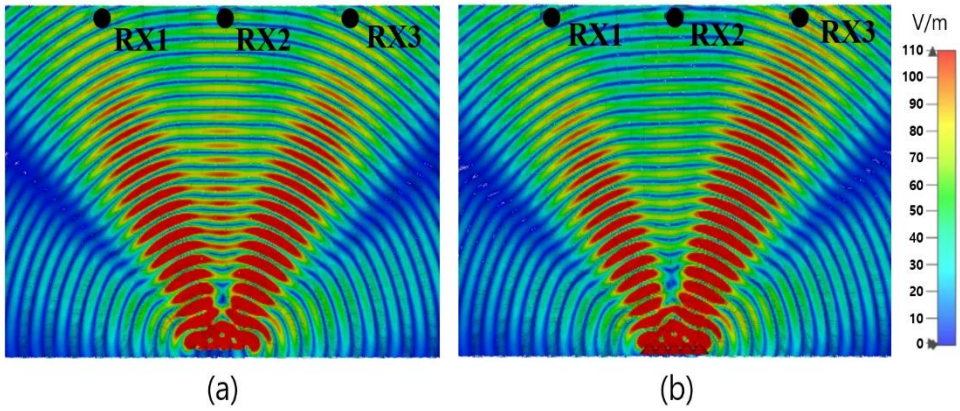

Fig. 3. 5. Electric field distribution of scenario 2 on the y = 0 mm plane considering the optimization (OPT) technique with the received power ratios (RPRs) of (a) 1:1:1 and (b) 1:1:2.

one beam with a smaller E-field magnitude targeted receiver 2. However, as receiver 2 was placed between receivers 1 and 3, it was also charged by the two beams that targeted receivers 1 and 3. When the RPR was 1:1:2, the beam of receiver 3 was larger than that of receiver 1. Based on the results of the scenario with three receivers, we validated that the OPT technique improves the performance of MPT for multiple receivers.

3.5 Summary

In this chapter, we developed an efficient MPT method capable of charging multiple receivers using a convex optimization algorithm. The optimization problem was formulated to maximize the PTE based on the constraint of charging multiple receivers with the desired RPR. We transformed the initial optimization problem into a CVP. Additionally, a 5 × 5 rectangular patch array antenna and patch element antenna operating at 10 GHz were designed as the transmitter and receiver, respectively. The MPT system was simulated using CST Microwave Studio and CVX. We considered multiple scenarios with three receivers arranged in linear and triangular positions. The E-field distribution was analyzed to verify the multi-beamforming of the MPT system. The performance parameters, such as the power received at each receiver and the PTE of the OPT, were compared with those of the multi-receiver TR technique considering several scenarios with three receivers. We determined that the actual RPR was equal to the desired RPR in each scenario when the OPT technique was used. By contrast, the multi-receiver TR technique failed to ensure the desired RPR. Therefore, we validated that the OPT technique achieves a greater PTE than the multi-receiver TR technique. Furthermore, the E-field distribution indicates that the receivers are charged by multibeam. Consequently, the proposed OPT technique was verified

to be superior to the multi-receiver TR technique in terms of power transmission to multiple receivers. The obtained results can aid in designing improved MPT and mmWave WPT systems.

3.6 Reference

[1] A. Costanzo and D. Masotti, "Smart Solutions in Smart Spaces: Getting the Most from Far-Field Wireless Power Transfer," in IEEE Microwave Magazine, vol. 17, no. 5, pp. 30-45, May 2016.

[2] B. Clerckx, A. Costanzo, A. Georgiadis and N. Borges Carvalho, "Toward 1G Mobile Power Networks: RF, Signal, and System Designs to Make Smart Objects Autonomous," in IEEE Microwave Magazine, vol. 19, no. 6, pp. 69-82, Sept.-Oct. 2018.

[3] W. Tang, Q. Zhu, J. Yang, D. Song, M. Su and R. Zou, "Simultaneous 3-D Wireless Power Transfer to Multiple Moving Devices With Different Power Demands," in IEEE Transactions on Power Electronics, vol. 35, no. 5, pp. 4533-4546, May 2020.

[4] K. Lee and H. -H. Choi, "Fast Wireless Power Transfer for Multiple Receivers in Linear Topology," in IEEE Systems Journal, vol. 14, no. 1, pp. 649-652, March 2020.

[5] H. Oh et al., "Mid-Range Wireless Power Transfer System for Various Types of Multiple Receivers Using Power Customized Resonator," in IEEE Access, vol. 9, pp. 45230-45241, 2021.

[6] J. Kim, D. -H. Kim and Y. -J. Park, "Free-Positioning Wireless Power Transfer to Multiple Devices Using a Planar Transmitting Coil and Switchable Impedance Matching Networks," in IEEE Transactions on Microwave Theory and Techniques, vol. 64, no. 11, pp. 3714-3722, Nov. 2016.

[7] K. Murata et al., "Efficient energy beamforming for multi-device microwave wireless power transfer under Tx/Rx power constraints," 2017 IEEE 28th Annual International Symposium on Personal, Indoor, and Mobile Radio Communications (PIMRC), 2017.

[8] Z. Feng, B. Clerckx and Y. Zhao, "Waveform and Beamforming Design for Intelligent Reflecting Surface Aided Wireless Power Transfer: Single-User and Multi-User Solutions," in IEEE Transactions on Wireless Communications, vol. 21, no. 7, pp. 5346-5361, July 2022.

[9] B. Clerckx and E. Bayguzina, "Waveform Design for Wireless Power Transfer," in IEEE Transactions on Signal Processing, vol. 64, no. 23, pp. 6313-6328, 1 Dec.1, 2016.

[10] Z. B. Zawawi, Y. Huang and B. Clerckx, "Multiuser Wirelessly Powered Backscatter Communications: Nonlinearity, Waveform Design, and SINR-Energy Tradeoff," in IEEE Transactions on Wireless Communications, vol. 18, no. 1, pp. 241-253, Jan. 2019.

[11] Z. Tang, X. Wang, X. Cao, M. Li, B. Ruan and M. Lu, "Microwave Power Transmission to Multiple Targets Simultaneously with Multibeam Forming," 2019 Photonics & Electromagnetics Research Symposium - Fall (PIERS - Fall), Xiamen, China, 2019, pp. 2831-2835.

[12] W. Hong et al., "Multibeam Antenna Technologies for 5G Wireless Communications," in IEEE Transactions on Antennas and Propagation, vol. 65, no. 12, pp. 6231-6249, Dec. 2017.

[13] D. Belo, D. C. Ribeiro, P. Pinho and N. Borges Carvalho, "A Selective, Tracking, and Power Adaptive Far-Field Wireless Power Transfer System," in IEEE Transactions on Microwave Theory and Techniques, vol. 67, no. 9, pp. 3856-3866, Sept. 2019.

[14] W. Geyi, Foundations of Applied Electrodynamics. New York, NY, USA: Wiley, 2010.

[15] X. Cai, X. Gu and W. Geyi, "Optimal Design of Antenna Arrays Focused on Multiple Targets," in IEEE Transactions on Antennas and Propagation, vol. 68, no. 6, pp. 4593-4603, June 2020.

[16] H. Y. Kim and S. Nam, "Optimization of Microwave Wireless Power Transmission with Specific Absorption Rate Constraint for Human Safety," in IEEE Transactions on Antennas and Propagation, vol. 68, no. 11, pp. 7721-7726, Nov. 2020.

[17] S. Boyd and L. Vandenberghe, Convex Optimization. Cambridge, U.K.: Cambridge Univ. Press, 2013.

[18] R. J. Duffin and E. L. Peterson, “Geometric programming with signomials,” J. Optim. Theory Appl., vol. 11, no. 1, pp. 3–35, Jan. 1973.

[19] C. S. Beightler and D. T. Phillips, Applied Geometric Programming. Hoboken, NJ, USA: Wiley, 1976.

[20] M. Grant, S. Boyd, and Y. Ye. (2015). CVX: MATLAB Software for Dis-ciplined Convex Programming. [Online]. Available: http://cvxr.com/cvx/M. Young, The Technical Writer's Handbook. Mill Valley, CA: University Science, 1989

Chapter 4. Efficiency Bound Estimation Algorithm of Practical Microwave Wireless Power Transmission System

4.1 Motivation

Recently, in conjunction with improvement in communication technologies, such as 5G and 6G, microwave and mmWave wireless power transmission (MPT) has attracted significant attention from academia and industries for powering widespread electronic devices and sensors in homes and offices [1], [2].

The MPT system consists of a power source connected to a transmitter (Tx) antenna system, a wireless channel, a receiver (Rx) antenna system, and a rectifier circuit that provides DC power to the electronics [3]. To develop the MPT system, the DC-to-RF conversion efficiency of the power source, power transfer efficiency (PTE) from Tx antenna to Rx antenna, RF-to-DC conversion efficiency and DC-to-DC conversion efficiency must be considered. For improving RF-to-DC conversion efficiency, the rectennas have been actively studied [4-8]. Especially, the enhancement method of PTE has been studied in various scenarios [9], [10]. An algorithm to maximize the PTE for charging multiple Rx was proposed using the optimization problem [9]. The convex optimization algorithm for exciting Tx antennas of a microwave

WPT system that transfers maximum power under a specific absorption rate constraint for human safety was developed [10].

The prior knowledge on the accurate upper bound of PTE for a given Tx and Rx antenna array is essential to successful design of an MPT system: the number of antennas and the element spacing of Tx and Rx array antenna should be properly determined in the initial stage of system design. In this study, the PTE bound is defined as the maximum PTE. Many studies have attempted to calculate the PTE of inductive and resonance WPT [11], [12] and MPT [13]–[18] systems: Goubau and Shinohara showed that a Gaussian beam is an optimal transmission source between two planar apertures, especially in the radiative near-field, and they calculated the PTE using the proposed theory [13], [14]. The PTE bound of the radiative WPT was derived for the aperture Tx and a practical mobile antenna [15]. In these studies, the PTE bound is calculated by continuous source of Tx, assuming that the Tx is an aperture antenna and Rx is an aperture or single antenna.

In practical MPT, the Tx and Rx use array antennas which have discrete element antennas. Therefore, an effective method for calculating the PTE bound of the array antennas is needed to design practical MPT systems. Recently, a rough upper bound of PTE was obtained by assuming that signals received by Rx element is added in-phase and Rx elements' power can be maximized simultaneously and combined [16]. Other research groups proposed methods to calculate the maximum PTE using scattering

parameter [17], [18]. The PTE can be calculated accurately if a full EM simulator is used to obtain the scattering parameters between the Tx and Rx of the MPT system. However, the size of the simulation space is limited by the available computer memory capacity and the simulation time is very long. It is the case especially for mmWave WPT because the number of array antennas increases to hundreds [1] and the electrical size increases significantly.

Therefore, we propose the PTE bound estimation method considering practical array antennas and estimating channels in the MPT system without computational burden. The convex optimization problem (CVP) is used to estimate the maximum PTE of an MPT system, which can be used as the upper bound of the power received at Rx under limited transmit power. A CVP is known to guarantee the existence of global optimum [19]. For the proposed CVP, channel state information (CSI) is estimated using Friis transmission equation and active element pattern (AEP) of the array antenna. The PTE bound is obtained by inputting the estimated CSI to the proposed CVP. This method is applied to MPT system with Tx and Rx composed of patch array antennas operating at 10 and 24 GHz. The PTE bounds are investigated by varying the distance and tilted angle between Tx and Rx antennas. The required computation time for the methods is also presented. The numerical results are compared to those obtained by previous studies. We obtained the PTE bound more accurately and faster

compared with the previous researches by using CSI obtained by AEP and the Friis equation in the proposed convex optimization process.

4.2 Efficiency Bound Calculation Algorithm Formulation

4.2.1 MPT system Model and Estimation of Channel State Information

We consider an MPT system in which a Tx and a Rx are array antennas operating at microwave and mmWave frequencies, as shown in Fig. 4. 1. The Tx and Rx arrays are square arrays as usual [1] and consist of ${N_t}^2$ and ${N_r}^2$ antennas where N_t and N_r are the number of elements per one side of Tx and Rx, respectively. In general, the edge effect that the radiation of edge element differs from that of center element is occurred in finite array. However, in the case of an array antenna consisting of hundreds of antennas, the edge effect is quite small in the radiation characteristics of the array because the ratio of the number of edge element to the total element is small enough to ignore the edge effect. For example, if the size of array antenna is 16x16, the ratio is 14%. In this study, since Tx and Rx are assumed to be large arrays, the edge effect can be ignored and the AEP can be used for the calculation of the CSI. By using the AEP, the magnitude and phase of CSI can be determined in closed form. In the far-field region of each element of Tx and Rx, the magnitude of CSI is calculated from Friis

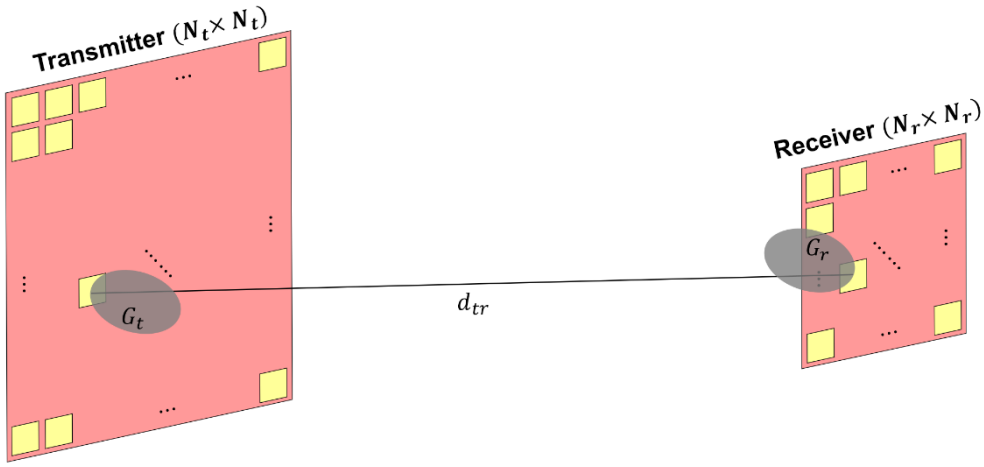

Fig. 4. 1. MPT system consisting of a transmitter and a receiver with array antenna.

transmission equation between element t of the Tx and element r of the Rx array, as follows

$$c_{tr\_far} = \sqrt{G_t(\theta_t, \varphi_t) G_r(\theta_r, \varphi_r)} \frac{\lambda}{4\pi d_{tr}} \qquad (4-1)$$

where $G_t(\theta_t, \varphi_t)$ and $G_r(\theta_r, \varphi_r)$ are the gain of the elements in angles θ and φ with respect to the Tx and Rx normal planes, respectively, λ is wavelength of operating frequency, and d_{tr} is the distance between those elements. The magnitude of CSI in the near-field is expressed as [13]

$$c_{tr\_near} = \sqrt{1 - \exp(-\tau^2)} \qquad (4-2)$$

where $\tau^2 = A_t A_r \cos\theta_t \cos\theta_r / (\lambda d_{tr})^2$, A_t and A_r are the aperture area of elements of Tx and Rx. $\cos\theta_t$ and $\cos\theta_r$ are contained in τ^2 to consider angles θ and φ with respect to the Tx and Rx normal planes. The phase of CSI is calculated by converting the distance between each element to phase terms, as follows $\phi = 2\pi d_{tr}/\lambda$. The PTE results obtained using the estimated CSI and the actual CSI are compared in section 4.4.3. In this study, the actual CSI is defined as a scattering parameter between Tx and Rx elements obtained through full-EM simulation.

4.2.2 Optimization Problem Formulation

Let the transmit signal be denoted by $x_t \in \mathbb{C}^{N_t^2 \times 1}$, and $\mathbf{S} = x_t x_t^H$, where sub-script H denotes the conjugate transpose. Let the CSI matrix between each element of Tx and Rx be noted by $\mathbf{C} \in \mathbb{C}^{N_t^2 \times N_r^2}$ where $\mathbf{C}$ is calculated using the method proposed in section A. The sum of power received by each element can be expressed as $P_R(\mathbf{S}) = \|\mathbf{C}x_t\|^2 = \mathrm{tr}(\mathbf{C}^H \mathbf{C}\mathbf{S})$ [6].

The objective of the optimization is to maximize the power received at the Rx under the transmit power constraint which exists across all Tx antennas denoted by $\|x_t\|^2 = \mathrm{tr}(\mathbf{S}) \leq P_t$, where P_t is the limited transmit power of the MPT system. The aforementioned design problem can be formulated as

$$\max \quad \mathrm{tr}(\mathbf{C}^H\mathbf{C}\mathbf{S}) \tag{4-3}$$

$$\text{subject to} \quad \mathrm{tr}(\mathbf{S}) \leq P_t \tag{4-4}$$

To convert the optimization problem (4−3)−(4−4) to CVP, we use the equivalent problem using epigraph form and adding transmit signal constraint, i.e.,

$$\max \quad P_r \tag{4-5}$$

$$\text{subject to} \quad \mathrm{tr}(\mathbf{C}^H\mathbf{C}\mathbf{S}) \geq P_r \tag{4-6}$$

$$\mathrm{tr}(\mathbf{S}) \leq P_t \tag{4-7}$$

$$\mathbf{S} \succcurlyeq 0. \tag{4-8}$$

The optimization problem (4−5)−(4−8) is a semidefinite program (SDP) [17] and CVP. Therefore, it can be solved by CVX [20]. Eq. (4−8) means that $\mathbf{S}$ is semidefinite. It can be said that the transmitted power is constant in this optimization problem because inequality (4−7) always satisfies equality condition when the optimization problem is solved completely. The proposed optimization problem maximizes the total received power with constant transmitted power, hence it is considered a problem of maximizing the PTE. The maximum efficiency of the MPT system can be obtained using estimated CSI and the proposed optimization problem. In this study, the PTE under the condition of the MPT system is defined as P_r/P_t.

We executed the PTE bound estimation method using the following process. First, we determined the specifications of the MPT system. Then, we designed the element of the array antenna and obtained A EP. The CSI was estimated using the designed element antenna, distance between Tx and Rx and tilted angle of Rx relative to broadside of Tx. Finally, the estimated CSI was fed to CVP (4-5)-(4-8), and we can obtain the PTE bound using the calculated maximum PTE.

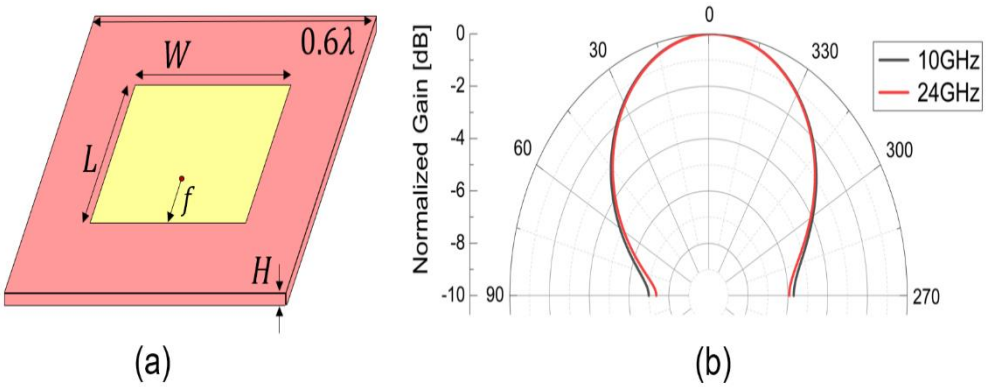

Fig. 4. 2. (a) Unit cell element of the patch antenna array with designed parameter and (b) its normalized gain of active element pattern.

TABLE 4. 1. Parameters of the Unit Cell Element

Parameter	W (mm)	L (mm)	f (mm)	H (mm)
10 GHz	11.5	9.59	2.10	0.50
24 GHz	4.78	3.95	1.00	0.25

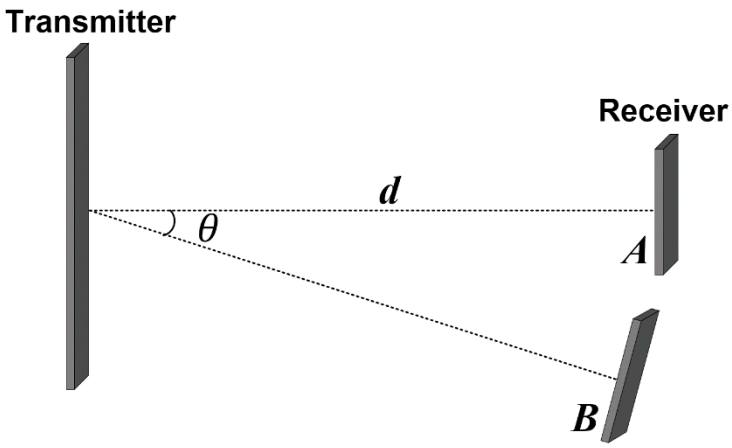

Fig. 4. 3. Simulation scenarios A and B of MPT system. In all cases, the receiver is facing the center of the transmitter. The positions of A and B are varied with distance d and angle **θ**, respectively.

4.3 Numerical Results

In this section, we provide simulation results to validate the proposed method. The MPT system consisting of a Tx and a Rx which are square array antennas was considered as shown in Fig. 4. 1. The AEP was obtained by using unit cell simulation of the CST Microwave Studio. The element antenna was microstrip patch antenna operating at 10 and 24 GHz, designed on a Taconic TLY−5 dielectric substrate with a relative permittivity of e=2.2, loss tangent of 0.00009, and the length of one side of 0.6 wavelength, as shown in Fig. 4. 2. The design parameters of the patch element for each operating frequency are listed in Table 4. 1. The gains of element antennas were calculated by AEP as shown in Fig. 4. 2. The PTE results of the proposed method were obtained by using MATLAB and CVX.

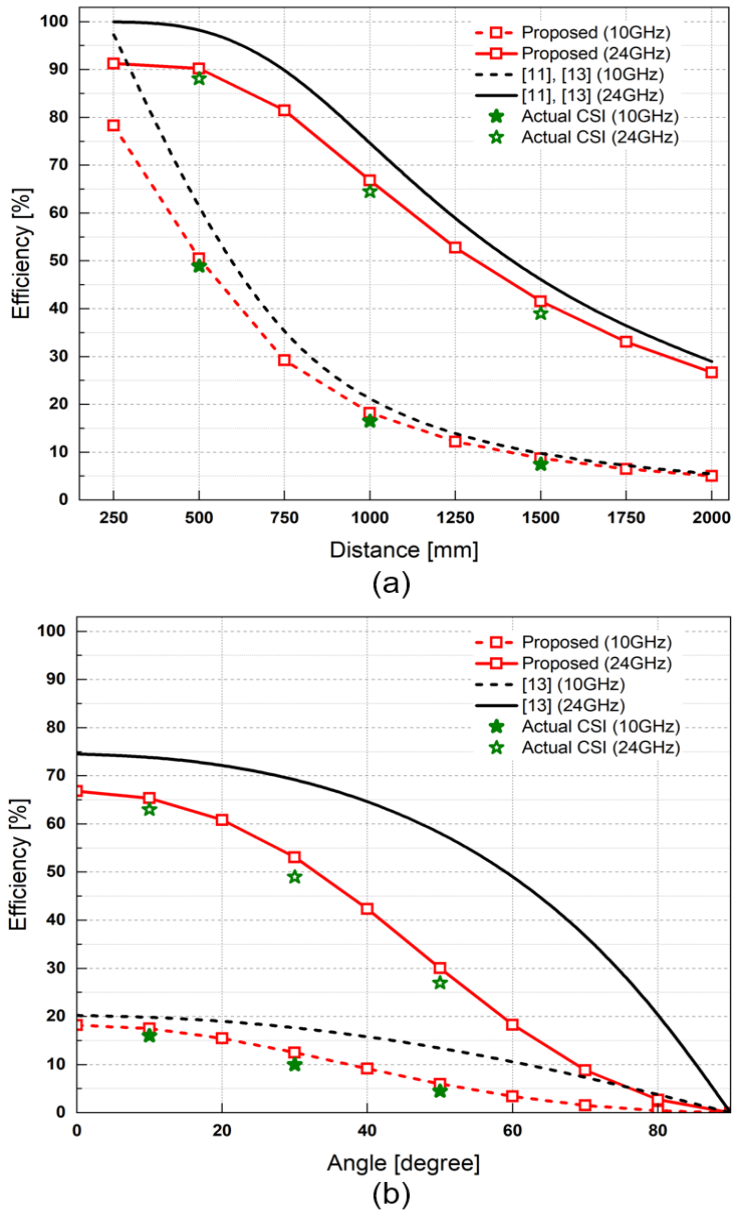

Fig. 4. 4. Comparison of the PTE bounds of the practical array antennas with operating frequencies of 10 (dashed line) and 24 GHz (solid line). The hollow symbols indicate the calculated points by proposed method using the estimated (square). The PTEs are calculated by the actual CSI (star) at 10 (solid) and 24 GHz (hollow). The proposed method is compared to [14] and [16]. The number of (Tx, Rx) elements are (11 x 11, 4 x 4) and (26 x 26, 10 x 10) at 10 and 24 GHz, respectively, under the condition of fixed physical size. (a) PTE bounds according to the distance between Tx and Rx when facing each other on the broadside. (b) PTE bounds according to the tilted angle of Rx relative to the broadside of Tx when distance is fixed to 1 m.

4.3.1 Power Transfer Efficiency Variation with Distance

The distance *d* between the Tx and Rx was varied under the condition of fixed physical sizes of Tx and Rx, as shown in Fig. 4. 3. These were fixed to 0.15 x 0.15 m and 0.06 x 0.06 m, respectively. The number of the antenna elements in the array was set according to physical size, spacing between elements, and operating frequency. As we designed the single element antenna structure with the size of 0.6 wavelength, the number of (Tx, Rx) elements were determined as (11 x 11, 4 x 4) and (26 x 26, 10 x 10) at 10 and 24GHz, respectively. The PTE bound of the proposed method was compared to those of [14] and [16], as shown in Fig. 4. 4.

We calculated the PTE bound using actual CSI over 500 mm intervals to validate our study. For obtaining the actual CSIs, the entire MPT system shown in Fig. 4. 1 was simulated by the time-domain solver of CST Microwave Studio running on the acceleration computer with two NVIDIA Tesla V100-PCIE-32GB GPUs. Even with GPU acceleration tokens, it required 121 hours to obtain three points (500, 1000 and 1500 mm) in the case of 24 GHz, whereas the estimated CSI was obtained in 5 minutes. The estimated CSIs were calculated by MATLAB with Tx and Rx parameters such as the number of element antennas, spacing and active element pattern. The time to obtain AEP using a full-EM simulation is less than 2 minutes.

The computation time for the actual CSI was significantly large because the electrical size of the MPT system was enormous in mmWave and the full-EM simulation was iterated the same number of times as that of the Rx elements.

We can observe that the PTEs calculated using the proposed method are in good agreement with those using the actual CSI. The error between PTEs of actual and estimated CSI is defined as $(\mathrm{PTE}_{\mathrm{estimated\ CSI}} - \mathrm{PTE}_{\mathrm{actual\ CSI}})/\mathrm{PTE}_{\mathrm{actual\ CSI}}$. The average errors of 10GHz and 24 GHz are 5% and 3.9%. These results demonstrate that the proposed method accurately reflects the practical MPT system. The small discrepancy between the results using the proposed CSI and actual CSI occurs owing to the limited number of the mesh cell in the EM simulation and the difference between the AEPs and the actual radiation pattern of the antenna elements in finite array. More than 2.4 billion of FDTD mesh cells are required to obtain accurate actual CSI in the 24 GHz scenario. However, the number of mesh cells that can be simulated is limited to 2.4 billion. Therefore, we reduced this even if the actual CSI accuracy is lower.

The PTE bounds of [14] and [16] are equal and show the maximum upper bound. As we mentioned in introduction, Tx and Rx were apertures in [14] and the powers received at Rx elements were independently maximized in [16]. It means that the PTE bound was roughly calculated as the largest value. The PTE bound of the proposed method is lower than that of [14] and [16] in the entire region. At distance of 1m and frequency of 24 GHz, the PTEs of the

proposed method and [14] are 66.8% and 74.6%, respectively. It means that PTE bound of [14] is larger than that of proposed method by 11.6% ratio. At distance of 1m and frequency of 10 GHz, the PTEs of the proposed method and [14] are 20.2% and 18.2%, respectively. It means that PTE bound of [14] is larger than that of proposed method by 10.9% ratio. As the distance increases, the PTE bound of the proposed method and that of [14] and [16] become closer since the beam focusing by the optimization algorithm becomes the same as the conventional beamforming using a transmit signal of the same magnitude and phase.

The result shows that the PTEs at 24 GHz are consistently larger than those at 10 GHz. This is because the focusing capability of the array antenna is increasing as the electrical size of the array increases. In the case of the far-field region, the antenna gain is approximately expressed as $4\pi A/\lambda^2$ for an array with a physical size A. Conversely, in the case of the near-field region, the difference between PTEs at 10 and 24 GHz reduces because the distance is close and most transmit power is transferred to Rx in both cases. It is noticeable that the higher the frequency, the larger the PTE for Tx and Rx arrays of same size. This suggests that frequency selection is important to determine the size of Tx and Rx when the desired MPT system specifications such as PTE and range are provided.

4.3.2 Power Transfer Efficiency Variation with Angle

The PTE estimation when Rx is tilted from the broadside of Tx is required for the MPT system design. Therefore, the PTE was calculated according to the tilted angle θ of Rx at the fixed distance of 1 m from the Tx as shown in Fig. 4. 4. The physical sizes and number of Tx and Rx elements were the same as subsection *A*. The PTE bounds of [14] are the most upper bound as with the results in the previous section. At angle of 50° and frequency of 24 GHz, the PTEs of the proposed method and [14] are 58.5 and 30%, respectively. It means that PTE bound of [14] is larger than that of proposed method by 95% ratio. The PTEs using the proposed method agrees well with those using the actual CSI. These results indicate that the proposed method can provide tighter PTE bound than other methods and can be applied to the design of practical MPT systems.

The greater the tilted angle of Rx, the lower the PTE at 10 and 24 GHz. This is because the element gain of RX is lower when the tilted angle is greater. In the case of 24 GHz, the total computation times to obtain three points (10, 30 and 50°) using the actual and estimated CSI were 151 h and 5 m, respectively. This demonstrates that the proposed method can be used to obtain the PTE bound accurately with much smaller time than other methods.

4.4 Summary

In this study, we proposed an efficient PTE bound estimation method for practical MPT system design with minimal computational burden. The maximum PTE of MPT system was obtained using the estimated CSI and the proposed CVP. For a fast and accurate PTE bound calculation, CSI was estimated by Friis transmission equation and AEP of array antenna under the assumption that Tx and Rx are large arrays. The proposed CVP was formulated to maximize received power under the transmit power constraint; therefore, the proposed CVP can maximize the PTE of MPT system. For an MPT system operating at 10 and 24 GHz, we calculated the PTE bound using the proposed method and compared it with those obtained by previous methods. The PTE bounds were obtained by varying the distance and tilted angle between Tx and Rx antennas. Analyzing the results according to the distance, it was found that the PTE bound obtained by the previous method was on average 10% larger than that of the proposed method using actual CSI. In addition, we showed that the PTE bound using the estimated CSI was on average 3.9% larger than that using the actual CSI obtained by the full EM simulation. The simulation time obtaining PTE of the proposed estimation method is several thousand times shorter than that of previous methods. Therefore, the proposed optimization method for

obtaining PTE using CSI estimation method is accurate and significantly shortens the overall simulation time of the WPT system. It is expected that the proposed method can be applied to determine the design parameters of the MPT system such as the number of element antennas and the spacing between the element antennas of Tx and Rx.

4.5 Reference

[1] M. Wagih, A. S. Weddell and S. Beeby, "Millimeter-Wave Power Harvesting: A Review," in IEEE Open Journal of Antennas and Propagation, vol. 1, pp. 560-578, 2020.

[2] U. Gustavsson et al., "Implementation Challenges and Opportunities in Beyond-5G and 6G Communication," in IEEE Journal of Microwaves, vol. 1, no. 1, pp. 86-100, winter 2021.

[3] A. Costanzo and D. Masotti, "Smart Solutions in Smart Spaces: Getting the Most from Far-Field Wireless Power Transfer," in IEEE Microwave Magazine, vol. 17, no. 5, pp. 30-45, May 2016.

[4] B. T. Malik, V. Doychinov, A. M. Hayajneh, S. A. R. Zaidi, I. D. Robertson and N. Somjit, "Wireless Power Transfer System for Battery-Less Sensor Nodes," in IEEE Access, vol. 8, pp. 95878-95887, 2020.

[5] M. Fairouz and M. A. Saed, " A Complete System of Wireless Power Transfer Using a Circularly Polarized Retrodirective Array," in Journal of Electromagnetic Engineering and Science, vol. 20(2), pp. 139-144, April. 2020.

[6] S. A. Rotenberg, S. K. Podilchak, P. D. H. Re, C. Mateo-Segura, G. Goussetis and J. Lee, "Efficient Rectifier for Wireless Power Transmission Systems," in IEEE Transactions on Microwave Theory and Techniques, vol. 68, no. 5, pp. 1921-1932, May 2020.

[7] P. Lu, K. Huang, Y. Yang, B. Zhang, F. Cheng and C. Song,

"Space Matching for Highly Efficient Microwave Wireless Power Transmission Systems: Theory, Prototype, and Experiments," in IEEE Transactions on Microwave Theory and Techniques, vol. 69, no. 3, pp. 1985−1998, March 2021.

[8] A. Eid, J. G. D. Hester, J. Costantine, Y. Tawk, A. H. Ramadan and M. M. Tentzeris, "A Compact Source–Load Agnostic Flexible Rectenna Topology for IoT Devices," in IEEE Transactions on Antennas and Propagation, vol. 68, no. 4, pp. 2621−2629, April 2020.

[9] R. Zhang and C. K. Ho, "MIMO Broadcasting for Simultaneous Wireless Information and Power Transfer," in IEEE Transactions on Wireless Communications, vol. 12, no. 5, pp. 1989−2001, May 2013.

[10] H. Y. Kim and S. Nam, "Optimization of Microwave Wireless Power Transmission With Specific Absorption Rate Constraint for Human Safety," in IEEE Transactions on Antennas and Propagation, vol. 68, no. 11, pp. 7721−7726, Nov. 2020.

[11] E. S. Lee, B. G. Choi, M. Y. Kim and S. H. Han, "Optimal Number of Turns Design of the IPT Coils for Laptop Wireless Charging," in IEEE Access, vol. 9, pp. 19548−19561, 2021.

[12] X. Dang, P. Jayathurathnage, S. A. Tretyakov and C. R. Simovski, "Self−Tuning Multi−Transmitter Wireless Power Transfer to Freely Positioned Receivers," in IEEE Access, vol. 8, pp. 119940−119950, 2020

[13] N. Shinohara, “Power without wires,” IEEE Microw. Mag.,

vol. 12, no. 7, pp. S64–S73, Dec. 2011.

[14] G. Goubau, “Microwave power transmission from an orbiting solar power station,” J. Microw. Power, vol. 5, no. 4, pp. 223–231, 1970.

[15] J. H. Kim, Y. Lim and S. Nam, "Efficiency Bound of Radiative Wireless Power Transmission Using Practical Antennas," in IEEE Transactions on Antennas and Propagation, vol. 67, no. 8, pp. 5750−5755, Aug. 2019

[16] A. Hajimiri, B. Abiri, F. Bohn, M. Gal−Katziri and M. H. Manohara, "Dynamic Focusing of Large Arrays for Wireless Power Transfer and Beyond," in IEEE Journal of Solid−State Circuits, vol. 56, no. 7, pp. 2077−2101, July 2021.

[17] W. Geyi, Foundations of Applied Electrodynamics. New York, NY, USA: Wiley, 2010.

[18] J. H. Park, D. I. Kim and K. W. Choi, "Analysis and Experiment on Multi−Antenna−to−Multi−Antenna RF Wireless Power Transfer," in IEEE Access, vol. 9, pp. 2018−2031, 2021.

[19] S. Boyd and L. Vandenberghe, Convex Optimization. Cambridge, U.K.: Cambridge Univ. Press, 2013.

[20] M. Grant, S. Boyd, and Y. Ye. (2015). CVX: MATLAB Software for Dis−ciplined Convex Programming. [Online]. Available: http://cvxr.com/cvx/

Chapter 5. Hybrid Beamfocusing Architecture and Algorithm in Practical Microwave Wireless Power Transmission System

5.1 Motivation

(MPT) is not limited by the location of the receiver and can charge at a long distance compared with inductive coupling and resonance wireless power transmission. Additionally, it can charge multiple receivers and considers human effects [1,2]. Therefore, the MPT technology has attracted significant attention for charging many electronic devices and sensors in industries and conferences [3-7].

In MPT, many studies to maximize power transmission efficiency (PTE) are underway. The overall PTE of an MPT system depends on several efficiencies, such as power source to TX antenna, TX to RX antenna, and RX antenna to received DC power [8,9]. We investigated the optimization of the PTE of the RF power source to the RX antenna part (RF-PTE). We considered RF signals to maximize the PTE of the MPT system. The methods to determine the optimal signal to transmit maximum power to a receiver include a method using a known channel response and feedback. The optimal magnitude and phase of the transmit signal were obtained using optimization techniques and eigenvalue decomposition in the

5.8 GHz MPT system using known channel response [10,11]. However, a study that utilizes a feedback algorithm exists. The optimal amplitude and phase of the transmit signal were obtained by transmitting orthogonal matrices with different phases from the transmitter and then feeding back the received power from the receiver to the transmitter. An experiment was conducted by manufacturing an MPT system operating at 10 GHz with a phase array antenna size of a transmitter of 20 x 20 [12]. A beam scanning algorithm that utilizes an iterative method to obtain the optimal phase of the transmit signal was proposed. A 5.8 GHz MPT system that comprises 64 transmit antennas and 16 receive antennas was presented [13]. In these studies on MPT, the signal was transmitted by controlling only the phase of the transmit signal or simultaneously controlling the amplitude and phase.

Theoretically, the phase and magnitude of the RF signal applied to each antenna of the transmitter must be controlled to maximize RF-PTE. However, the implementation of the MPT system is limited in terms of cost and complexity when the operating frequency is increased. For example, a transmit array antenna that operates at 24 GHz with a side length of 20 cm (16 wavelengths) and an element spacing of 0.5 wavelengths exists. One thousand and twenty-four antennas exist and the number of amplitude controllers and phase shifters that must be connected to each antenna is 1024. Comparing the case of the MPT with that of the phase-only change, an additional 1024 magnitude controllers must

be inserted. The amplitude controllers and phase shifters are expensive at high frequencies because they are active RF components. Therefore, the power consumption and cost of the entire system are significantly increased.

The PTE is not maximum when only the phase of the transmit signal is controlled. However, it is advantageous in terms of price and system complexity because it does not require components that control amplitude. Additionally, the number of variables is small; thus, less time is required to determine the optimal signal value in practical MPT systems. Consequently, this study aims to determine an algorithm to design an efficient MPT system with low price, low complexity, and high PTE. Therefore, we apply the hybrid beamforming used in communication to the MPT.

In communication, studies on hybrid beamforming, which combines the advantages of analog and digital beamforming, are underway [14−18]. Hybrid beamforming is advantageous in terms of price and system complexity. It can achieve performance close to digital beamforming using fewer RF chains compared with the number of transmit antennas. Generally, the optimal hybrid beamforming architecture is obtained by creating an optimization problem that maximizes spectral efficiency. Hybrid beamforming is divided into two types, partially−connected and fully−connected hybrid beamforming depending on the architecture. The spectral efficiency of the latter has the maximum value [19].

This study applies the concept of hybrid beamforming used in

communication to MPT. In MPT, the receiver is often located in the radiative near field of the transmitter; therefore, the optimal transmit signal at each antenna has a different phase and magnitude for the power to be focused on the receiver. We define the proposed MPT scheme as hybrid beamfocusing (HBF). We propose an optimization algorithm to determine the optimal magnitude and phase required for each phase shifter and magnitude controller of the HBF architecture. The optimal RF signal to be transmitted from each antenna for maximum PTE is obtained using the convex optimization problem [8]. The phase and magnitude of the HBF architecture are obtained by comparing the optimal signal obtained in [8] with the transmit signal in the HBF architecture to minimize the difference. This problem is resolved by dividing the HBF architecture into partially and fully-connected cases. The proposed algorithm was applied to various scenarios of wireless power transmission systems operating at 10 GHz and simulated. The performance of HBF was derived. In the given scenarios, the simulation was performed by varying the number of magnitude controllers. Moreover, a partially-connected HBF with fewer magnitude controllers can achieve performance close to the optimal PTE. Further, we propose a subarray beamfocusing architecture to effectively reduce the price, complexity, and computational load of the system. Additionally, we validated the algorithm by applying the proposed algorithm to an MPT system operating at 5.8 GHz.

5.2 Optimization Problem Formulation

5.2.1 Fully−digital Beamfocusing architecture

This section provides a brief overview of the fully−digital beamfocusing architecture, which can be used as a comparative reference for HBF. In the case of a fully−digital beamfocusing structure, each antenna of the transmitter is connected to a phase shifter and amplitude controller, allowing the amplitude and phase of the signal transmitted from all antennas to be flexibly controlled based on the channel, as shown in Fig. 5. 1 (a).

We assumed an MPT scenario in which the transmitter and receivers each comprised square planar array antennas. The transmitter and receiver are composed of N_t and N_a antennas, respectively. The received voltage on the receiving antenna can be obtained as $V_R(\mathbf{S}) = \sum_{n=0}^{N-1} \hbar_n s_n = \mathbf{H}^T\mathbf{S}$ with $\mathbf{H} = [\hbar_0, \hbar_1 \cdots \hbar_{N-1}]^T$, where $\hbar_n = A_n e^{j\phi_n}$ is the channel response between the $n-th$ transmitting antenna and the receiver. A_n and ϕ_n are the amplitude and phase of the channel response, respectively. The phase and amplitude of the optimal transmit signal can be obtained using the convex optimization problem proposed in [8].

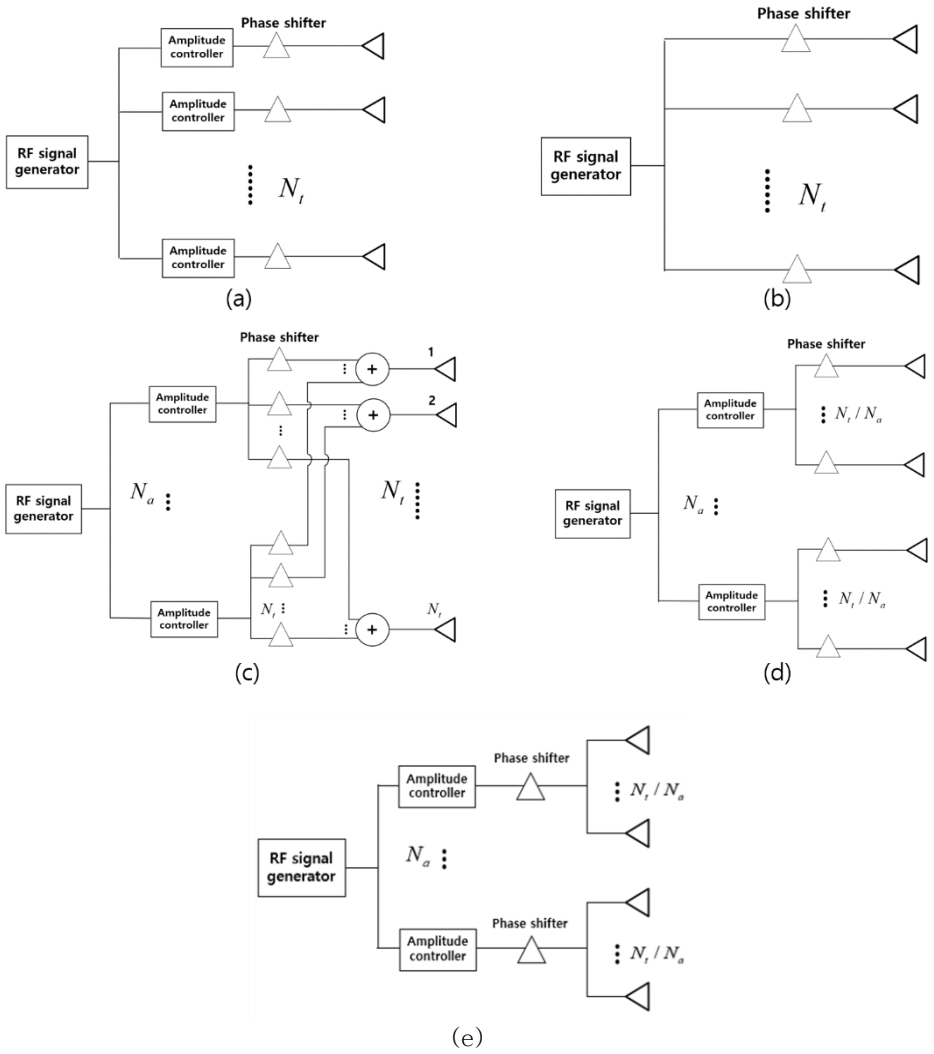

Fig. 5. 1. Architectures of the MPT system using hybrid beamfocusing. (a) Fully digital beamfocusing, (b) Analog beamfocusing (c) Fully-connected beamfocusing (d) Partially-connected beamfocusing (e) Subarray beamfocusing

5.2.2 Hybrid Beamfocusing Architecture

In a fully connected HBF architecture, each amplitude controller is connected to all antennas; thus, the N_t RF transmitted signals are summed using a power combiner at each antenna, as shown in Fig. 5.

1 (c). In a partially−connect HBF architecture, each N_a amplitude controller is connected to an N_t/N_a number of subarrays, as shown in Fig. 5. 1 (d). The number of amplitude controllers N_a is set to a divisor of N_t such that the ratio N_t/N_a is an integer. The structure of phase shifters in the HBF architecture is known as analog beam−focusers instead of analog beam−formers used in a phased array.

Here, we propose an optimization problem to obtain the coefficient values of an amplitude controller and a phase shifter that achieve the maximum RF−PTE with the proposed HBF architecture for a given MPT scenario. The RF signal applied by the analog beam−focuser, which is the output signal of the magnitude controller is defined as $\mathbf{x}_{\boldsymbol{RF}} = [x_1, x_2 \cdots x_{N_{RF}}]^T$, where $x_n = v_n e^{j\psi_n}$ is the output signal of the n−th amplitude controller. v_n and ψ_n are the amplitude and phase of the signal, respectively. The final optimal values of $\mathbf{x}_{\boldsymbol{RF}}$ are real and complex numbers in the case of Fig. 5. 1 (b)−(d) and Fig. 5. 1 (e), respectively. The analog beam−focuser is an $N_t \times N_a$ matrix and is defined differently depending on whether it is partially or fully−connected. In the case of a fully−connected architecture, the values of the matrix elements are complex numbers with a magnitude of 1 with an arbitrary phase. In the case of a partially−connected architecture, the matrix is expressed as follows:

$$\mathbf{A}_p = \begin{bmatrix} \mathbf{p}_1 & \mathbf{0} & \cdots & \mathbf{0} \\ \mathbf{0} & \mathbf{p}_2 & & \mathbf{0} \\ \vdots & & \ddots & \vdots \\ \mathbf{0} & \mathbf{0} & \cdots & \mathbf{p}_{N_a} \end{bmatrix} \tag{5-1}$$

where $\mathbf{p}_i = \left[\exp\left(j\phi_{(i-1)\frac{N_t}{N_a}+1}\right), \ldots, \exp\left(j\phi_{i\frac{N_t}{N_a}}\right)\right]^T$. The transmit signal from the transmit antenna is expressed as $L_{RF}\mathbf{A}\mathbf{x}_{RF}$ by multiplying $\mathbf{x}_{RF}$ by the analog beamfocusing matrix A and the loss caused by the RF component. L_{RF} is the RF power loss caused in RF components, such as an RF power splitter and combiner. This study defines the phenomenon in which the power of the RF signal is divided into N-ways; thus, the power decreases to one-nth in each RF path as RF loss by the RF power splitter. RF loss by the RF power combiner denotes a decrease in power caused by different phases and amplitudes of RF input signals. L_{RF} is expressed as $\sqrt{N_a/N_t}$ and $1/\sqrt{N_a N_t}$ in the partially and fully-connected cases, respectively. L_{RF} is RF signal loss coefficient regardless of the phase and magnitude of the power combiner input signal and is applied to output signal of amplitude controller. No RF loss was assumed, except for the RF power combiner and splitter. A loss was assumed in the amplitude controller and phase shifter; however, the loss of each product differs and can be compensated for by calibration. The received signal in the receiver is expressed as $L_{RF}\mathbf{H}\mathbf{A}\mathbf{x}_{RF}$ by multiplying a signal

transmitted from the transmit antenna by a channel response characteristic. H is the $N_r \times N_t$ channel response. An optimization problem to maximize the receive power and RF−PTE is as follows.

$$\max \quad \mathrm{P} = |L_{RF}\mathbf{HAx}_{\boldsymbol{RF}}|^2 \tag{5−2}$$

$$\text{subject to} \quad \text{condition of} \quad (\mathbf{A})_{i,j}, \forall i, j \tag{5−3}$$

$$\mathbf{x}_{\boldsymbol{RF}}{}^{H}\mathbf{x}_{\boldsymbol{RF}} \leq P \tag{5−4}$$

Equation (5−2) is an objective function representing the RF power received from a receiver. Equation (5−3) is a condition of matrix A according to the type of HBF architecture, such as partially−connected and fully−connected HBF. Equation (5−4) is a constraint function to limit the RF transmit power. The aforementioned optimization problem is a multiple variable optimization problem and the element−wise constraints of A; thus, jointly optimizing these two variables is highly complicated. A solution can be obtained with an alternating minimization algorithm that decouples the optimization problem of these two variables [20]. As a principle of alternating minimization, we alternatively solve for $\mathbf{x}_{\boldsymbol{RF}}$ and A while fixing the others.

Therefore, first, the optimal value $\boldsymbol{y}_{\boldsymbol{opt}}$ to be transmitted from each antenna is obtained using the method proposed in [8]. That is, an optimal transmission signal when the fully−digital beamfocusing is obtained. The optimal value of the HBF can be obtained through a

novel optimization problem that minimizes the difference in magnitude between the transmit signal of HBF and $\boldsymbol{y_{opt}}$. Therefore, we propose the objective function of the optimization problem as the square of 2−norm of the difference between the two transmission signals:

$$\min \quad |L_{RF}\mathbf{A}\mathbf{x}_{\boldsymbol{RF}} - \boldsymbol{y}_{OPT}|_2^2 \ , \tag{5-5}$$

$$\text{subject to} \quad (\mathbf{A})_{i,j}, \forall i, j \ \text{ depending on architecture} \tag{5-6}$$

$$\mathbf{x}_{\boldsymbol{RF}}{}^H \mathbf{x}_{\boldsymbol{RF}} \leq P \tag{5-7}$$

This optimization problem can be solved using the constraint least square problem if A is fixed; $\mathbf{x}_{\boldsymbol{RF}}$ can be obtained. An initial condition of all components of $\mathbf{x}_{\boldsymbol{RF}}$ are set to 1. In case of partially−connected, non−zero components of A are set to 1. In case of fully−connected, all components of A are set to 1. The constraint least square problem is a convex optimization problem; thus, it is solved using MATLAB and CVX [21]. The A structure is defined depending on HBF architectures; A of the partially−connected and fully−connected are block diagonal and full matrix, respectively. However, the method for solving problem is the same. Conversely, provided $\mathbf{x}_{\boldsymbol{RF}}$ is fixed, A is obtained by a closed form. Therefore, we update A and $\mathbf{x}_{\boldsymbol{RF}}$ alternatively until the solution of the optimization problem converges and solve the two problems to obtain the optimal solution. Generally, the solution converges after 3 iterations. A is solved differently when

$\mathbf{x}_{RF}$ is fixed depending on the A structure and the detailed process is as follows.

First, in the fully-connected case, Equation (5-5) expressed as follows.

$$\min \quad \sum_{i=1}^{N_t} \left| L_{RF}\left(\sum_{j=1}^{N_a} a_{i,j} x_{RF,j}\right) - y_{opt,i} \right|^2 \qquad (5-8)$$

$a_{i,j}$ is the component of matrix A with a complex number of magnitude 1. Each term according to i in the first sigma of Equation (5-8) is independent. Additionally, variables L_{RF}, $x_{RF,j}$, and $y_{opt,i}$ excluding $a_{i,j}$ are fixed values. Therefore, $a_{i,j}$ that minimizes $\left| L_{RF}\left(\sum_{j=1}^{N_a} a_{i,j} x_{RF,j}\right) - y_{opt,i} \right|^2$ can be obtained. $a_{i,j}$ is a complex number with a magnitude of 1, expressed as $e^{j\phi_{i,j}}$. Hence, $x_{RF,j} = \alpha_j e^{j\theta_j}$ and $y_{opt,i} = \beta_i e^{j\psi_i}$ are defined. Substituting the symbols defined in the expression in the first sigma of Equation (5-8), we obtained:

$$\min \quad \left| L_{RF}\left(\sum_{j=1}^{N_a} \alpha_j e^{j(\phi_{i,j}+\theta_j)}\right) - \beta_i e^{j\psi_i} \right|^2. \qquad (5-9)$$

The methods to minimize this expression are divided into two cases. First, in the case of $L_{RF}\sum_{j=1}^{N_a} \alpha_j < \beta_i$, Equation (5-9) cannot be equated to zero. Therefore, the phase of the first and second terms should be the same, resulting in a considerably small value. The phase value to satisfy the condition is $\phi_{i,j} = \psi_i - \theta_j$. In the case

of $L_{RF}\sum_{j=1}^{N_a}\alpha_j \geq \beta_i$, using the trigonometric formula, Expression (5-9) can be equated to zero. Consider two complex numbers, $a_i e^{j\Phi_{i,1}}$ and $b_i e^{j\Phi_{i,2}}$, with magnitudes of $a_i = L_{RF}\alpha_1$ and $b_i = L_{RF}\sum_{j=2}^{N_a}\alpha_j$. Suppose $\Phi_{i,1} = \phi_{i,1} + \theta_1$ and $\Phi_{i,2} = \phi_{i,2} + \theta_2 = \cdots = \phi_{i,N_a} + \theta_{N_a}$. In that case, the phases of two complex numbers can be determined for their sum to be $\beta_i e^{j\psi_i}$. Thus, the phase difference between $a_i e^{j\Phi_{i,1}}$ and $b_i e^{j\Phi_{i,2}}$ is determined using the triangular formula as $\omega_i = \cos^{-1}\left[\frac{\beta_i^2 - a_i^2 - b_i^2}{2a_i b_i}\right]$.

Therefore, $a_i e^{j\Phi_{i,1}} + b_i e^{j\Phi_{i,2}}$ can be expressed as $(a_i + b_i e^{j\omega_i})e^{j\tau_i}$. τ_i that satisfies $(a_i + b_i e^{j\omega_i})e^{j\tau_i} = \beta_i e^{j\psi_i}$ is $\psi_i - \gamma_i$, where $\gamma_i = \cos^{-1}\left[\frac{a_i^2 + \beta_i^2 - b_i^2}{2a_i\beta_i}\right]$. Consequently, $\phi_{i,1} = \psi_i - \gamma_i - \theta_1$, $\phi_{i,j} = \omega_i + \psi_i - \gamma_i - \theta_j$, $j = 2 \ldots N_{RF}$ are obtained.

In the case of a partially-connected architecture, **A** in Equation (5-1) is substituted into Equation (5) and developed as follows.

$$\min \quad \sum_{i=1}^{N_t}\left|L_{RF}x_{RF,l}e^{j\phi_i} - y_{opt,i}\right|^2 \qquad (5-10)$$

l is defined as the quotient of i/N_a. To minimize the value of (5-10) when the value of $x_{RF,l}$ is fixed, the value of each term must be minimized because each term in sigma is independent. Thus, the phase of $L_{RF}x_{RF,l}e^{j\phi_i}$ and $y_{opt,i}$ must be equal. Therefore, the optimal phase of partially-connected architecture is obtained as $\phi_i = \psi_i - \theta_l$.

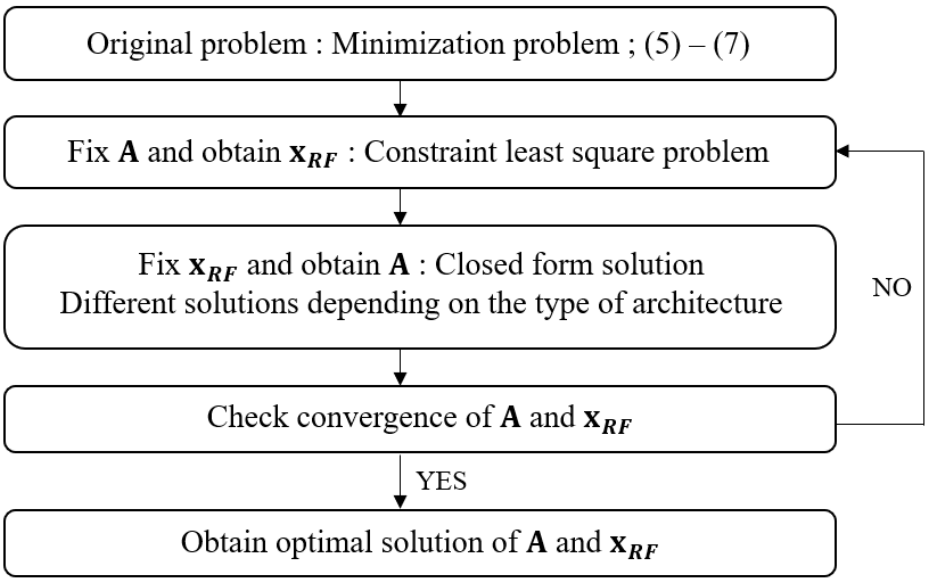

Fig. 5. 2. Flowchart of the proposed iterative minimization problem.

The process of solving the proposed optimization problem is shown in Fig. 5. 2. In an analog beamfocusing architecture, an RF signal generator is connected to N_t transmit antennas, as shown in Fig. 5. 1 (b). The solution of analog beamfocusing is obtained when $\mathbf{x}_{RF}$ is 1 in the partially−connected architecture. Finally, A which represents the phase of the transmit signal is obtained. In a subarray beamfocusing architecture, the various N_a amplitude controllers and phase shifters are connected to N_t/N_a number of subarrays, as shown in Fig. 5. 1 (e). The solution of subarray beamfocusing is obtained when the components of A are given as 1 in the partially−connected architecture. Finally, the vector $\mathbf{x}_{RF}$ composed of complex number is obtained.

5.3 Numerical Results

5.3.1 Power Transfer Efficiency Variation with Distance

In this section, the maximum RF-PTE of fully-digital beamfocusing, analog beamfocusing, and broadside beamforming was calculated and compared when the size of the transmitter and receiver antenna was fixed and the distance between the transmitter and receiver was varied. As shown in Fig. 5. 3, it is a scenario in which the transmitter and receiver face each other. The maximum RF-PTE of fully-digital beamfocusing was calculated using the algorithm proposed in [8] in MATLAB and CVX. Analog beamfocusing is the case in which each antenna signal is the same amplitude and the phase is controlled. Broadside beamforming is the case in the broadside direction based on the far field because the amplitude and phase of the transmission signal of each antenna are the same. Suppose a channel is given between the transmitter and receiver. In that case, the calculation is simple.

The transmitter and receiver are square patch array antennas operating at 10 GHz and the distance between element antennas is 0.6 wavelength. The antenna was designed using CST microwave studio. The active element pattern was obtained using the designed element antenna, the channel between the transmitter and the receiver was obtained, and the RF-PTE was calculated using

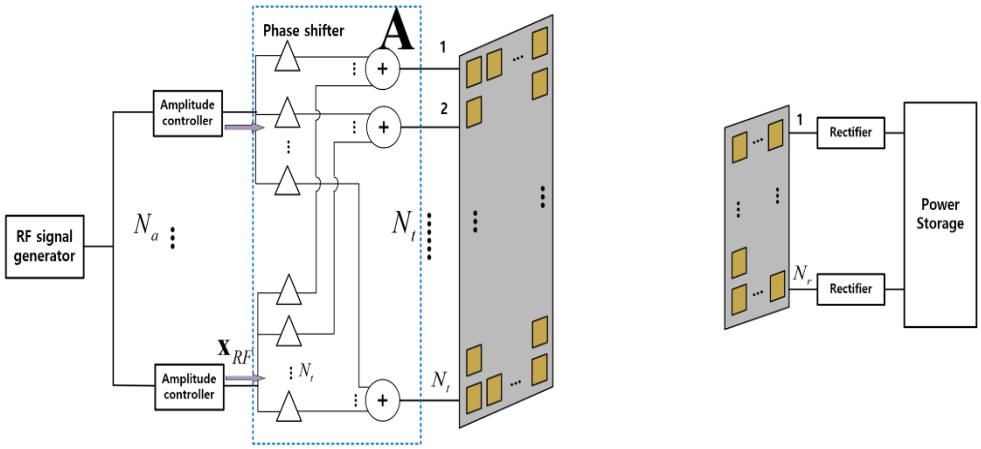

Fig. 5. 3. MPT system scenario comprising a transmitter and a receiver with an array antenna when the transmitter and the receiver face each other.

MATLAB. The rectangular patch antenna is a coaxially fed microstrip patch antenna designed on a Taconic TLY-5 dielectric substrate with a relative dielectric constant of e=2.2, loss tangent of 0.00009, and a dimension of 11.5 mm × 9.59 mm. The dimension of the transmitter array antenna is 16 × 16. The dimensions of the receiver array antenna are 8 × 8 and 12 ×12. The RF-PTE for each case when the distance between the transmitter and the receiver is increased from 0.1 to 2 m in 0.1 m increments is shown in Fig. 5. 4.

Overall, the RF-PTE decreases in the order of fully-digital beamfocusing, analog beamfocusing, and broadside beamforming. Full-digital beamfocusing has a high degree of freedom because it can both control the size and phase of signals transmitted from the

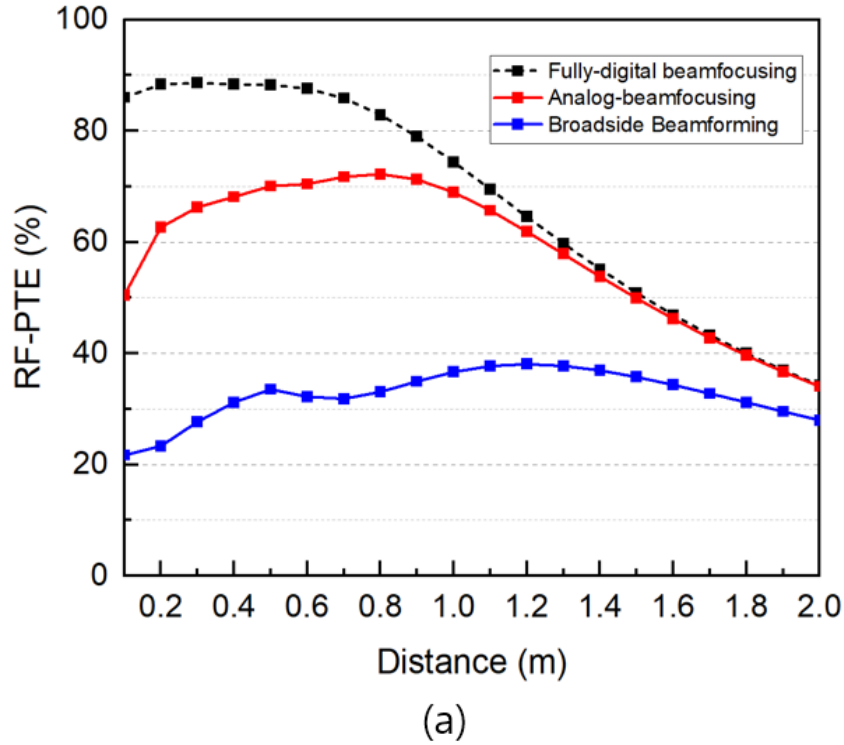

(a)

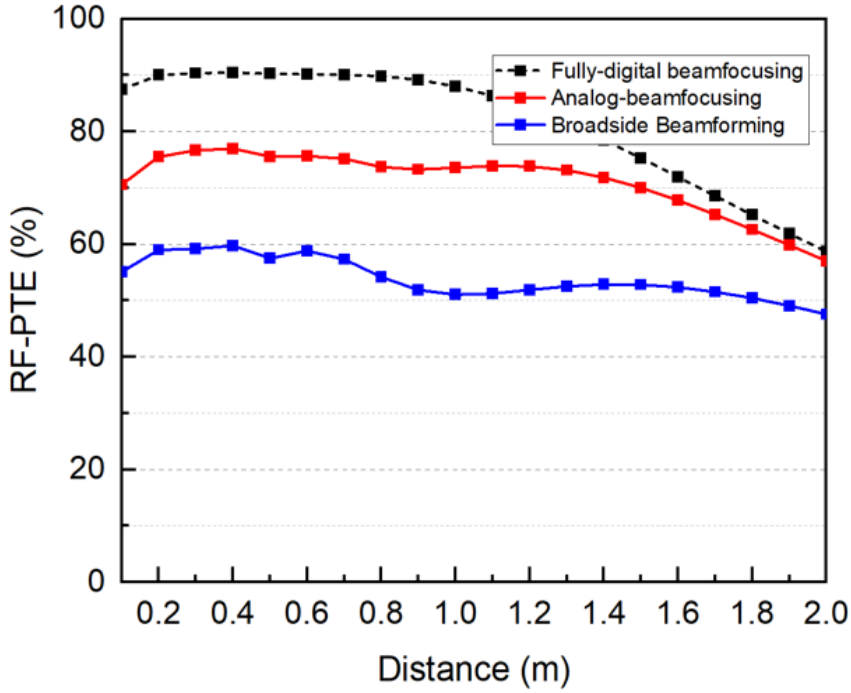

(b)

Fig. 5. 4. The PTE with 16x16 transmitter when the distance between the transmitter and the receiver is increased from 0.1 m to 2 m in increments of 0.1m. (a) RX : 8x8 (b) RX : 12x12

antenna. Therefore, when the location of the receiver is close, the RF-PTE can be increased by increasing the RF-PTE magnitude of the signal transmitted from the antenna in the middle and reducing the size of the edge. Conversely, analog beamfocusing is limited in terms of increasing efficiency by controlling only the phase when the location of the receiver is close. Therefore, a large difference in efficiency exists between the two methods when the receiver's position is close. Broadside beamforming is the best method of transmitting power in that direction provided the receiver is located in the far field of the transmitter. However, suppose the receiver is present in the near field or radial near field. In that case, it is disadvantageous for power transmission. For example, suppose the size of the receiver is 12 × 12 and the distance is 1 m, compared with RF-PTE, full-digital beamfocusing is 88% and analog beamfocusing is 73%, whereas broadside beamforming is only 51%. Currently, MPT uses frequencies above 10 GHz to increase efficiency under transmitter conditions with limited physical sizes; thus, far field is far away. In the case of a 16 × 16 patch array antenna, operating at a frequency of 10 GHz assumed in this study, the far-field reference is 5.5 m. Therefore, MPT is limited in the beamforming method.

As the distance increases, the difference in the efficiency between full-digital and analog beamfocusing decreases. Suppose the receiver is 8 × 8. In that case, a 0.8% difference exists at 1.6 m. Suppose the receiver is 12 × 12. In that case, a 1.6% difference

exists at 2 m. This is because the difference in the channel magnitude between antennas is insignificant as the distance increases. Therefore, suppose only the phase is controlled without controlling the amplitude of the transmission signal of each antenna. In that case, the difference between the case in which the amplitude and phase are both controlled and the maximum RF−PTE is insignificant.

Comparing (a) and (b), the larger the size of the receiver, the higher the efficiency at the same distance. This is because the RF−PTE increases as the area in which the power can be received increases. Additionally, the larger the receiver, the greater the difference in efficiency between full−digital and analog beamfocusing. The difference in efficiency is 5.4% for 8 × 8 and 14.5% for 12 × 12 at a distance of 1 m. Full−digital beamfocusing allows the receiver antenna to receive a relatively even distribution of power; thus, it can transmit power more effectively when the size of the receiver increases.

When the receiver is 8 × 8, analog beamfocusing RF−PTE decreases as the distance between the transmitter and the receiver decreases to less than 0.8 m. Analog beamfocusing transmits the same amount of power from each antenna and in the case of the element antenna at the edge, the channel amplitude is very small owing to the large angular difference from the receiver. However, in the case of fully−digital beamfocusing, because all the power of the antenna can be controlled, the power of the edge can be reduced and can be focused in the center to increase efficiency. Therefore, analog

beamfocusing and general beamforming are limited in terms of their applications to MPT and RF-PTE should be improved via hybrid beamfocusing. Suppose the receiver is 12 × 12. In that case, the RF-PTE changes by changing the amplitude controller for several scenarios, as undermentioned.

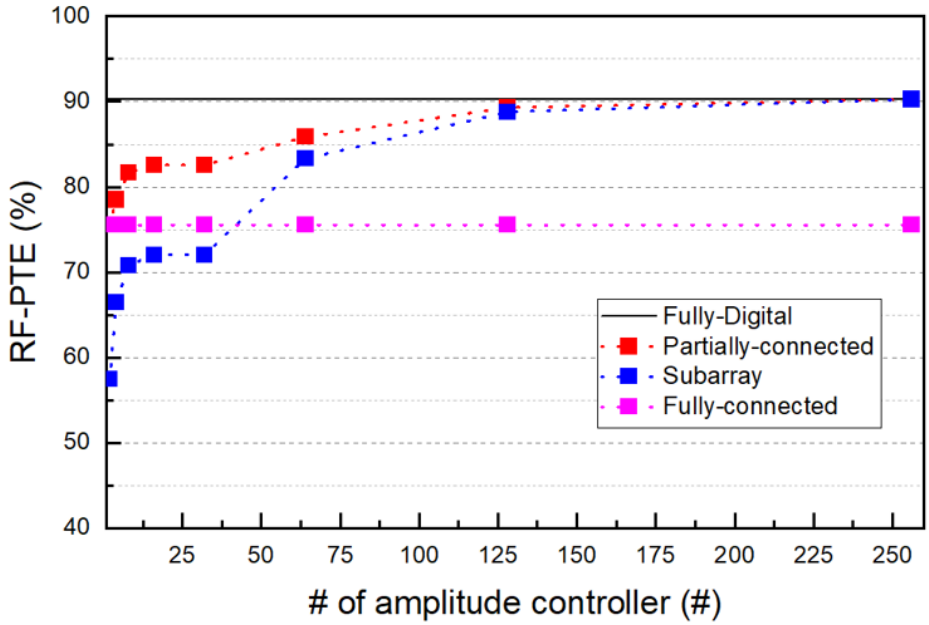

(a)

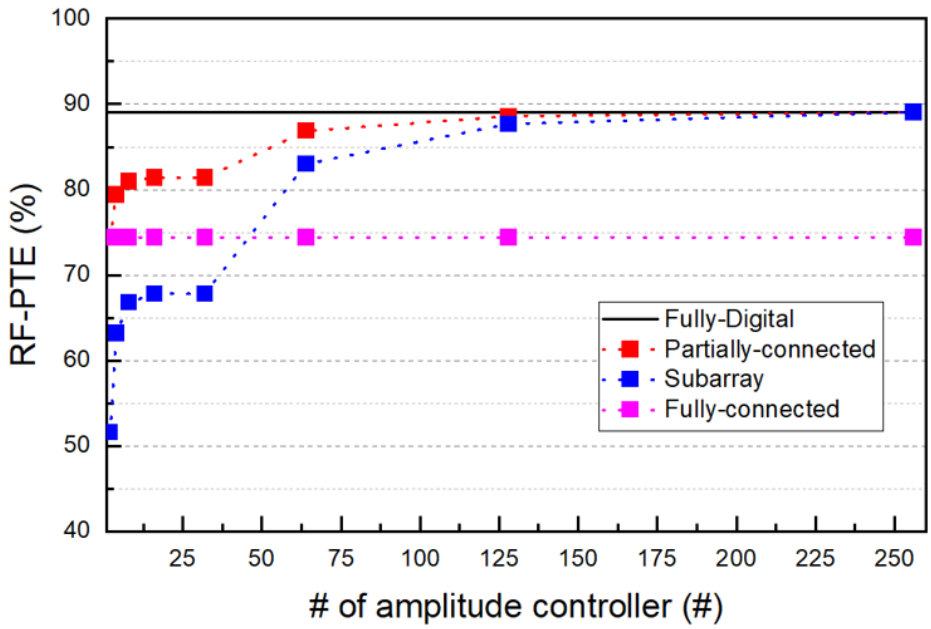

(b)

Fig. 5. 5. Comparison of PTE of hybrid beamfocusings when the number of amplitude controller is increased from 1 to 256. Distance between TX and RX is (a) 0.5m, (b) 1m.

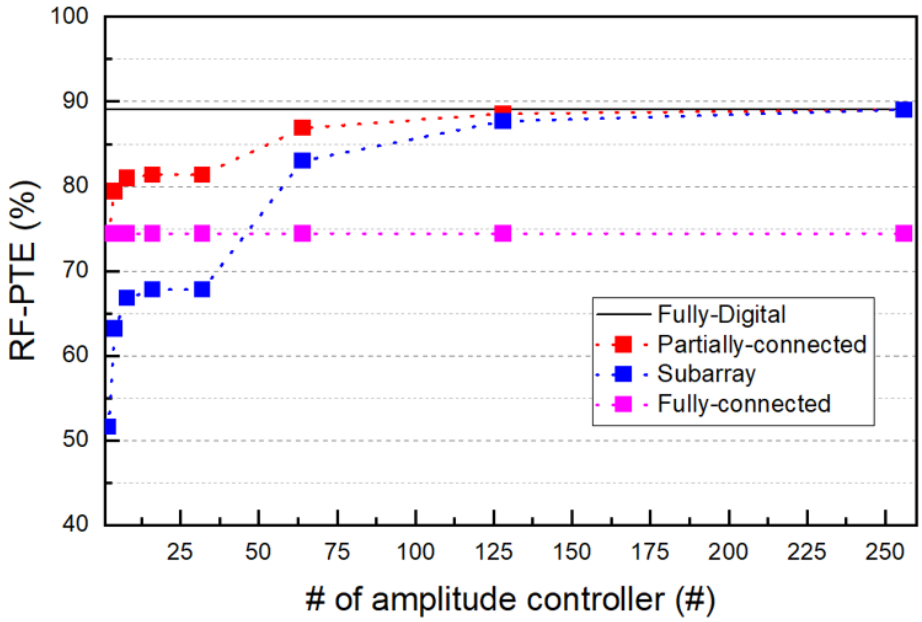

(a)

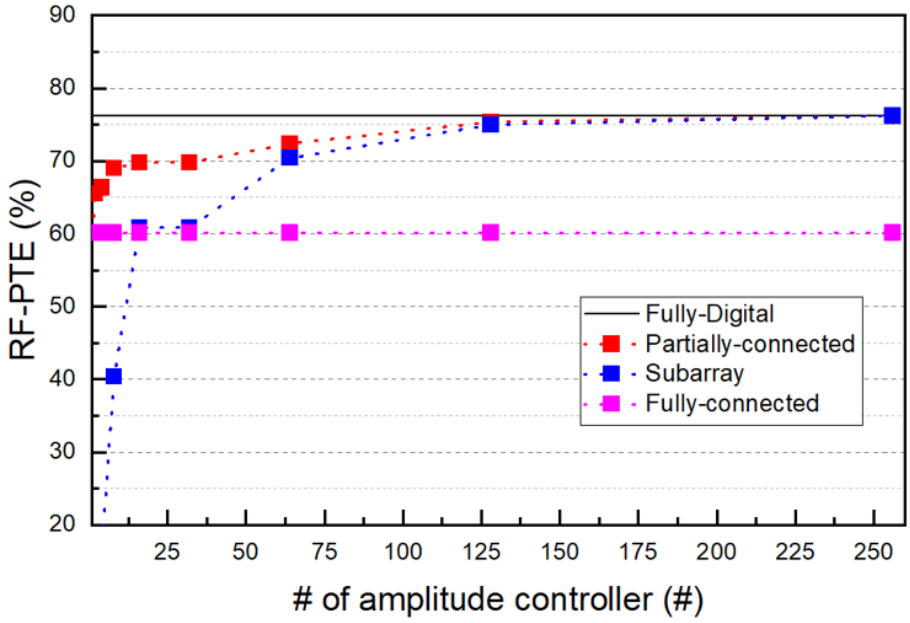

(b)

Fig. 5. 6. Comparison of the RF−PTE of hybrid beamfocusing when the number of amplitude controllers is increased by a power of 2 from 1 to 256. (a) The distance between TX and RX is 0.5 m and the tilted angle is 30 °. (b) Two receivers with a distance of 0.5 m between them, each at a position of 30 ° twisted in opposite directions

5.3.2 Power Transfer Efficiency Variation with Amplitude Controller

In this section, the RF-PTE according to the number of amplitude controllers was compared. Among the aforementioned scenarios, the proposed HBF algorithm was applied to the scenario in which the transmitter was 16 × 16 and the receiver was 12 × 12. We compared the fully-digital beamfocusing, partially-connected, fully-connected, and subarray HBF. The subarray HBF has the same number of phase shifters and amplitude controllers, as shown in Fig. 5. 1 (e). The amplitude and phase of the transmit signal in the common subarray are equal. That is, the number of phase shifters required is the same as the amplitude controller and is reduced compared with that of the partially-connected HBF. For the four scenarios, the number of amplitude controllers is increased by a power of 2, from 1 to 256 and the results of comparing RF-PTE are shown in Figs. 5. 5 and 6. In the first and second scenarios, the receiver is in front of the transmitter and the distance between the two is 0.5 m and 1 m, respectively. In the third scenario, the receiver is located at an angle of 30 ° to the transmitter and the distance between them is 0.5 m; the receiver is facing the center of the transmitter. The last scenario has two receivers, the distance equals 0.5 m at a position of 30 ° twisted in opposite directions.

In fully-connected HBF, the RF-PTE is constant even when the

number of amplitude controllers increases. In a fully-connected structure, the RF power combiner is located in front of each transmit antenna. When RF signals with different amplitudes and phases passing through each phase shifter are combined, RF loss occurs. This results in a smaller RF-PTE. Because RF loss does not occur when signals of the same phase and amplitude are combined in the RF power combiner, the algorithm obtains signals of the same phase and amplitude as the optimal value of fully-connected. That is, the size of each element of $\mathbf{x}_{RF}$ and the phase shifters connected to the amplitude controller are the same regardless of whether the number of amplitude controllers increases. Therefore, the value of the RF-PTE remains unchanged, even if the number of amplitude controllers increases. Conversely, the RF-PTE of partially-connected HBF and subarray HBFs approaches the RF-PTE of the fully digital case as the number of amplitude controllers increases; the value becomes the same when the number of amplitude controllers is 256. Suppose the distance is 1 m. In that case, the RF-PTE values of fully-digital, fully-connected, partially-connected, and subarray with one amplitude controller are 89.0%, 74.4, 74.4%, and 51.6%, respectively. In the case of 64 amplitude controllers, the RF-PTEs of partially-connected and subarray are 86.8% and 83%, respectively. An RF-PTE with an error within 5% of the fully-digital RF-PTE can be achieved on average using the number of transmit antennas and an amplitude controller of 25%.

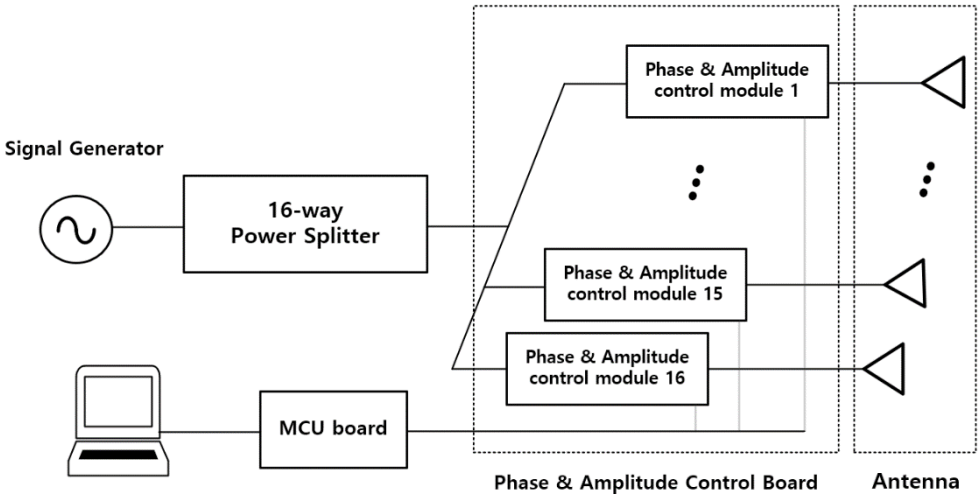

Fig. 5. 7. Block diagram of the proposed testbed transmit system.

5.4 Microwave Wireless Power Transmission System Design and Implementation

This section describes the design, structure, and fabrication of all hardware components in the testbed for experimentation. A block diagram of the proposed testbed transmit system is shown in Fig. 5. 7. The implemented MPT system comprises a 16 × 1 patch array antenna transmitter and a 4 × 1 patch array antenna receiver operating at 5.8 GHz. The transmitter comprises a signal generator, power splitter, phase/amplitude control board, and patch array antenna, each connected using a coaxial cable. First, a power splitter is required to divide the RF power generated by the signal generator into 16 RF paths. The power splitter comprises two 8-way power splitters and one 2-way power splitter, which distributes signals to 16 RF paths. A phase/amplitude control module was required to change the amplitude and phase of the divided signal. In this study, 16 phase/amplitude control modules were used to measure RF-PTE for all cases from 1 to 16 amplitude controllers of the partially-connected HBF. Each module is designed for digital control and comprises a 7-bit true time delay line and a 5-bit commercial attenuator [21]. The true time delay line provides a 360 ° coverage of the phase shift value with a resolution of 16 ° at 5.8 GHz. The smallest controllable unit of the attenuator is 0.5 dB and the largest is 8 dB, which can attenuate an RF power of up to 15.5 dB.

Microstrip patch antennas are used for both transmitters and receivers. We conducted an experiment to validate the HBF algorithm proposed in the scenario; thus, the experiment was conducted using an antenna with a basic structure. The layout of a 4 × 1 antenna array with antenna patch dimensions is shown in Fig. 5. 8. The dimensions of the 16 × 1 antenna array are similar to that of 4 × 1 antenna arrays. The dimensions of the patch are W = 19 mm and L = 16.5 mm. The spacing between the two patch antenna elements and the vertical length of the substrate are L_s = 31 mm and H_s = 62 mm, respectively. The distance between the feeding point and the center of the patch antenna is L_f = 2.9 mm. The antenna was designed with CST Microwave Studio to operate at 5.8 GHz. Based on the simulation results, the 16 × 1 and 4 × 1 array antennas manufactured on the Duroid 5880 board with a thickness of 30 mm, are shown in Fig. 5. 9. The reflection coefficient of each antenna element was measured using a network analyzer and was lower than −15 dB on all ports. The transmitter system and receiver are implemented as shown in Fig. 5. 9. Each patch antenna was fed to the coaxial feed from the back of the board connected to the transmitter and receiver modules via a coaxial cable.

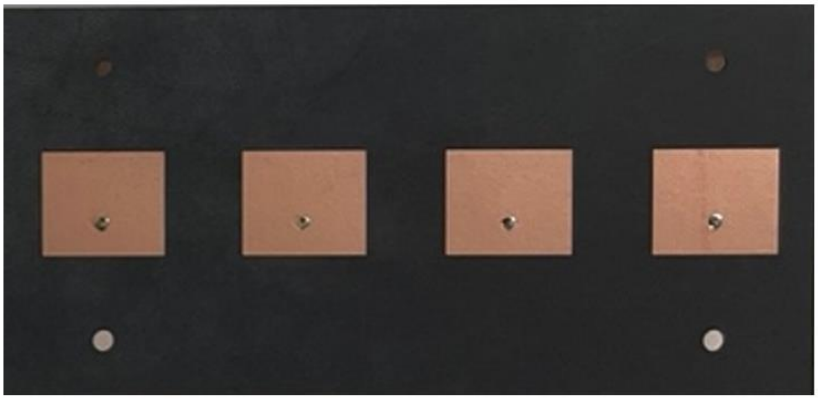

(a)

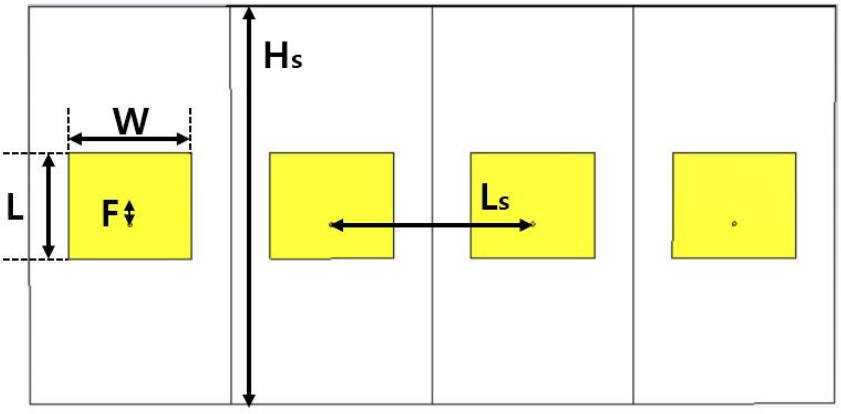

(b)

Fig. 5. 8. (a) Implemented microstrip patch antenna 4x1 (b) Dimension of microstrip patch antenna 4x1

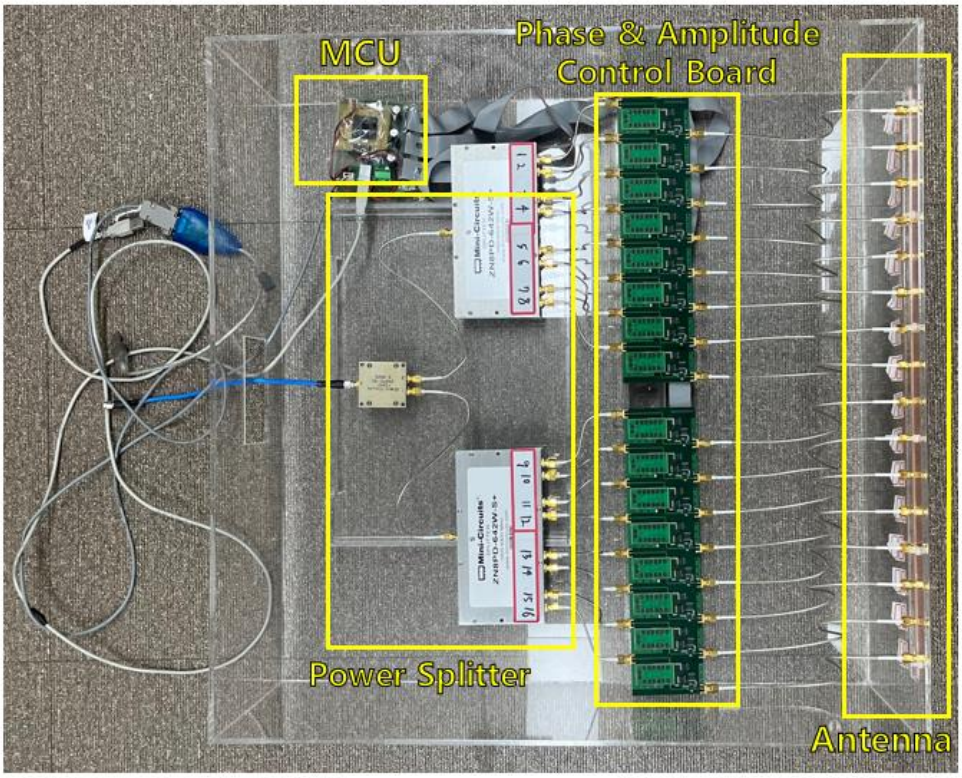

(a)

(b)

Fig. 5.9. (a) Implemented transmit system (b) Implemented receiver

5.5 Experiment Result

The experiment was conducted with an MPT testbed manufactured to validate the feasibility of the algorithm and the experimental results are examined. The experimental setup is shown in Fig. 5. 10. At the transmitter, the signal generator applies the RF signal to the power splitter. Additionally, the micro controller unit (MCU) is connected to the laptop to control the phase and amplitude control board. A vector network analyzer was connected to each receiver antenna to measure a received signal.

First, we measured the s-parameter between the transmitter and the receiver single antenna using a vector network analyzer to obtain a channel response between the transmitter and the receiver. Next, we used the measured channel response in the HBF algorithm and derived each optimal phase and amplitude controller value when the number of amplitude controller changes from 1 to 16 by a power of 2. Finally, we input the derived phase and amplitude to the phase/amplitude control board of the transmitter through the MCU and RF power is transmitted. The RF power received from the receiver was measured using a spectrum analyzer. The RF-PTE was calculated using the measured RF power. The transmit power used in calculating the RF-PTE of the partially-connected HB in the algorithm is only considered a loss by the power splitter. Therefore, the RF loss of the phase/amplitude control module and cable of each of the 16 paths were measured. The commercial attenuator has a

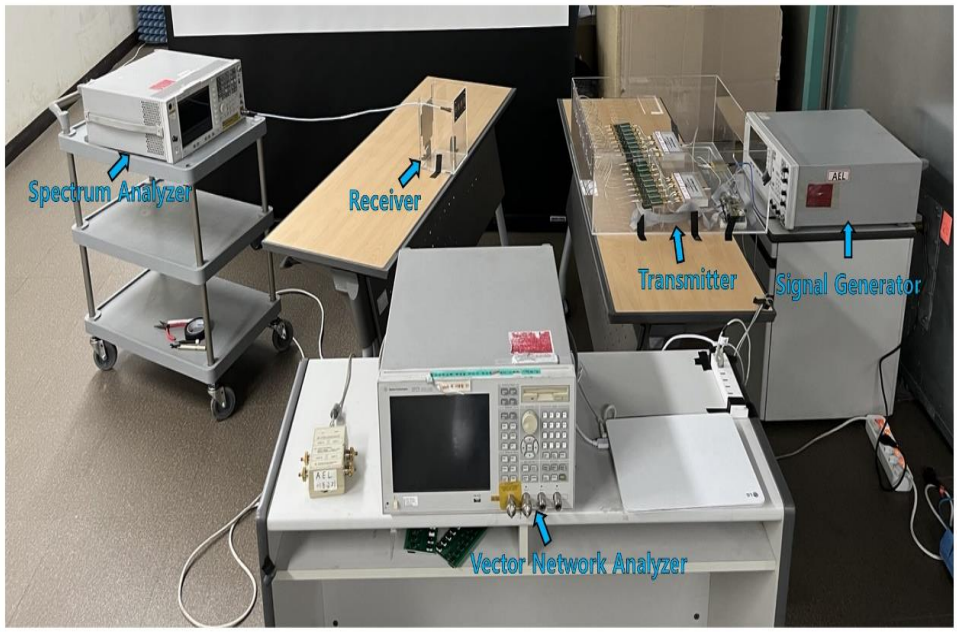

Fig. 5. 10. Experiment setup of the implemented testbed MPT system.

phase difference based on the attenuation state. When the RF-PTE was calculated, the magnitude and phase of RF the signal were calibrated by considering the RF loss and phase difference of the attenuator.

Experiments were conducted on four scenarios. Three scenarios were when the transmitter and receiver were located in front of each other and the distances between them were 0.1, 0.3, and 0.5 m. The fourth scenario was when the two receivers were located 0.2 m from the transmitter and the angle relative to the transmitter was 30 ° and −30 ° , respectively. A graph comparing the RF-PTE of

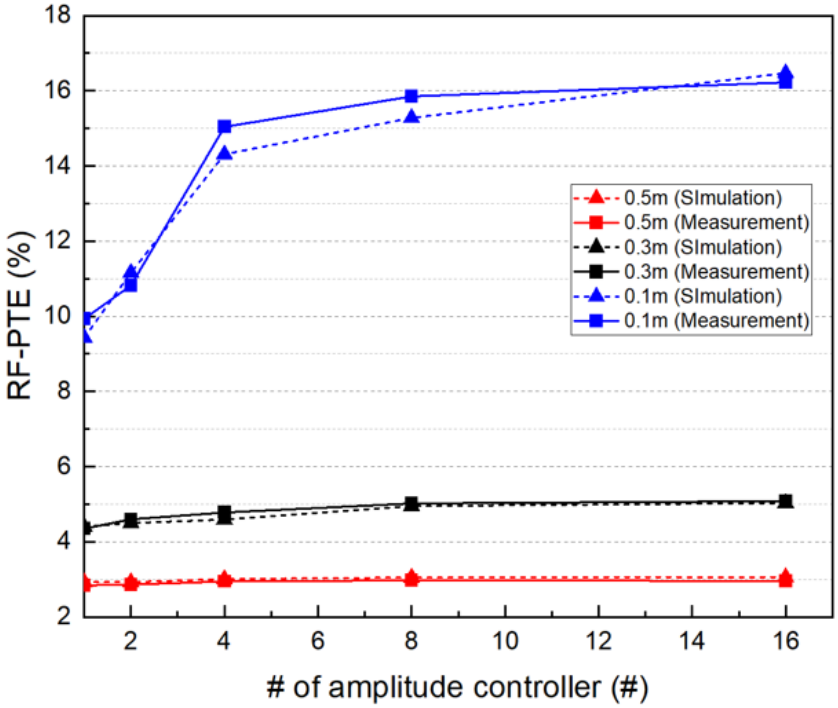

(a)

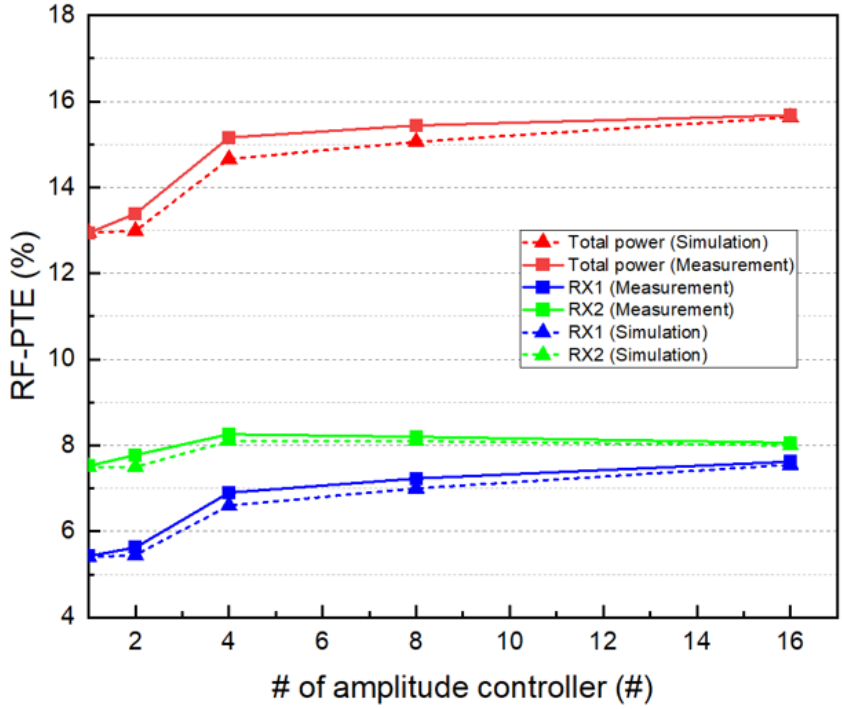

(b)

Fig. 5. 11. Experiment results in case of (a) One receiver (b) Two Receiver

measurement and simulation by varying the number of amplitude controllers from 1 to 16 by powers of 2 for each scenario is shown in Fig. 5. 11.

The simulation and measurement results were in good agreement for all scenarios. Moreover, when the number of amplitude controllers increased, the RF-PTE increased. When the number of amplitude controllers and antennas were the same, the RF-PTEs of full-digital and HBF were equal. The RF-PTE value increased with a decrease in distance. In the case of one amplitude controller and a distance of 0.1 and 0.5 m, the RF-PTEs were 10% and 2.8%, respectively. These results were so because the channel response decreased as the distance increased. With 16 amplitude controllers at a distance of 0.1 m, the RF-PTE increased by 7%. The absolute RF-PTE value would be larger provided the transmitter was larger, indicating that the use of the partially-connected HBF is advantageous in terms of efficiency compared with analog beamfocusing. Additionally, when the number of amplitude controllers was 4, the RF-PTE was 15%, an increase of over 5% compared with the RF-PTE by one amplitude controller. The aforementioned performance was achieved using an amplitude controller of 25% of the total number of antennas, indicating that HBF is highly efficient and can reduce the cost and complexity of the system. As shown in Fig. 5. 11 (b), the total RF-PTE added to the power received from the two receivers and the RF-PTE of each receiver was measured in the case of two receivers. The efficiencies

of the two receivers differed in the case of one amplitude controller and became almost the same when the number of amplitude controllers was 16. The magnitude of the efficiency differed because the channels of the two receivers were not symmetrical owing to the unsymmetrical nature of the experimental environment, as shown in Fig. 5. 10. Therefore, the HBF algorithm could be applied to a practical system.

5.6 Summary

In this chapter, we proposed an optimization algorithm that enabled efficient wireless power transmission by applying the HBF architecture to MPT to obtain the optimal values required for each phase shifter and amplitude controller. The optimization problem to achieve maximum RF−PTE in HBF architecture was to minimize the difference between the optimal transmission signal obtained in the fully−digital beamfocusing structure and the transmission signal in the HBF architecture. Further, we solved the optimization problem for HBF.

We obtained the results by applying the proposed algorithm to various scenarios of an MPT system with an operating frequency of 10 GHz. The transmitter was fixed with a 16 × 16 patch array antenna and the receiver was fixed with a 12 × 12 patch array antenna. We compared the results of HBF and fully−digital beamfocusing when the number of amplitude controllers was increased. The partially−connected PTE validated that an RF−PTE with an error within 4% of the fully digital RF−PTE can be achieved on average using the number of transmit antennas and an amplitude controller of 25%. Additionally, the subarray architecture could achieve a high RF−PTE using a relatively small number of amplitude controllers, which can be an additional option of the MPT architecture. When the proposed HBF MPT system was created and the optimal signal was obtained without the knowledge of the channel, the computational time could

be effectively reduced because the number of variables to be used was significantly reduced.

The experiment was conducted by designing a wireless power transmission testbed system that operated at 5.8 GHz to validate the feasibility of the proposed algorithm. A 16 × 1 transmitter patch array antenna and a 4 × 1 receiver patch array antenna were used and the RF−PTE of the partially−connected HBF was measured by changing the number of amplitude controllers in various scenarios and compared with the simulation results. As the number of amplitude controllers increased, RF−PTE increased, and RF−PTE close to full−digital beamfocusing was achieved with the number of amplitude controllers of 25–50%. Therefore, applying partially connected HBF to the MPT was advantageous in terms of cost and complexity and could create an MPT system that could transmit power with optimal efficiency. Our findings have guiding significance to determining the structure of the system when implementing an MPT system in the future.

5.7 Reference

[1] H. Y. Kim and S. Nam, "Optimization of Microwave Wireless Power Transmission With Specific Absorption Rate Constraint for Human Safety," in IEEE Transactions on Antennas and Propagation, vol. 68, no. 11, pp. 7721-7726, Nov. 2020.

[2] H. Y. Kim and S. Nam, "Efficient Microwave Wireless Power Transmission using Optimization Algorithm," 2022 16th European Conference on Antennas and Propagation (EuCAP), 2022.

[3] M. A. Ullah, R. Keshavarz, M. Abolhasan, J. Lipman, K. P. Esselle and N. Shariati, "A Review on Antenna Technologies for Ambient RF Energy Harvesting and Wireless Power Transfer: Designs, Challenges and Applications," in IEEE Access, vol. 10, pp. 17231-17267, 2022.

[4] O. L. A. López, D. Kumar, R. D. Souza, P. Popovski, A. Tölli and M. Latva-Aho, "Massive MIMO With Radio Stripes for Indoor Wireless Energy Transfer," in IEEE Transactions on Wireless Communications, vol. 21, no. 9, pp. 7088-7104, Sept. 2022.

[5] O. L. A. López, H. Alves, R. D. Souza, S. Montejo-Sánchez, E. M. G. Fernández and M. Latva-Aho, "Massive Wireless Energy Transfer: Enabling Sustainable IoT Toward 6G Era," in IEEE Internet of Things Journal, vol. 8, no. 11, pp. 8816-8835, 1 June1, 2021.

[6] M. Tavana, M. Ozger, A. Baltaci, B. Schleicher, D. Schupke and C. Cavdar, "Wireless Power Transfer for Aircraft IoT

Applications: System Design and Measurements," in IEEE Internet of Things Journal, vol. 8, no. 15, pp. 11834-11846, 1 Aug.1, 2021.

[7] S. H. Chae, C. Jeong and S. H. Lim, "Simultaneous Wireless Information and Power Transfer for Internet of Things Sensor Networks," in IEEE Internet of Things Journal, vol. 5, no. 4, pp. 2829-2843, Aug. 2018.

[8] H. Kim and S. Nam, "Efficiency Bound Estimation for Practical Microwave and mmWave Wireless Power Transfer System Design," Journal of Electromagnetic Engineering and Science, vol. 22, no. 1, pp. 171–177, 2023.

[9] A. Costanzo and D. Masotti, "Smart Solutions in Smart Spaces: Getting the Most from Far-Field Wireless Power Transfer," in IEEE Microwave Magazine, vol. 17, no. 5, pp. 30-45, May 2016.

[10] X. Cai, X. Gu and W. Geyi, "Optimal Design of Antenna Arrays Focused on Multiple Targets," in IEEE Transactions on Antennas and Propagation, vol. 68, no. 6, pp. 4593-4603, June 2020.

[11] H. Sun and W. Geyi, "Optimum Design of Wireless Power Transmission Systems in Unknown Electromagnetic Environments," in IEEE Access, vol. 5, pp. 20198-20206, 2017.

[12] A. Hajimiri, B. Abiri, F. Bohn, M. Gal-Katziri and M. H. Manohara, "Dynamic Focusing of Large Arrays for Wireless Power Transfer and Beyond," in IEEE Journal of Solid-State Circuits, vol. 56, no. 7, pp. 2077-2101, July 2021.

[13] J. H. Park, N. M. Tran, S. I. Hwang, D. I. Kim and K. W. Choi,

"Design and Implementation of 5.8 GHz RF Wireless Power Transfer System," in IEEE Access, vol. 9, pp. 168520-168534, 2021, doi: 10.1109/ACCESS.2021.3138221.

[14] M. Rihan, T. Abed Soliman, C. Xu, L. Huang and M. I. Dessouky, "Taxonomy and Performance Evaluation of Hybrid Beamforming for 5G and Beyond Systems," in IEEE Access, vol. 8, pp. 74605-74626, 2020.

[15] S. Payami et al., "Developing the First mmWave Fully-Connected Hybrid Beamformer With a Large Antenna Array," in IEEE Access, vol. 8, pp. 141282-141291, 2020.

[16] I. Ahmed et al., "A Survey on Hybrid Beamforming Techniques in 5G: Architecture and System Model Perspectives," in IEEE Communications Surveys & Tutorials, vol. 20, no. 4, pp. 3060-3097, Fourthquarter 2018.

[17] A. F. Molisch et al., "Hybrid Beamforming for Massive MIMO: A Survey," in IEEE Communications Magazine, vol. 55, no. 9, pp. 134-141, Sept. 2017.

[18] Y. Hu, J. Zhan, Z. H. Jiang, C. Yu and W. Hong, "An Orthogonal Hybrid Analog–Digital Multibeam Antenna Array for Millimeter-Wave Massive MIMO Systems," in IEEE Transactions on Antennas and Propagation, vol. 69, no. 3, pp. 1393-1403, March 2021.

[19] X. Yu, J. -C. Shen, J. Zhang and K. B. Letaief, "Alternating Minimization Algorithms for Hybrid Precoding in Millimeter Wave MIMO Systems," in IEEE Journal of Selected Topics in Signal

Processing, vol. 10, no. 3, pp. 485-500, April 2016.

[20] O. El Ayach, S. Rajagopal, S. Abu-Surra, Z. Pi, and R. W. Heath, “Spatially sparse precoding in millimeter wave MIMO systems,” IEEETrans. Wireless Commun., vol. 13, no. 3, pp. 1499–1513, Mar. 2014.

[21] M. Grant, S. Boyd, and Y. Ye, “CVX: MATLAB software for disciplined convex programming,” 2015. [Online]. Available: http://cvxr.com/cvx/

[22] Minyoung Yoon and Sangwook Nam, “7-Bit Multilayer True-Time Delay up to 1016 ps for Wideband Phased Array Antenna," IEICE Transactions on Electronics, vol.E102-C,no.8, Aug. 2019

Chapter 6. Conclusions & Future Works

In this thesis, algorithms for achieving maximum power transmission efficiency (PTE) of microwave wireless power transmission (MPT) and methods for implementing efficient systems were proposed and analyzed. A simulation was conducted on a wireless power transmission scenario to prove the proposed algorithm, and a testbed was implemented and an experiment was conducted.

In the second chapter, we propose a novel convex optimization algorithm for controlling the transmit antennas of MPT systems that transmit maximum power under certain absorption rate (SAR) constraints for human safety. The received power and PTE of the proposed optimization technique were compared with the time-reversal (TR) technique at 0.9 GHz. We show that OPT techniques can transfer more power than TR techniques with lower PTEs within the SAR limit and that the proposed techniques can be applied to various MPT scenarios.

In the third chapter, an optimization method for MPT capable of charging multiple receivers was presented. Optimization algorithms find the optimal transmission signal to transfer the desired power to multiple receivers with maximum PTE. Considering various scenarios, the received power of each receiver and the PTE of the optimization method and the PTE of the multi-receiver TR method

were compared. The OPT algorithm transmits multiple beams to simultaneously charge multiple receivers. In addition, it was verified that the OPT technology can accurately deliver power to the receiver at the desired ratio with a larger PTE than the TR technology in the MPT system.

In the fourth chapter, an efficient method for finding the PTE for a practical microwave and mmWave wireless power transmission system consisting of a transmitter and a receiver array antenna was studied. For MPT systems designed for 10 GHz and 24 GHz, the estimated PTE boundaries were compared with previous studies. In addition, the calculation time required for each method was compared. It was shown that the proposed method provides faster and more accurate PTE boundaries without electromagnetic simulation of an MPT system composed of Tx and Rx array antennas.

In the fifth chapter, MPT with hybrid beam focusing was studied. An algorithm for deriving an optimal signal with maximum PTE for partially-connected and fully-connected hybrid beam focusing methods was proposed. Through simulation and experimental results, it was confirmed that the optimal efficiency can be approached with only a smaller number of amplitude controllers than the total number of antennas. Therefore, it was verified that when the hybrid beam focusing method is used for MPT, it is possible to design an MPT system with optimal efficiency and advantages in terms of cost, complexity, and computational time.

In this thesis, we propose an algorithm that can determine the specifications of an optimal transmission signal and an efficient MPT system in a given scenario using optimization. However, since the optimal signal was obtained by assuming that the channel information was known, there are limitations in applying the practical MPT system. Therefore, in a given system, if channel information is not known, a method for finding an optimal transmission signal should be studied in the future. Even if an optimal value cannot be found by using optimization, power can be transmitted by finding a suboptimal by an alternative method. A typical method is to use feedback. After the transmitter transmits a random test pattern, the signal received at the receiver is fed back to the transmitter. The feedback signal is DC power or RF power received from the receiver. The test patterns used are orthogonal sets, and the phase that can send the maximum power for each test pattern is derived by changing the phase of the transmission signal from 0 degrees to 360 degrees. The optimal signal can be obtained by finding the optimal phase of each test pattern and accumulating the signals. Next, the optimal signal obtained can be applied to HBF system. The optimal signal to be transmitted from each antenna found above is input data to the algorithm proposed in chapter 5. In the case of partially-connected HBF, the coefficients that each amplitude controller and phase shifter can be obtained by HBF algorithm. The practical HBF MPT system can be completed using this method.

초 록

본 논문에서는 마이크로웨이브 무선 전력 전송(MPT)의 최대 파워 전송 효율과 효율적인 시스템 제작을 위한 최적화 알고리즘 연구를 진행하였다 먼저 배열 안테나를 이용한 마이크로웨이브 무선 전력 전송 시 파워 전송 효율을 최대로 하기 위한 최적의 전송 신호를 구하는 최적화 알고리즘을 연구하였다. 마이크로웨이브 무선 전력 전송에서 고려하는 중요한 두 가지 요소가 있다. 첫 번째는 전자파가 인체에 미치는 영향을 최소화하는 것이며, 두 번째는 여러 개의 수신기를 동시에 충전하는 것이다. 따라서 두 경우를 각각 만족시키며 최대 파워 전송 효율을 도출하는 최적화 알고리즘을 제안하였다. 또한 효율적인 무선 전력 전송 시스템을 만들 위해 필요한 가이드 라인을 제공하여 주는 최적화 알고리즘을 연구하였다. 빠른 채널 예측 방법을 통하여 무선 전력 전송 시스템의 효율 경계를 계산할 수 있는 알고리즘을 개발하였다. 추가적으로, 하이브리드 빔포밍 방식의 무선 전력 전송 방식을 제안하였다. 연구의 주된 내용은 아래와 같다.

첫 번째, 인체 안전을 위한 특정 흡수율(SAR) 제약 조건에서 최대 전력 전송이 가능하도록 하는 최적의 MPT 시스템 송신 신호를 구하기 위해서 새로운 볼록 최적화 알고리즘을 제안하였다. 초기 NP-hard 문제를 convex 최적화 문제로 변환하는 방법에 대해 자세히 설명하였다. 상자 모양의 팬텀 모델 옆에 하나의 수신기가 배치되어 있으며, 다중 송신 안테나가 그것들을 둘러싸고 있는 MPT 시나리오에 알고리즘을 적용하였다. 최적화 프로세스에 필요한 송수신기의 채널 응답과 팬텀의 전기장 응답은 전파 전자기 시뮬레이션 (CST Microwave Studio)을 사용하여 얻었다. 제안된 최적화 기법의 수신 전력 및 전력 전달 효율을 0.9GHz에서 TR(Time-Reversal) 기법과 비교하였다. 최적화 기법이 SAR 한도 내에서 TR 기법보다 더 많은 전력을 전달할 수 있고 제안 기법이 다양한 MPT 시나리오에 적용될 수 있음을 보여주었다.

두 번째, 다중 수신기를 충전할 수 있는 MPT을 위한 최적화 방법을 개발하였다. 최적화 알고리즘은 원하는 전력을 최대 파워 전달 효율(PTE)로 여러 수신기에 전달하기 위한 최적의 전송 신호를 찾는다. 송신기와 수신기로써 10GHz에서 동작하는 5 × 5 직사각형 패치 어레이 안테나와 패치 단일 안테나를 설계하였으며 최적화 방법을 이용한 MPT 시스템의 동작 과정을 분석하였다. 또한 다양한 시나리오를 고려하여 각 수신기의 수신 전력 및 최적화 기법의 PTE와 다중 수신기 TR 기법의 PTE을 비교하였다. 최적화 알고리즘은 다중 빔을 생성하여 여러 수신기를 동시에 충전한다. 또한 MPT 시스템에서 최적화 기술이 TR 기술보다 더 큰 PTE로 원하는 비율로 정확하게 수신기에 전력을 전달할 수 있음을 검증하였다.

세 번째, 송신기와 수신기 어레이 안테나로 구성된 실용적인 마이크로파 및 mmWave 무선 전력 전송 시스템에 대한 PTE를 찾는 효율적인 방법을 연구하였다. MPT 시스템의 PTE 경계는 송신 전력 제약 하에서 수신 어레이에서 수신되는 전력을 최대화하는 볼록 최적화 문제로 공식화함으로써 얻어진다. 송신기와 수신기의 각 요소 사이의 채널 상태 정보(CSI)는 제안된 convex 최적화 문제의 입력 파라미터이다. CSI는 송신기와 수신기가 대형 어레이로 가정되기 때문에 어레이 안테나의 Friis 전송방정식 및 Active Element Pattern를 이용하여 추정한다. 10GHz와 24GHz로 설계된 MPT 시스템의 경우 송신기와 수신기 사이의 거리와 기울어진 각도를 변화시키면서 추정된 PTE 경계를 이전 연구와 비교하였다. 또한 각 방법에 필요한 계산 시간을 비교하였다. 제안된 방법이 송신기 및 수신기 어레이 안테나로 구성된 MPT 시스템의 EM 시뮬레이션 없이 더 빠르고 정확한 PTE 경계를 구할 수 있음을 확인하였다.

네 번째, MPT에 대한 하이브리드 빔포커싱 방법을 연구하였다. 하이브리드 빔포커싱 구조를 위한 최대 RF 전력 전달 효율(RF-PTE)을 갖는 위상 변위기와 진폭 제어기의 최적 계수를 얻기 위한 최적화 알고리즘을 제안한다. 최적화 문제를 반복적으로 푸는 최적화 알고리즘을 제안한다. 이 알고리즘은 10GHz에서 작동하는 패치 어레이 안테나로 구성

된 송신기와 수신기가 있는 MPT 시스템에 적용하여 시뮬레이션되었다. 또한 5.8GHz에서 작동하는 테스트 베드를 구현하였다. 시뮬레이션과 실험을 통해 부분적으로 연결된 하이브리드 빔포커싱 구조의 진폭 제어기 개수를 완전 디지털 빔포커싱에 비해 절반으로 줄여 최적의 RF-PTE를 달성할 수 있다. 따라서 하이브리드 빔포커싱 방식을 이용하여 경제적이고 덜 복잡한 MPT 시스템을 구현할 수 있다.

주요어: 무선 전력 전송, 어레이 안테나, 파워 전달 효율, convex 최적화

학 번: 2016-20889

감사의 글

전파공학 연구실에 석박 과정으로 받아 주시고, 부족한 저를 진심으로 지도해주신 남상욱 교수님께 감사의 말씀을 드립니다. 교수님께서 항상 책을 보며 공부하시는 모습을 보면서 성실하신 모습에 감명을 받았습니다. 또한 교수님의 겸손하신 모습을 오랫동안 보면서 제 자신을 되돌아보며 변화할 수 있는 계기가 되었습니다. 교수님의 지도 덕분에 공학적 문제를 만들고 해결하는 방법을 습득할 수 있게 되었고 사회에 가서도 교수님께 배운 점들을 활용하기 위해 노력하겠습니다.

가족들에게 진심으로 감사의 말씀을 드립니다. 언제나 뒤에서 든든하게 기도하고 지원해주신 부모님께 감사합니다. 앞으로 더 효도하고 그 동안의 보살핌에 감사하며 살도록 하겠습니다. 또한 항상 내가 주는 관심보다 더 많은 관심을 주는 동생에게도 감사의 마음을 전합니다. 또한 지금까지 저를 인도하여 주신 하나님께 감사합니다.

바쁘신 와중에도 시간을 내어 학위논문을 지도해 주신 이정우 교수님, 이범선 교수님, 이정해 교수님, 그리고 오정석 교수님께도 감사의 인사를 드립니다. 교수님들의 세심한 논문 지도 덕분에 학위과정을 잘 마무리할 수 있었습니다.

마지막으로 연구실 구성원들께 감사의 말씀드립니다. 좋은 분들과 박사 과정 기간 동안 연구실 구성원으로써 지낼 수 있어서 영광이었습니다. 앞으로 사회에 나가서도 좋은 인연을 유지하며 지냈으면 좋겠습니다.

2023년 2월

김호열